FINAL REPORT FOR

Grant No. NAG 1-500

SEMICONDUCTOR SUPERLATTICE PHOTODETECTORS

June 1, 1984 to December 31, 1986

Submitted to

Dr. Ivan Clark

National Aeronautics and Space Administration
Langley Research Center, Mail Stop 473
Hampton, VA 23665

Prepared by

S. L. Chuang
Department of Electrical and Computer Engineering
University of Illinois
Urbana, IL 61801

K. Hess, J. J. Coleman and J. P. Leburton
Department of Electrical and Computer Engineering
and Coordinated Science Laboratory
University of Illinois
Urbana, IL 61801

FINAL REPORT FOR

Grant No. NAG 1-500

SEMICONDUCTOR SUPERLATTICE PHOTODETECTORS

June 1, 1984 to December 31, 1986

Submitted to

Dr. Ivan Clark

National Aeronautics and Space Administration
Langley Research Center, Mail Stop 473
Hampton, VA 23665

Prepared by

S. L. Chuang
Department of Electrical and Computer Engineering
University of Illinois
Urbana, IL 61801

K. Hess, J. J. Coleman and J. P. Leburton
Department of Electrical and Computer Engineering
and Coordinated Science Laboratory
University of Illinois
Urbana, IL 61801

TABLE OF CONTENTS

I. INTRODUCTION

The research grant NAG 1-500 entitled "Semiconductor Superlattice Photodetectors" was awarded to the University of Illinois at Urbana-Champaign by National Aeronautics and Space Administration-Langley Research Center on June 27, 1984. The grant was continued on July 1, 1985 and extended to December 31, 1986. Dr. Ivan Clark is the Technical Officer, and Mr. John F. Royall is the Grants Officer.

This report is the final report.

1. Period:

   June 1, 1984 to December 31, 1986

2. Reporting Date:

   January 10, 1987.

3. Technical Personnel:

   S. L. Chuang — Assistant Professor of Electrical and Computer Engineering

   J. J. Coleman — Professor of Electrical and Computer Engineering

   K. Hess — Professor of Electrical and Computer Engineering and Research Professor of Coordinated Science Laboratory

   J. P. Leburton — Assistant Professor of Electrical and Computer Engineering and Research Assistant Professor of Coordinated Science Laboratory

   Two research assistants

II. TECHNICAL PROGRESS

Superlattice photodetectors have been investigated during the past two and one-half years. We have studied a few major physical processes in the quantum-well heterostructures related to the photon detection and electron conduction mechanisms, namely, the impact ionization of hot electrons, the tunneling-assisted process, the field effect on the wave functions and the energy levels of the electrons, and the optical absorption with and without the phonon assistance. The results are summarized below. The details are reported in the appendix where reprints and preprints of papers supported by this grant are included.

1. Superlattice photomultiplier

Tunneling-assisted impact ionization across the conduction-band-edge discontinuity of a quantum-well heterostructure is investigated and applied to a new superlattice structure (Appendix A). We consider multiquantum-well structures where the quantum-well regions are heavily doped and the undoped barrier regions are essentially insulating. Incident hot electrons due to the applied electric field perpendicular to the heterointerface interact with the two-dimensional electrons confined to the quantum wells through Coulomb force. The resultant electrons can either have enough energy to get out of the wells or tunnel through the triangular barriers. A new analytical approximation for the impact ionization rate is given which compares favorably with numerical results. The tunneling-assisted impact ionization rates and the ionization coefficients are calculated. It is shown that the tunneling effect reduces the ionization threshold and enhances the ionization rate significantly. Some experimental results of

this single-carrier type photomultiplier have been reported by Capasso's group at AT&T Bell Laboratories.

We also carried out the variational calculations of subband eigenstates in an infinite quantum well with an applied electric field using Gram-Schmidt orthogonalized trial wave functions (Appendix B). The results agree very well with the exact numerical solutions even up to 1200 kV/cm. We also show that for increasing electric fields the energy of the ground state decreases, while that of higher subband states increases slightly up to 1000 kV/cm and then decreases for a well size of 100 A.

We have also performed the exact numerical calculations for the energy level and the resonance width of quasibound states in a quantum well with an applied electric field (Quantum-well Stark Resonance) by solving the Schrödinger equation directly (Appendix C). This calculation gives both the resonance positions and widths for the complex eigenvalue $E_o - i\Gamma/2$ of the system. Our theory also shows that the energy shifts of the ground states for the electrons and holes have the same behavior in high fields without any turnaround phenomenon, contrary to the results of Austin and Jaros.

2. Superlattice Photodetector Based on the Real Space Transfer Mechanism

We have investigated the free carrier absorption process of a superlattice photodetector which makes use of the real space transfer mechanism. In particular, we have formulated and numerically computed the free carrier absorption coefficient for bulk GaAs in which we considered a second-order process involving both a photon and a phonon. Additionally, we carried out the computations for the free carrier absorption coefficient

in a quantum well for the above cited second-order process involving a photon and a phonon.

We also carried out new calculations for the electric field dependence of the intersubband optical absorption within the conduction band of a quantum well (Appendix D). We show that for increasing electric field the absorption peak corresponding to the transition of states 1 → 2 is shifted higher in energy and the peak amplitude is increased. These features are different from those of the exciton absorption. It is also found that the forbidden transition for states 1 → 3 when F = 0 is possible when F is nonzero. These results are significant for applications to infrared photodetectors and infrared lasers making use of the intersubband transitions in the quantum wells.

IV. PUBLICATIONS

The following manuscripts submitted for publication were supported either fully or partially by this Grant. The support by this Grant has been acknowledged in these manuscripts.

1. S. L. Chuang and K. Hess, "Impact ionization across the conduction-band-edge discontinuity of quantum-well heterostructures," J. Appl. Phys., vol. 59, pp. 2885-2894, 1986.

2. S. L. Chuang and K. Hess, "Impact ionization across the band-edge discontinuity for a superlattice photomultiplier," presented at the 1986 Device Research Conference, Amherst, Massachusetts, June 21-23, 1986.

3. S. L. Chuang, "Lateral shift of an optical beam due to leaky surface-plasmon excitations," J. Opt. Soc. Am., vol. 3, pp. 593-599, 1986.

4. S. L. Chuang and K. Hess, "Tunneling-assisted impact ionization for a superlattice," J. Appl. Phys., to appear in February 1987.

5. D. Ahn and S. L. Chuang, "Variational calculations of subbands in a quantum well with uniform electric field: Gram-Schmidt orthogonalization approach," Appl. Phys. Lett., vol. 49, pp. 1450-1452, 1986.

6. D. Ahn and S. L. Chuang, "Exact calculations of quasibound states of an isolated quantum well with uniform electric field: Quantum-well Stark resonance," Phys. Rev. B, vol. 34, PP.9034-9037, 1986.

7. D. Ahn and S. L. Chuang, "Intersubband optical absorption in a quantum well with applied electric field," Phys. Rev. B, accepted for publication.

8. S. L. Chuang, "A coupled-mode formulation by reciprocity and a variational principle," IEEE J. Lightwave Technology, vol. LT-5, pp.5-15, 1987.

9. S. L. Chuang, "A coupled-mode theory for multiwaveguide system satisfying the reciprocity theorem and power conservation," IEEE J. Lightwave Technology, vol. LT-5, pp.174-183, 1987.

10. S. L. Chuang, "Application of the strongly coupled-mode theory to integrated optical devices," IEEE J. Quantum Electronics, to appear in May, 1987.

11. L. Tsang and S. L. Chuang, "Strongly coupled-mode theory for reciprocal anisotropic multiwaveguide system," IEEE J. Lightwave Technology, submitted for publication.

12. D. Ahn and S. L. Chuang, "Nonlinear intersubband optical absorption in a semiconductor quantum well," Appl. Phys. Lett, submitted for publication.

Appendix A

S. L. Chuang and K. Hess, "Tunneling-assisted impact ionization for a superlattice," J. Appl. Phys., to appear in February 1987.

859703JAP

Tunneling-assisted impact ionization for a superlattice

S. L. Chuang
Department of Electrical and Computer Engineering, University of Illinois at Urbana-Champaign, Urbana, Illinois 61801

K. Hess
Department of Electrical and Computer Engineering and Coordinated Science Laboratory, University of Illinois at Urbana-Champaign, Urbana, Illinois 61801

(Received 4 August 1986; accepted for publication 21 October 1986)

Tunneling-assisted impact ionization across the conduction-band-edge discontinuity of quantum-well heterostructures is investigated and applied to a new superlattice structure. We consider multiquantum-well structures where the quantum-well regions are heavily doped and the undoped barrier regions are essentially insulating. Incident hot electrons due to the applied electric field perpendicular to the heterointerface interact with the two-dimensional electrons confined to the quantum wells through Coulomb force. The resultant electrons can either have enough energy to get out of the wells or tunnel through the triangular barriers. A new analytical approximation for the impact ionization rate is given which compares favorably with numerical results. The tunneling-assisted impact ionization rates and the ionization coefficients are calculated. It is shown that the tunneling effect reduces the ionization threshold and enhances the ionization rate significantly.

I. INTRODUCTION

Superlattice photodetectors have been of interest to many researchers because they involve new device physics and have the potential of minimizing the excess noise factor.[1-4] The basic concept is based on the well-known fact that to minimize the excess noise due to the feedback process in an avalanche photodiode, one requires that the impact ionization coefficients of the electrons and the holes differ greatly, and the carrier type with the larger ionization coefficient initiates the impact ionization process.[5-7] Since the ionization coefficients, α and β, of the electrons and holes, respectively, can be very close, one tries to artificially enhance the α/β or β/α ratio using superlattice structures.[1-4] These include a multiquantum-well structure,[1,2] a staircase photomultiplier,[2,3] etc. One notes that most of these proposed devices deal with impact ionization across the energy band gap E_g. We have studied recently the possibilities of a superlattice photomultiplier which makes use of the impact ionization across the conduction-band-edge discontinuity ΔE_c.[8] Independent experimental work on this process has also been reported recently,[9] where both $Al_{0.48}In_{0.52}As/Ga_{0.47}In_{0.53}As$ and AlSb/GaSb superlattices are considered.

The multiquantum-well device we consider is shown in Fig. 1, where the GaAs regions are doped with donors N_D and the $Al_xGa_{1-x}As$ regions are undoped.[8] Ohmic contacts are provided to the GaAs regions for replenishment of electrons in the wells once they are impact ionized by incident electrons which are heated up in the AlGaAs regions by the external electric field. A theoretical study of the impact ionization in this structure has been done numerically in Ref. 8 without considering the tunneling effect. Since the impact ionization process is due to the electron confined to the wells and virtually no holes are involved, the electron ionization coefficient α will be much larger than the hole ionization coefficient β. In this paper, we also develop an anlytical approximation for the impact ionization of electrons from the quantum wells and compare its results with those of our previous numerical approach. We demonstrate very good agreement between the two methods. On this basis, tunneling-assisted impact ionization across the band-edge discontinuity is calculated. Previous studies,[10,11] including the pioneering work of Keldysh and Kyuregyan, involve mainly tunneling-assisted impact ionization across the energy gap E_g. We include Fowler–Norheim tunneling[12,13] by using a numerical approach involving Airy functions instead of using the WKB method since the WKB method will not be appropriate when the energy of the electron is close to the barrier height (ΔE_c in this case). A comparison of the results using Airy functions and those for the WKB method is made. It is shown that tunneling reduces the threshold energy for impact ionization and enhances the ionization rate, especially at the low-energy side. Numerical results for the electron ionization coefficient α are then presented with and without the tunneling effect. The multiplication factor is also shown versus the applied voltage.

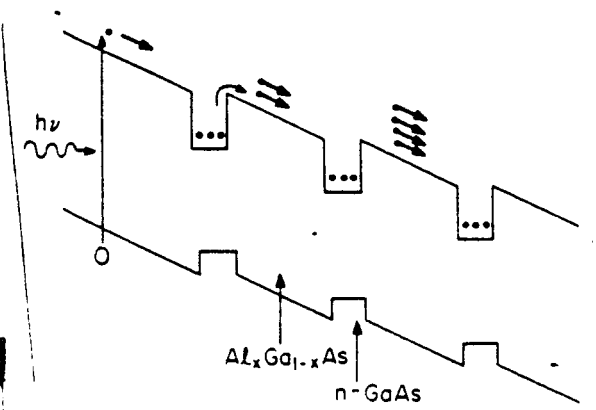

FIG. 1. Geometrical configuration of a multiquantum-well structure exhibiting impact ionization across the conduction-band-edge discontinuity for a solid-state photomultiplier.

II. THEORY

In this section, we present (in Sec. II A) an analytical approximation for the impact ionization of electrons confined to quantum wells excluding tunneling effects. We compared the results with those obtained by using a direct numerical approach from Ref. 8. We then include the tunneling effect in the impact ionization process in Sec. II B.

A. Analytical approximation for the average impact ionization rate

The total transition rate per unit volume P_{tr} between the incident hot electrons in the free states and the cold electrons confined to the quantum wells is given by[8]

$$P_{tr} = \frac{1}{V}\sum_{\mathbf{k}_1}\sum_{\mathbf{k}_2}\sum_{\mathbf{k}_1'}\sum_{\mathbf{k}_2'} \times P^{\mathbf{k}_1'\mathbf{k}_2'}_{\mathbf{k}_1\mathbf{k}_2} f(\mathbf{k}_1) f(\mathbf{k}_2)[1-f(\mathbf{k}_1')][1-f(\mathbf{k}_2')], \quad (1)$$

where

$$P^{\mathbf{k}_1'\mathbf{k}_2'}_{\mathbf{k}_1\mathbf{k}_2} = \frac{2\pi}{\hbar}|\langle 12|H_s|1'2'\rangle|^2 \delta(E_1+E_2-E_1'-E_2'). \quad (2)$$

The square of the matrix element $|\langle 12|H_s|1'2'\rangle|^2$ due to Coulomb interactions has been calculated in Ref. 8 where the initial state consists of electron 1 in free state above the well and electron 2 in bound state inside the well. The final state consists of both electron 1′ and electron 2′ in free states above the well. The average ionization rate $\langle 1/\tau\rangle$ is given by Eq. (25) of Ref. 8:

$$\left\langle\frac{1}{\tau}\right\rangle = \frac{P_{tr}}{n_0} \cong \int \frac{dk_{0z}}{2\pi}\left(\frac{\pi\hbar^2}{2m_a^* k_B T_e}\right)^{1/2} \times \exp\left(-\frac{\hbar^2 k_{0z}^2}{2m_a^* k_B T_e}\right)\frac{1}{\tau(E_{0z})}, \quad (3)$$

where n_0 is the concentration of the incident electrons, m_a^* is the effective mass in the AlGaAs region, and

$$\frac{1}{\tau(E_{0z})} = \sum_n \frac{4\pi e^4}{\hbar\epsilon^2}\left(\frac{L_{zn}}{L}\right)^2 \int \frac{d\mathbf{k}_{2t}}{(2\pi)^2 L_{zn}} \times f(\mathbf{k}_{2t})[S(\mathbf{k}_1,\mathbf{k}_{2n}^+)+S(\mathbf{k}_1,\mathbf{k}_{2n}^-)]. \quad (4)$$

The summation is over all the occupied subbands in the wells and E_{0z} is the energy of the incident electron measured from the conduction-band edge of the barrier region. All parameters are defined as in Ref. 8. An effective well width L_{zn} is used to account for the finite barrier height.[8] The integral $S(\mathbf{k}_1,\mathbf{k}_2)$ due to the electron-electron interactions is defined as

$$S(\mathbf{k}_1,\mathbf{k}_2) = \int_{k_{1z}+k_{2z}-k_{th}'<k_{1z}'<k_{th}'} \frac{d\mathbf{k}_1'}{(2\pi)^3} \times \frac{\delta(E_1+E_2-E_1'-E_2')}{[|\mathbf{k}_1-\mathbf{k}_1'|^2+q^2]^2}\Bigg|_{\mathbf{k}_2'=\mathbf{k}_1+\mathbf{k}_2-\mathbf{k}_1'}, \quad (5)$$

where the range of integration for k_{1z}' is limited since both k_{1z}' and k_{2z}' must be $\geq k_{th}'$ for electrons 1′ and 2′ to get out of wells if the tunneling effect is not included. The screening parameter q has been discussed in Ref. 8. The above integral has also been evaluated numerically in Ref. 8 where $\mathbf{k}_2$ has both transverse component $\mathbf{k}_{2t}$ and z-component $\pm z(n\pi/L_{zn})$. We know that $\mathbf{k}_{2t}$ is limited by the doping concentration which determines the Fermi energy E_F in the wells,

$$f(\mathbf{k}_{2t}) = \begin{cases} 1 & \text{if } 0<k_{2t}<K_{2t}^{(n)} \\ 0 & \text{otherwise} \end{cases}, \quad (6a)$$

$$K_{2t}^{(n)} = \sqrt{(2m^*/\hbar^2)E_F - (n\pi/L_{zn})^2}, \quad (6b)$$

where n refers to the nth subband. The electron concentration is

$$n \simeq N_D = \int_{E_{Q1}}^{\infty} f(E)g(E)dE = \sum_n N_n, \quad (7)$$

where

$$N_n = \frac{m^*}{\pi\hbar^2 L_{zn}} k_B T \ln(1+e^{(E_F-E_{Qn})/k_B T}) \simeq \frac{m^*}{\pi\hbar^2 L_{zn}}(E_F-E_{Qn}) \quad (8)$$

(for $E_F - E_{Qn} \gg k_B T$) is the electron concentration in the nth subband and E_{Qn} is the energy level of the nth subband. Since $\hbar\mathbf{k}_1$ is the momentum of the incident hot electrons which is usually much larger than the momentum of the electrons in the wells, and $\mathbf{k}_1$ is essentially directed in the z

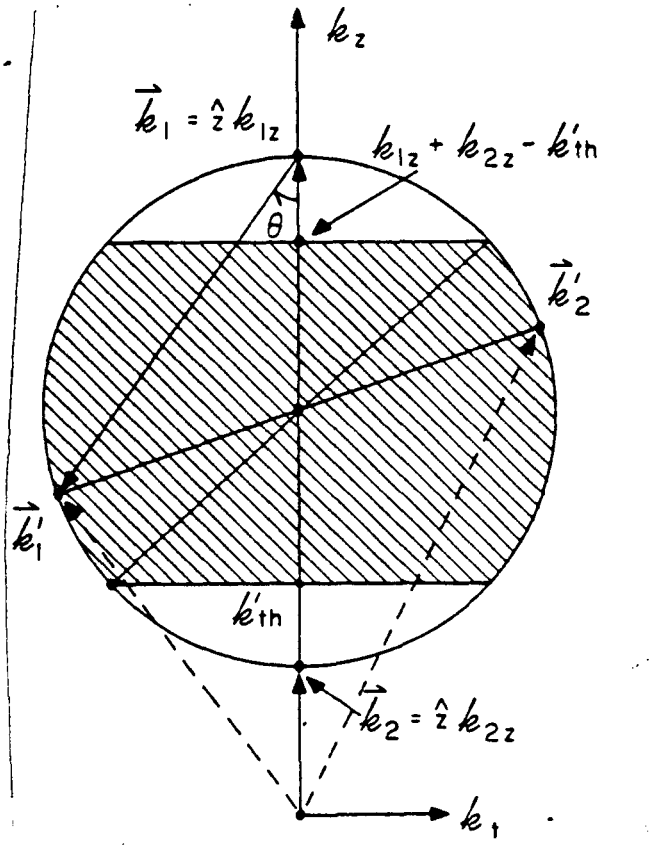

FIG. 2. A momentum space diagram illustrating the range of integrations for $\mathbf{k}_1'$. Because of both energy and momentum conservation, the four wave vectors $\mathbf{k}_1$, $\mathbf{k}_2$, $\mathbf{k}_1'$, and $\mathbf{k}_2'$ lie on a spherical surface in the momentum space assuming parabolic band structures.

direction, $\mathbf{k}_1 = \hat{z}k_1$, we thus assume

$$S(\mathbf{k}_1,\mathbf{k}_2) \simeq S(\mathbf{k}_1,\hat{z}k_{2z}) , \tag{9}$$

and ignore the transverse components $\mathbf{k}_{2t}$ in the integrand of the integral $S(\mathbf{k}_1,\mathbf{k}_2)$. Using the geometrical configuration shown in Fig. 2 in which $\mathbf{k}_1$, $\mathbf{k}_2$, $\mathbf{k}_1'$, and $\mathbf{k}_2'$ lie on the same spherical surface[8] due to both energy and momentum conservation, we integrate Eq. (5) analytically noting that

$$\delta(E_1 + E_2 - E_1' - E_2') = (m^*/\hbar^2)\delta[(\mathbf{k}_1' - \mathbf{k}_1)\cdot(\mathbf{k}_2 - \mathbf{k}_1')] , \tag{10}$$

and making a change of variable

$$\mathbf{k} = \mathbf{k}_1' - \mathbf{k}_1 , \tag{11}$$

we obtain

$$S(\hat{z}k_{1z},\hat{z}k_{2z}) = \begin{cases} \left(\dfrac{m^*}{8\pi^2\hbar^2}\right) \dfrac{(k_{1z} + k_{2z} - 2k_{th}')}{[(k_{1z} - k_{2z})(k_{1z} - k_{th}') + q^2][(k_{1z} - k_{2z})(k_{th}' - k_{2z}) + q^2]} & \text{if } k_{2z} < k_{th}' < \dfrac{k_{1z} + k_{2z}}{2} \quad (12a) \\ \left(\dfrac{m^*}{8\pi^2\hbar^2 q^2}\right) \dfrac{|k_{1z} - k_{2z}|}{|k_{1z} - k_{2z}|^2 + q^2} & \text{if } k_{th}' < k_{2z} \quad (12b) \\ 0 \quad \text{otherwise} & (12c) \end{cases}$$

In the first case, the condition $k_{2z} < k_{th}' < (k_{1z} + k_{2z})/2$ corresponds to the integral over the shaded region in Fig. 2. If the threshold value k_{th}' is $< k_{2z}$, the integral will be over the whole spherical surface[8] and results in the second Eq. (12b). The threshold wave number k_{th}' for electrons 1′ and 2′ is given by

$$k_{th}' = \sqrt{2m_b^*\Delta E_c}/\hbar \tag{13}$$

which is larger than k_{2z} usually where the voltage drop across the quantum-well region is assumed to be zero since it is heavily doped and ohmic contacted. Here m_b^* (or m^*) is the average effective mass in the GaAs region with the nonparabolic effect included.[8] Thus, the threshold energy of the incident hot electrons for impact ionization E_i, measured from the conduction-band edge in the barrier region, is calculated from

$$k_{1z} = k_{1z}' + k_{2z}' - k_{2z} > 2k_{th}' - k_{2z} , \tag{14}$$

$$E_i = (\hbar^2/2m_b^*)(2k_{th}' - k_{2z})^2 - \Delta E_c . \tag{15}$$

If one ignores $k_{2z} = \pi/L_{z1}$ of the ground state, we have $E_i \simeq 3\Delta E_c$. Thus, the threshold energy E_i is in general $\simeq 3\Delta E_c$ or less when k_{2z} is included. The integration over $\mathbf{k}_{2t}$ is easily done using the distribution function $f(\mathbf{k}_{2t})$ in (6) and the fact that $S(\mathbf{k}_1,\mathbf{k}_2)$ is independent of $\mathbf{k}_{2t}$.

$$\frac{1}{\tau(E_0)} = \sum_n \frac{4\pi e^4}{\hbar^2\epsilon^2}\left(\frac{L_{zn}}{L}\right)^2 \frac{K_{2t}^{(n)^2}}{4\pi L_{zn}} \times \left[S\left(\mathbf{k}_1,\hat{z}\frac{n\pi}{L_{zn}}\right) + S\left(\mathbf{k}_1,-\hat{z}\frac{n\pi}{L_{zn}}\right)\right] , \tag{16}$$

where $E_0 = E_{0z}$ since the incident electron 1 is assumed to be traveling in the z direction only. The last integral over k_{0z} (or E_0) in (3) to obtain the average ionization rate $\langle 1/\tau \rangle$ is calculated numerically by Simpson's rule. We ignore $\mathbf{k}_{2t}$ in the integrand of Eq. (5) which means that we assume that all electrons in the same subband in the quantum wells are ionized at the same rate independent of $\mathbf{k}_{2t}$. Numerical results as shown in Fig. 3(a) indicate that this is an excellent approximation which speeds up our computation by more than a factor of 100. The results using the direct numerical inte-

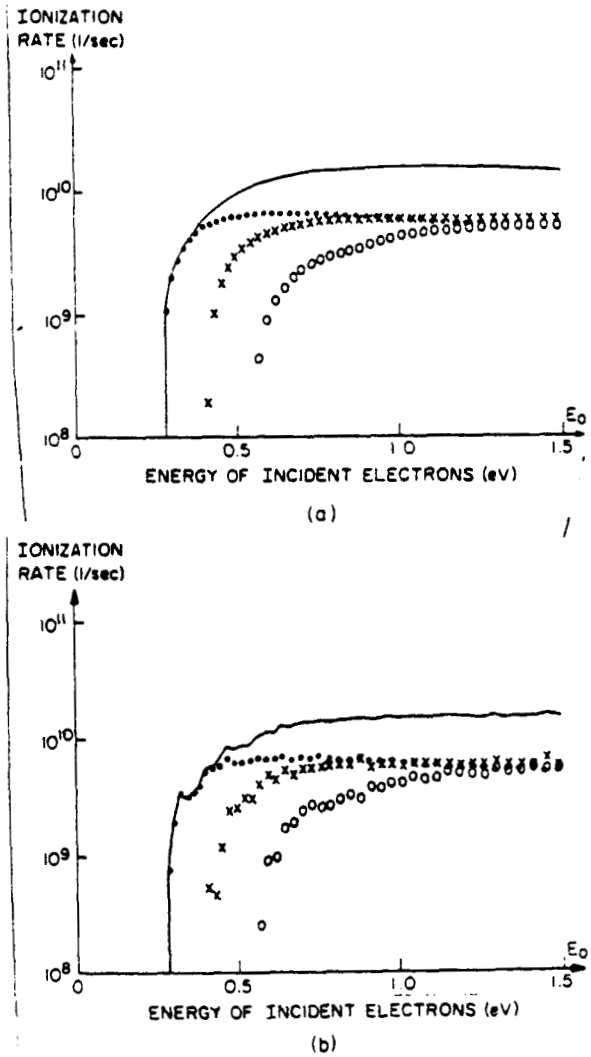

FIG. 3. (a) The impact ionization rate $[1/\tau(E_0)]$ as a function of the incident electron energy E_0 measured from the conduction-band edge of the AlGaAs region using the analytical approximation (12) in Eq. (4). (circles = first subband, crosses = second subband, dashed line = third subband, solid line = total.) (b) $1/\tau(E_0)$ calculated using direct numerical integrations of multiple integrals as has been done in Fig. 4(b) of Ref. 8.

grations[8] of multiple variables are shown in Fig. 3(b) for comparison. It is clear that our analytical approximations lead to very accurate results and eliminate the fluctuations due to numerical instabilities in the previous numerical integrations for all subbands as shown in Fig. 3(b).

B. Tunneling-assisted impact ionization

The impact ionization of electrons in the wells which subsequently tunnel through the triangular barrier is calculated from

$$P_{tr} = \frac{1}{V}\sum_{k_1}\sum_{k_2}\sum_{k_1'}\sum_{k_2'} P_{k_1k_2} T(E_1')T(E_2') f(\mathbf{k}_1) f(\mathbf{k}_2) \times [1-f(\mathbf{k}_1')][1-f(\mathbf{k}_2')], \quad (17)$$

where $T(E_1')$ and $T(E_2')$ are the transmission coefficients through a triangular barrier with a barrier height $V_0 = \Delta E_c$ as shown in Fig. 4 at energies E_1' and E_2', respectively. The tunneling coefficient using the WKB method is given by[13]

$$T(E) = T(E_z) = \begin{cases} \dfrac{4\sqrt{E_z(V_0-E_z)}}{V_0} e^{-4\eta_0^{3/2}/3} & \text{if } \eta_0 \gg 1 \quad (18a) \\ \dfrac{4\sqrt{(E_z-V_0)/E_z}}{(1+\sqrt{(E_z-V_0)/E_z})^2} & \text{if } \eta_0 \ll -1, \quad (18b) \end{cases}$$

where

$$\eta_0 = (K_F/eF)(V_0 - E_z), \quad (19)$$

$$K_F = (2m^* eF/\hbar^2)^{1/3}, \quad (20)$$

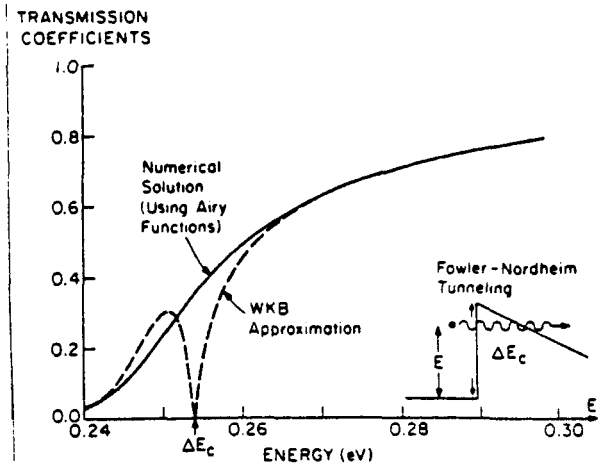

FIG. 4. The transmission coefficient for electron tunneling through a triangular barrier with a height $\Delta E_c = 0.254$ eV. The solid curve is using the numerical approach with Airy functions and their derivatives. The dashed curve is from the WKB method.

where the effective mass difference between the well and the barrier regions has been ignored. If one includes the effective mass difference, the tunneling coefficient will be a function of both the longitudinal and the transverse energies,[13,14] E_z and E_t. The effect is small, however, since the effective mass difference is small. A more accurate result for the tunneling coefficient without any asymptotic expansion can be obtained by use of Airy functions[13]:

$$T(E_z) = \frac{4K_F}{\pi k_z} \frac{1}{[\mathrm{Bi}(\eta_0) - (K_F/k_z)\mathrm{Ai}'(\eta_0)]^2 + [\mathrm{Ai}(\eta_0) + (K_F/k_z)\mathrm{Bi}'(\eta_0)]^2}, \quad (21)$$

where

$$k_z = (2m^* E_z/\hbar^2)^{1/2} \quad (22)$$

where η_0 is defined in (19), $\mathrm{Ai}(\eta_0)$ and $\mathrm{Bi}(\eta_0)$ are the Airy functions, and $\mathrm{Ai}'(\eta_0)$ and $\mathrm{Bi}'(\eta_0)$ are their derivatives with respect to the arguments. A numerical comparison of the two results using (18) and (21) is shown in Fig. 4 for a barrier height $V_0 = \Delta E_c = 0.254$ eV. It is clear that the results using the WKB method are good only if the condition $|\eta_0| \gg 1$ is valid. For energies E_z near the barrier height, which are important for our calculation of the tunneling-assisted impact ionization, the WKB method is not accurate since the prefactor in (18) goes to zero, while the more precise result shows a smooth transition. If one sets the prefactor equal to one as done by other researchers,[13,14] the dashed curve will shift to 1 at $E = V_0$, and will deviate more from the solid curve, which is obtained from the exact numerical approach, than the dashed line. Thus, we conclude that (21) should be used to incorporate the effect of the tunneling-assisted impact ionization.

Since the tunneling coefficient is a function of E_z only, we have

$$S(\hat{z}k_{1z}, \mathbf{k}_2) \simeq S(\hat{z}k_{1z}, \hat{z}k_{2z}) = \frac{m^*}{8\pi^2\hbar^2}\int_{k_{2z}}^{k_{1z}} dk_{1z}' \times \frac{T(E_{1z}')T(E_{2z}')}{[(k_{1z}-k_{1z}')(k_{1z}-k_{2z})+q^2]^2}, \quad (23)$$

where $T(E_{1z}')$ and $T(E_{2z}')$ are obtained from (21) and the range of integration is from k_{2z} to k_{1z}, i.e., over the whole spherical surface in Fig. 2, instead of from k_{th}' to $k_{1z} + k_{2z} - k_{th}'$ since the tunneling effect is taken into account in $T(E_{1z}')$ and $T(E_{2z}')$. The previous calculations without tunneling correspond to

$$T(E_{1z}') = \begin{cases} 1 & \text{if } E_{1z}' \geq \Delta E_c \\ 0 & \text{if } E_{1z}' < \Delta E_c \end{cases}, \quad (24)$$

and a similar expression holds for $T(E_{2z}')$. Thus, the results of impact ionization without tunneling will have threshold energies decided by (15), which are higher than that of the tunneling-assisted impact ionization since the transmission

coefficient differs significantly from zero even if E'_{1z} and $E'_{2z} < \Delta E_c$.

III. NUMERICAL RESULTS

Various effects of multiple subbands, the quantum-well width L_z, the band-edge discontinuity ΔE_c, and the doping concentration have been discussed in Ref. 8. We have used the 60–40% rule for the conduction- and valance-band-edge discontinuities.[15] The validity of our new analytical approximation in Eq. (12) has been presented in Fig. 3(a) and compared with the direct numerical integrations shown in Fig. 3(b) using Eq. (4). The results of the analytical formula in Fig. 3(a) do not show the fluctuations of the multiple numerical integrations in Fig. 3(b).

In Fig. 5, we show the ionization rate as a function of the incident electron energy E_0 measured from the conduction-band edge of the barrier region at the heterointerface with and without tunneling. The doping concentration N_D is 1×10^{17} cm^{-3} and only one subband is filled in this case. It can be seen that the threshold energy for impact ionization is reduced significantly when tunneling is included. The ionization rate is also enhanced especially at the low-energy end. When the energy of the incident electron is very high, the tunnelings of the final electrons 1′ and 2′ are not important which is expected, since they all have enough energy to get out of wells without tunneling assistance. In Fig. 6, we calculate the ionization coefficient α for a doping concentration $N_D = 7\times10^{18}$ cm^{-3} and assume the saturation velocity of the electrons $v_s = 1\times10^7$ cm/s. The ionization coefficient is obtained using $\alpha = \langle 1/\tau\rangle/v_s$. The electron temperature T_e versus the electric field F is obtained from the average energy by a Monte Carlo simulation and is roughly, e.g., $T_e = 4630$ K at $F = 100$ kV/cm; $T_e = 3860$ K at $F = 50$ kV/cm; and $T_e = 2300$ K at $F = 10$ kV/cm. The multiplication factor M_n for electrons as a function of the applied voltage V for a multiple-quantum-well structure of 50 periods is shown in Fig. 7. We assume a well size $L_z = 200$ Å, and a period

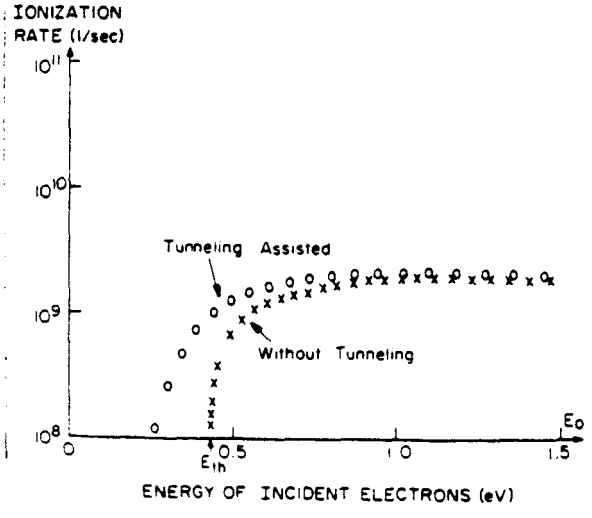

FIG. 5. The impact ionization rates $[1/\tau(E_0)]$ as functions of the incident electron energy with tunneling-assisted process (circles) and without tunneling (crosses) are compared.

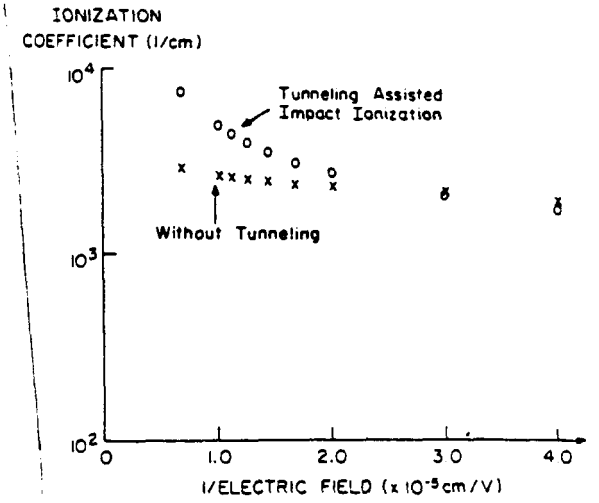

FIG. 6. The electron ionization coefficients α with and without tunneling assistance vs the reciprocal of the electric field are shown.

$L = 600$ Å. At this high-doping concentration, there are four occupied subbands. The average effective mass $m_b^* = 0.091\, m_0$ for the GaAs region is used to take care of the effect of the nonparabolicity.[8] We have $m_a^* = 0.083\, m_0$ in the $Al_xGa_{1-x}As$ region assuming the Al mole fraction $x = 0.25$. The conduction-band-edge discontinuity is $\Delta E_c = 0.187$ eV.

All the calculations are done assuming $T = 77$ K since the confinement of the carriers by the quantum wells will be better at low temperature. This dynamic storage of carriers[9] in the quantum wells is very crucial in the design of this device. According to Eqs. (4) and (12), the impact ionization can also be written as

$$\frac{1}{\tau(E_0)} = \sum_n \frac{N_n}{2}\frac{4\pi e^4}{\hbar\epsilon^2}\left(\frac{L_{zn}}{L}\right)^2 \times\left[S\left(\mathbf{k}_1, \hat{z}\,\frac{n\pi}{L_{zn}}\right) + S\left(\mathbf{k}_1, -\hat{z}\,\frac{n\pi}{L_{zn}}\right)\right], \qquad (25)$$

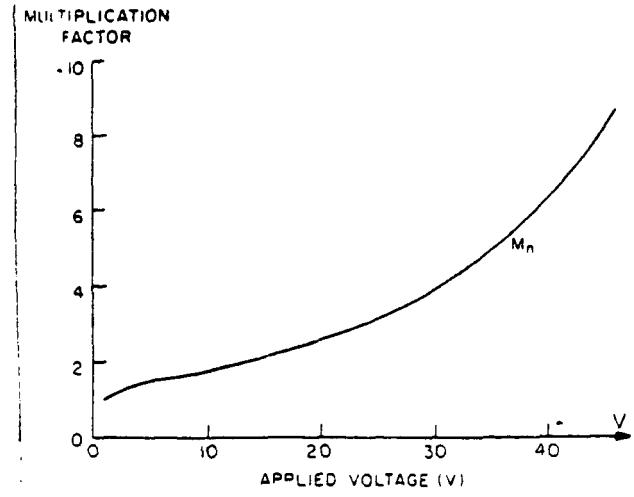

FIG. 7. The multiplication factor for electrons vs the applied voltage in a multiquantum-well structure with 50 periods is illustrated above.

i.e., the impact ionization rate due to electrons in each subband of the quantum well is proportional to the electron concentration in that subband. This is true provided that $S(\mathbf{k}_1,\mathbf{k}_2) \simeq S(\mathbf{k}_1,\hat{z}k_{2z})$, i.e., the transverse component $\mathbf{k}_{2t}$ is negligible in the S integrals. To increase the ionization rate, one either increases ΔE_c or increases L_z to have more electrons N_D stored in the wells. However, larger ΔE_c will increase the threshold energy, and larger L_z will decrease the energy of the confined electrons. Both tend to decrease the impact ionization rate. Thus, one needs to choose optimum parameters for ΔE_c, L_z, and doping concentration N_D for best performance of the device. The multiplication factor for electrons is calculated from

$$M_n = (1 + \alpha L)^N, \tag{26}$$

where the 1 accounts for the primary electrons, αL accounts for the secondary electrons and N is the number of periods. If the total length of the avalanche region is W, we have $W = NL$, and in the limit $N \to \infty$

$$M_n = \lim_{N \to \infty} [1 + \alpha(W/N)]^N = e^{\alpha W}, \tag{27}$$

which is the same as that of an ideal avalanche photodiode[16] with an avalanche region W. However, since L is finite, we use (26) instead of (27). The multiplication factor increases steadily or almost exponentially for this superlattice photomultiplier instead of increasing sharply at a certain reverse-biased voltage which would be the case for a two-carrier-type avalanche photodiode.[16]

IV. CONCLUSIONS

Tunneling-assisted impact ionization across the conduction-band-edge discontinuity has been investigated theoretically. An excellent analytical approximation has been found for electron-electron interactions between the incident free electrons and the bound two-dimensional electrons in the quantum wells. It is shown that the tunneling-assisted process lowers the threshold energy and enhances the ionization rate. The tunneling may increase the ionization coefficient by a factor of 2 or 3 depending on the electric field strength and the size of the quantum wells.

ACKNOWLEDGMENTS

This research is supported by the NASA grant NAG1-500 and the Joint Services Electronics Program.

[1] R. Chin, N. Holonyak, Jr., G. E. Stillman, J. Y. Tang, and K. Hess, Electron. Lett. **16**, 467 (1980).
[2] F. Capasso, *Physics of Avalanche Photodiodes in Semiconductors and Semimetals*, Vol. 22, series edited by R. K. Willardson and A. C. Beer, volume edited by W. T. Tsang (Academic, New York, 1985), Part D, Chap. 1.
[3] F. Capasso, W. T. Tsang and G. F. Williams, IEEE Trans. Electron Devices **ED-30**, 381 (1983).
[4] T. Tanoue and H. Sakaki, Appl. Phys. Lett. **41**, 67 (1982).
[5] R. J. McIntyre, IEEE Trans. Electron Devices **ED-13**, 164 (1966).
[6] R. J. McIntyre, IEEE Trans. Electron Devices **ED-19**, 703 (1972).
[7] G. E. Stillman, V. M. Robbins, and N. Tabatabaie, IEEE Trans. Electron Devices **ED-31**, 1643 (1984).
[8] S. L. Chuang and K. Hess, J. Appl. Phys. **59**, 2885 (1986).
[9] F. Capasso, J. Allam, A. Y. Cho, K. Mohammed, R. J. Malik, A. L. Hutchinson, and D. Sivco, Appl. Phys. Lett. **48**, 1294 (1986).
[10] L. V. Keldysh, Sov. Phys. JETP **34**, 665 (1958).
[11] A. S. Kyuregyan, Sov. Phys.-Semicond. **10**, 410 (1976).
[12] R. H. Fowler, and L. Nordheim, Proc. R. Soc. London Ser. A **119**, 173 (1928).
[13] C. B. Duke, *Tunneling in Solids* (Academic, New York, 1969), Chap. IV.
[14] S. M. Sze, *Physics of Semiconductor Devices*, second edition (Wiley, New York, 1981), Chap. 9.
[15] R. C. Miller, A. C. Gossard, D. A. Kleinman, and O. Munteanu, Phys. Rev. B **29**, 3740 (1984).
[16] P. P. Webb, R. J. McIntyre, and J. Conradi, RCA Rev. **35**, 235 (1974).

Appendix B

D. Ahn and S. L. Chuang, "Variational calculations of subbands in a quantum well with uniform electric field: Gram-Schmidt orthogonalization approach," Appl. Phys. Lett., vol. 49, pp. 1450-1452, 1986.

Variational calculations of subbands in a quantum well with uniform electric field: Gram–Schmidt orthogonalization approach

Doyeol Ahn and S. L. Chuang
Department of Electrical and Computer Engineering, University of Illinois at Urbana–Champaign, Urbana, Illinois 61801

(Received 14 August 1986; accepted for publication 30 September 1986)

We present variational calculations of subband eigenstates in an infinite quantum well with an applied electric field using Gram–Schmidt orthogonalized trial wave functions. The results agree very well with the exact numerical solutions even up to 1200 kV/cm. We also show that for increasing electric fields the energy of the ground state decreases, while that of higher subband states increases slightly up to 1000 kV/cm and then decreases for a well size of 100 Å.

Electronic as well as optical properties of quantum wells subject to external electric fields have received much attention.[1-9] These areas are interesting both from a fundamental and a practical point of view. The possible device applications include the use of quantum confined Stark effect[2] in optical modulators[8] and optical switching devices.[9] As yet, most of the theoretical works has been confined to the calculations of the ground state. Very recently, Matsuura and Kamizato[7] reported an exact numerical calculation of subbands in an infinite well and concluded that the higher subbands behave very differently from that for the ground state when the electric field strength is increased. Exact solutions employing two independent Airy functions[2,5] are sometimes too complicated to use in real problems. The variational approach has the advantage of providing analytical expressions for the eigenstate energies and the wave functions, and numerical results with reasonable accuracy can be obtained. Analytic form of the trial wave function for the ground states has been known,[1,2] but no useful forms of the trial solutions for the higher subbands which yield accurate results compared with the exact ones are given yet. Recently, a trial wave function of the form $f_n(z)\exp(-\beta_c z)$ for the nth subband has been suggested,[5] where $f_n(z)$ is the zero-field nth quantum well bound state wave function and β_c is a variational parameter. However, it is pointed out that the solutions may yield very different results from the exact ones (for $n > 1$) because these trial functions are not orthogonal to each other.[7] That observation is also confirmed in this paper and the numerical results are illustrated. Thus, it is important to find an orthogonalized set of trial wave functions for the variational calculations of subband energies and wave functions.

We report in this letter variational calculations on subband states in an external uniform electric field based on the infinite well model. We find analytic forms of orthogonalized trial wave functions by the Green–Schmidt orthogonalization procedure. Our calculations agree very well with exact numerical results up to 1200 kV/cm with an error less than 9% for $L = 100$ Å. For comparison, we also show the numerical results for which the trial wave functions are not orthogonalized.

It is well known that the variational method can also be used to obtain one of the higher energy levels if the function is orthogonal to the eigenfunctions of all the lower states.[10] The most common method of obtaining an orthogonal set of functions is the Gram–Schmidt orthogonalization procedure,[11] which is the construction of an orthonormal set $\{\phi_1,\phi_2,...\}$ from a finite or an infinite independent set $\{u_1,u_2,...\}$ which is not necessarily orthonormal.

Let us consider an electron with charge $-|e|$ and effective mass m^*, in an infinite quantum well width L in the presence of a constant electric field F along the positive direction of the well z. We choose the origin to be at the center of the well. The Hamiltonian of the system in the effective mass approximation is given by[1,2]

$$H = H_0 + |e|Fz\,, \tag{1}$$

where H_0 is the unperturbed Hamiltonian whose eigenvalues are given by

$$E_n^{(0)} = (\hbar^2\pi^2/2m^*L^2)n^2 \quad n = 1,2,... \tag{2}$$

For our specific problem, we chose the nth vector u_n to be

$$u_n(z) = \sin\left[\frac{n\pi}{L}\left(z+\frac{L}{2}\right)\right] \times \exp\left[-\beta_n\left(\frac{z}{L}+\frac{1}{2}\right)\right], \quad |z| < \frac{L}{2}, \tag{3}$$

which is not an orthogonal set, where β_n is the nth variational parameter. One can easily see that for $n = 1$, u_1 is the trial solution introduced by Bastard *et al.*[1] We also define the inner product between two functions f and g, $\langle f|g\rangle$, by

$$\langle f|g\rangle \equiv \int_{-L/2}^{L/2} f^*(z)g(z)dz\,, \tag{4}$$

where the superscript * denotes a complex conjugate.

The procedure we use is as follows:

$n = 1$, (i) Let $\psi_1 = u_1$. (5a)

(ii) Minimize $E_1(\beta_1) = \langle\psi_1|H|\psi_1\rangle/\langle\psi_1|\psi_1\rangle$, (5b)

and find β_1.

(iii) $\phi_1 = \psi_1/\langle\psi_1|\psi_1\rangle^{1/2}$. (5c)

$n = 2$, (i) Let $\psi_2 = u_2 - \langle u_2|\phi_1\rangle\phi_1$. (6a)

(ii) Minimize $E_2(\beta_2) = \langle\psi_2|H|\psi_2\rangle/\langle\psi_2|\psi_2\rangle$, (6b)

 0003-6951/86/471450-03$01.00

and find β_2.

(iii) $\phi_2 = \psi_2/\langle\psi_2|\psi_2\rangle^{1/2}$. (6c)

$n = l$, (i) Let $\psi_l = u_l - \sum_i^{l-1}\langle u_l|\phi_i\rangle\phi_i$. (7a)

(ii) Minimize $E_l(\beta_l) = \langle\psi_l|H|\psi_l\rangle/\langle\psi_l|\psi_l\rangle$, (7b)

and find β_l.

(iii) $\phi_l = \psi_l/\langle\psi_l|\psi_l\rangle^{1/2}$. (7c)

This procedure requires mainly three inner products which are in analytical forms:

$$\langle u_n|u_m\rangle = \frac{L}{2}(\beta_n+\beta_m)\left(\frac{1-(-1)^{n-m}\exp[-(\beta_n+\beta_m)]}{(n-m)^2\pi^2+(\beta_n+\beta_m)^2} - \frac{1-(-1)^{n+m}\exp[-(\beta_n+\beta_m)]}{(n+m)^2\pi^2+(\beta_n+\beta_m)^2}\right), \tag{8}$$

$$\langle u_n|H_0|u_m\rangle = \frac{1}{2}LE_1^{(0)}\left\{\left[(\beta_n+\beta_m)\left(m^2-\frac{\beta_m^2}{\pi^2}\right)+m\beta_m(n-m)\right]\frac{1-(-1)^{n-m}\exp[-(\beta_n+\beta_m)]}{(n-m)^2\pi^2+(\beta_n+\beta_m)^2}\right.$$
$$\left. -\left[(\beta_n+\beta_m)\left(m^2-\frac{\beta_m^2}{\pi^2}\right)-m\beta_m(n+m)\right]\frac{1-(-1)^{n+m}\exp[-(\beta_n+\beta_m)]}{(n+m)^2\pi^2+(\beta_n+\beta_m)^2}\right\}, \tag{9}$$

and

$$\langle u_n\left||e|Fz\right|u_m\rangle = \frac{1}{2}|e|FL^2\frac{1}{(n+m)^2\pi^2+(\beta_n+\beta_m)^2}\left[\left(1+\frac{\beta_n+\beta_m}{2}-\frac{2(\beta_n+\beta_m)^2}{(n+m)^2\pi^2+(\beta_n+\beta_m)^2}\right)\right.$$
$$\left.\times\{1-(-1)^{n+m}\exp[-(\beta_n+\beta_m)]\}+(\beta_n+\beta_m)(-1)^{n+m}\exp[-(\beta_n+\beta_m)]\right]$$
$$-\frac{1}{2}|e|FL^2\frac{1}{(n-m)^2\pi^2+(\beta_n+\beta_m)^2}\left[\left(1+\frac{\beta_n+\beta_m}{2}-\frac{2(\beta_n+\beta_m)^2}{(n-m)^2\pi^2+(\beta_n+\beta_m)^2}\right)\right.$$
$$\left.\times\{1-(-1)^{n-m}\exp[-(\beta_n+\beta_m)]\}+(\beta_n+\beta_m)(-1)^{n-m}\exp[-(\beta_n+\beta_m)]\right]. \tag{10}$$

The minimization of an analytical function and finding $\beta^{\min}$ can be directly done in the computer by calling some subroutines, e.g., using International Mathematical Statistical Libraries (IMSL) subroutines.

For the expectation value of the ground-state energy $E_1(\beta_1)$, we have

$$E_1(\beta_1) = \langle\phi_1|H|\phi_1\rangle$$
$$= E_1^{(0)}\left[\left(1+\frac{\beta_1^2}{\pi^2}\right)+\tilde{F}\left(\frac{1}{2\beta_1}+\frac{\beta_1}{\beta_1^2+\pi^2}-\frac{1}{2}\coth\beta_1\right)\right], \tag{11}$$

where the parameter $\tilde{F}$ is defined by

$$\tilde{F} = |e|FL/E_1^{(0)}, \tag{12}$$

which turns out to be the normalized electric field.[7]

In the low field limit, $\tilde{F} \ll 1$,

$$\beta_1^{\min} = \frac{1}{2}\tilde{F}\left(\frac{\pi^2}{6}-1\right) \tag{13}$$

and

$$\Delta E_1 \equiv E_1(\beta_1^{\min}) - E_1^{(0)} = -\frac{1}{8}\left(\frac{1}{3}-\frac{2}{\pi^2}\right)^2\frac{m^*e^2F^2L^4}{\hbar^2}. \tag{14}$$

In the high field limit, $\tilde{F} \gg 1$

$$\beta_1^{\min} = (\tfrac{1}{4}\pi^2\tilde{F})^{1/3} \tag{15}$$

and

$$\Delta E_1 = -\frac{1}{2}|e|FL + \left(\frac{3}{2}\right)^{5/3}\left(\frac{e^2F^2\hbar^2}{m^*}\right)^{1/3}. \tag{16}$$

Equations (11)–(16) have already been obtained by Bastard *et al.*[1] except they missed the factor of 1/2 in front of β in Eq. (7) and the expressions for $\beta_1^{\min}$ of Ref. 1 in the low and high field limits are not correct. This does not affect their final results for ΔE_1, which are correct. Calculations of higher energy levels are straightforward following the procedures in Eqs. (5)–(7). The results of the normalized energy $\tilde{E}_n = E_n/E_1^{(0)}$ for the first three states are plotted versus the normalized electric field $\tilde{F}$ in Fig. 1. The plot in terms of these two normalized parameters is universal which can be seen from the original Schrödinger wave equation.[7] It is readily seen that the shift of the subband energy due to the electric field is different between the $n = 1$ state and the higher energy states. For increasing electric fields, the ground state shows a large negative shift, while higher states have small positive shifts for fields up to $\tilde{F} \simeq 20$ and then negative shifts. We have also plotted the subband energies obtained from the exact numerical solution. We find that both methods of calculation give very close results, even up to $\tilde{F} = 25$. The parameters we use are $m^* = 0.065m_0$ and $L = 100$ Å where m_0 denotes the free-electron mass. $\tilde{F} = 10$ corresponds to 578.5 kV/cm for this L. The results of calculations employing unorthogonalized trial functions[5] defined

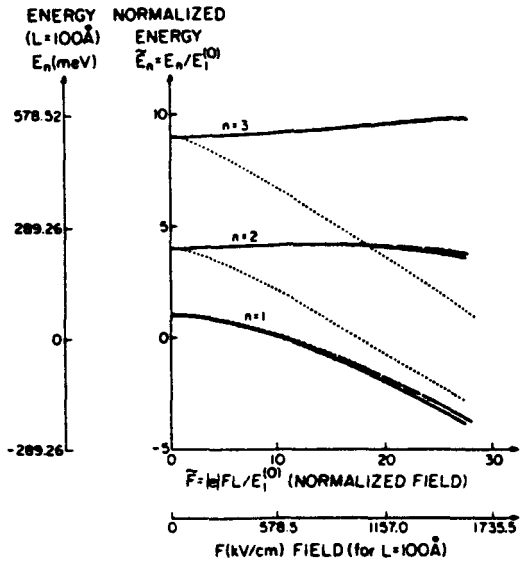

FIG. 1. Normalized subband energies ($\tilde{E}_n = E_n/E_1^{(0)}$) are plotted vs the normalized electric field ($\tilde{F} = |e|FL/E_1^{(0)}$). (1) The exact solution — (solid lines), (2) the variational method with Gram–Schmidt orthogonalization procedure ----- (dashed lines), (3) the variational method (see Ref. 5) without orthogonalization · · · · · (dotted lines).

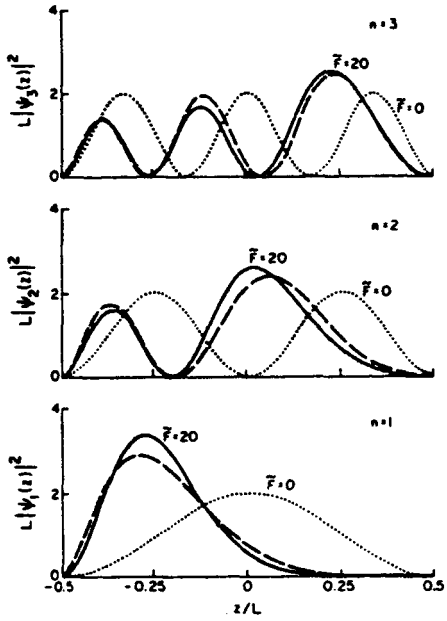

FIG. 2. Magnitudes of the wave functions, $L|\psi_n(z)|^2$, are plotted vs the normalized distance z/L for the first three subbands. The dotted lines are for the zero electric field. The solid lines are the exact solutions and the dashed lines are those for the variational method with the Gram–Schmidt orthogonalization procedure for a quantum well with an applied electric field ($\tilde{F} = 20$).

in Eq. (3) are plotted in Fig. 1 (dotted lines). One readily notices that these solutions begin deviating significantly from the exact ones at around $\tilde{F} = 1.5$ ($F = 86.8$ kV/cm for $L = 100$ Å). In Fig. 2 we plot the square of the wave functions $|\psi|^2$ for the first three states when the electric field is $\tilde{F} = 20$. $|\psi|^2$ is normalized to L. We see in Fig. 2 that the ground-state wave function is shifted to $z < 0$ region significantly, while higher subband wave functions still have a large amplitude in the $z > 0$ region even at $\tilde{F} = 20$.

In conclusion, we have derived orthogonalized trial wave functions which yield very close results to those of the exact numerical solutions. It is shown that for decreasing electric fields the energy of the lowest subband decreases, while that of the higher subbands increases slightly up to $\tilde{F} = 20$ ($F \gtrsim 1000$ kV/cm for $L = 100$ Å).

This work was partially supported by the NASA grant NAG 1-500 and the Air Force contract F33615-84-K-1557.

[1]G. Bastard, E. E. Mendez, L. L. Chang, and L. Esaki, Phys. Rev. B 28, 3241 (1983).
[2]D. A. B. Miller, D. S. Chemla, T. C. Damen, A. C. Gossard, W. Wiegmann, T. H. Wood, and C. A. Burrus, Phys. Rev. Lett. 53, 2173 (1984).
[3]E. J. Austin and M. Jaros, Phys. Rev. B 31, 5569 (1985).
[4]F. Borondo and J. Sánches-Dehesa, Phys. Rev. B 33, 8758 (1986).
[5]G. Bastard, Superlattice and Microstructure 1, 265 (1985).
[6]J. Singh, Appl. Phys. Lett. 48, 434 (1986).
[7]M. Matsuura and T. Kamizato, Phys. Rev. B 33, 8385 (1986).
[8]S. Tarucha and H. Okamoto, Appl. Phys. Lett. 48, 1 (1986).
[9]D. A. B. Miller, D. S. Chemla, T. C. Damen, T. H. Wood, C. A. Burrus, A. C. Gossard, and W. Wiegmann, IEEE J. Quantum Electron. 21, 1462 (1985).
[10]L. I. Schiff, *Quantum Mechanics* (McGraw-Hill, New York, 1968).
[11]I. Stakgold, *Boundary Value Problems of Mathematical Physics* (Collier-MacMillan, London, 1972), Vol. 1.

Appendix C

D. Ahn and S. L. Chuang, "Exact calculations of quasibound states of an isolated quantum well with uniform electric field: Quantum-well Stark resonance," Phys. Rev. B, vol. 34, PP.9034-9037, 1986.

PHYSICAL REVIEW B VOLUME 34, NUMBER 12 15 DECEMBER 1986

Exact calculations of quasibound states of an isolated quantum well with uniform electric field: Quantum-well Stark resonance

D. Ahn and S. L. Chuang
Department of Electrical and Computer Engineering, University of Illinois at Urbana-Champaign, Urbana, Illinois 61801
(Received 1 October 1986)

We present universal plots from exact numerical calculations for the energy level and the resonance width of quasibound states in a quantum well with an applied electric field (quantum-well Stark resonance) by solving the Schrödinger equation directly. This calculation gives both the resonance positions and widths for the complex eigenvalue $E_0 - i\Gamma/2$ of the system. Our theory also shows that the energy shifts of the ground states for the electrons and holes have the same behaviors in high fields without any turnaround phenomenon, contrary to the results of Austin and Jaros.

Electronic and optical properties of quantum wells with applied external electric fields are of increasing interest. Studies of these areas are important both from a fundamental and a practical point of view. Optical modulators[1] and optical switching devices[2] based on the quantum confined Stark effect have been suggested. Possible device applications of the field-induced tunneling in quantum-well and quantum-barrier heterostructures include high-speed resonant tunneling devices.[3-6]

More recent theoretical studies[7-9] of the effects of external electric fields on the quantum-well systems have predicted both the field-induced level shifts and the field dependence of the carrier lifetime. In this paper, we report exact numerical calculations on quasibound states of a quantum well in an external electric field (quantum-well Stark resonance) by solving the Schrödinger equation for Stark resonance directly. It is found that the previous results based on phase-shift analysis[7,9] and the stabilization method[8] agree very well with our results over a wide range of the electric field. At an extremely high electric field, there is no turnaround behavior in the energy shift for both the electrons and the holes, contrary to the results in Ref. 7, where no explanation can be provided for that phenomenon. We believe that our direct numerical approach is very reliable even at a very high electric field, while the results using the phase-shift analysis may have drawbacks in the high-field limit. Our approach has an advantage over the previous results[7-9] in that both the Stark resonance position (quasibound-state level) and the width can be obtained from the single complex energy eigenvalue of the quantum-well Stark resonance problem. The disadvantage is that numerical subroutines of the Airy functions with complex arguments are required.

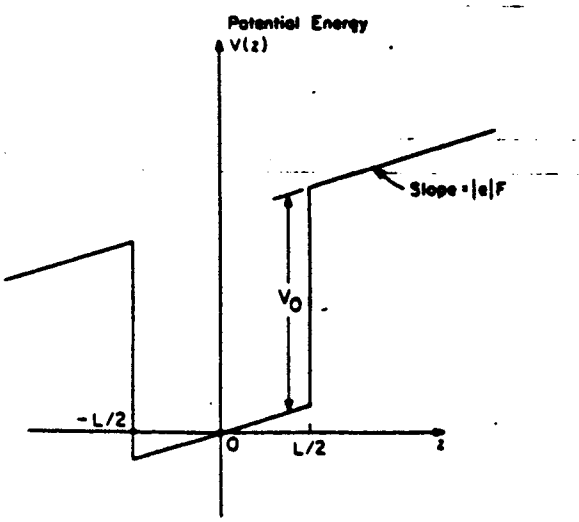

FIG. 1. Potential-energy profile $V(z)$ for a single quantum well with depth V_0 and width L subject to an external electric field F.

Consider an electron with charge $-|e|$ and effective mass m^*, in a finite quantum well of width L and depth V_0 in the presence of a constant electric field F along the positive direction of the well z (Fig. 1). We choose the origin to be at the center of the well. The Schrödinger equation of the system in the effective-mass approximation is given by[7,9]

$$\begin{aligned} &-\frac{\hbar^2}{2m^*}\frac{d^2}{dz^2}\psi(z)+|e|Fz\psi(z)=E\psi(z), \quad |z|\le L/2, \\ &-\frac{\hbar^2}{2m^*}\frac{d^2}{dz^2}\psi(z)+(V_0+|e|Fz)\psi(z)=E\psi(z), \\ &\qquad\qquad |z|>L/2. \end{aligned} \tag{1}$$

Since the potential energy term in Eq. (1) tends to $-\infty$ as z goes to $-\infty$, the system does not, strictly speaking, have true bound states.[7,10] In other words, the particle initially confined in a well can always lower its potential energy by tunneling out of the well when the field is not zero. It may happen, however, that the tunneling probability is very small. In such a case, we can regard the system as having quasibound states, in which the particles move "inside the well" for a considerable period of time and leave through tunneling only when a fairly long time interval τ has elapsed. In discussing the quasibound states, we may use the following formal method. Instead of considering the solutions of the Schrödinger equation with a boundary condition requiring the finiteness of the wave function at

infinity, we shall look for solutions which represent outgoing waves at infinity;[10] this implies that the particle finally leaves the well by tunneling. Since such a boundary condition is complex, we cannot assert that the eigenvalues (energy) must be real. By solving the Schrödinger equation, we obtain a set of complex eigenvalues, which we write in the form

$$E = E_0 - i\Gamma/2 , \tag{2}$$

where Γ is found to be positive. E_0 and Γ correspond to the quasibound-state energy level and the resonance width, respectively. The tunneling probability per unit time is defined by

$$\omega = \Gamma/\hbar . \tag{3}$$

The solutions to Eq. (1) with the outgoing-wave condition are linear combinations of two independent Airy functions[11]

$$\psi(z) = \begin{cases} a_1[\mathrm{Bi}(\eta_2) + i\,\mathrm{Ai}(\eta_2)], & z < -L/2, \\ a_0\mathrm{Ai}(\eta_1) + b_0\mathrm{Bi}(\eta_1), & |z| \le L/2, \\ a_2\mathrm{Ai}(\eta_2), & z > -L/2 , \end{cases} \tag{4}$$

with

$$\eta_1 = -\left[\frac{2m^*}{(e\hbar F)^2}\right]^{1/3}(E - |e|Fz) , \tag{5a}$$

and

$$\eta_2 = -\left[\frac{2m^*}{(e\hbar F)^2}\right]^{1/3}(E - V_0 - |e|Fz) . \tag{5b}$$

The wave function for $z < -L/2$ represents an electron traveling to $z = -\infty$ after tunneling. The complex energy E can be found by solving the secular equation obtained by matching the value of ψ and its first derivative at the points, $z = \pm L/2$. The resulting determinantal equation is

$$\det\begin{pmatrix} \mathrm{Ai}(\eta_1^+) & \mathrm{Bi}(\eta_1^+) & -\mathrm{Ai}(\eta_2^+) & 0 \\ \mathrm{Ai}'(\eta_1^+) & \mathrm{Bi}'(\eta_1^+) & -\mathrm{Ai}'(\eta_2^+) & 0 \\ \mathrm{Ai}(\eta_1^-) & \mathrm{Bi}(\eta_1^-) & 0 & -[\mathrm{Bi}(\eta_2^-) + i\,\mathrm{Ai}(\eta_2^-)] \\ \mathrm{Ai}'(\eta_1^-) & \mathrm{Bi}'(\eta_1^-) & 0 & -[\mathrm{Bi}'(\eta_2^-) + i\,\mathrm{Ai}'(\eta_2^-)] \end{pmatrix} = 0 , \tag{6}$$

where $\eta_1^\pm$ and $\eta_2^\pm$ are the values of η_1 and η_2 evaluated at $z = L/2$ and $-L/2$, respectively. If we introduce a new parameter $E^{(0)}$ defined by

$$E^{(0)} = \frac{\hbar^2}{2m^*}\left(\frac{\pi}{L}\right)^2 \tag{7}$$

(which happens to be the ground-state energy of an infinite quantum well with width L), and define the normalized energy $\tilde{E} = E/E^{(0)}$, the normalized electric field $\tilde{F} = |e|FL/E^{(0)}$, and the normalized well depth $\tilde{V}_0 = V_0/E^{(0)}$, we may express $\eta_1^\pm$ and $\eta_2^\pm$ by these three normalized quantities: $\tilde{E}$, $\tilde{F}$, and $\tilde{V}_0$.

$$\eta_1^\pm = -\left[\frac{\pi^2}{\tilde{F}^2}\right]^{1/3}(\tilde{E} \mp \tfrac{1}{2}\tilde{F}) , \tag{8a}$$

$$\eta_2^\pm = -\left[\frac{\pi}{\tilde{F}^2}\right]^{1/3}(\tilde{E} - \tilde{V}_0 \mp \tfrac{1}{2}\tilde{F}) . \tag{8b}$$

TABLE I. Comparison of the numerical results for $E_0 - i\Gamma/2$ using the exact numerical method of this paper, the phase-shift analysis (Refs. 7 and 9), and the stabilization method (Ref. 8).

F(kV/cm)		This paper (eV)	Phase-shift analysis (eV)	Stabilization method (eV)
75	E_0	0.025167	0.025167	0.025167
	Γ	1.86×10^{-6}	1.9×10^{-6}	8.6×10^{-6}
100	E_0	0.0242107	0.0242105	0.0242106
	Γ	3.64×10^{-5}	3.6×10^{-5}	4.1×10^{-5}
150	E_0	0.0213716	0.0213816	0.021170
	Γ	6.41×10^{-4}	6.4×10^{-4}	6.5×10^{-4}

This means that the solution of $\tilde{E}$ from Eq. (6) is universal and can be used for both electrons and holes with the replacement of the parameter $E^{(0)}$ with their corresponding effective masses.[12] (Here the effective masses inside and outside the well are assumed to be equal.) The normalized energy $\tilde{E}$ can be expressed in terms of only two normalized parameters, $\tilde{V}_0$ and $\tilde{F}$. Thus it is clear that both electrons and holes should have the same behaviors in their energy shift and the resonance width. To obtain the results of E_0

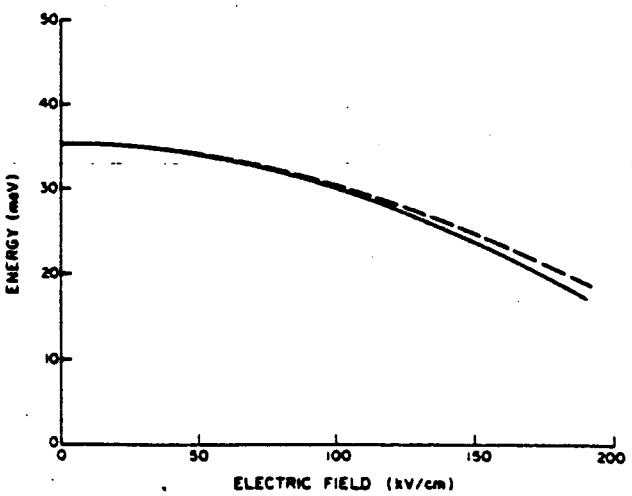

FIG. 2. Comparison of the ground-state energy of the variational calculation (Refs. 13 and 15) for infinite-well with appropriate effective-well width (dashed line) and the real part of the energy eigenvalue E_0 from exact calculation (solid line) of this paper.

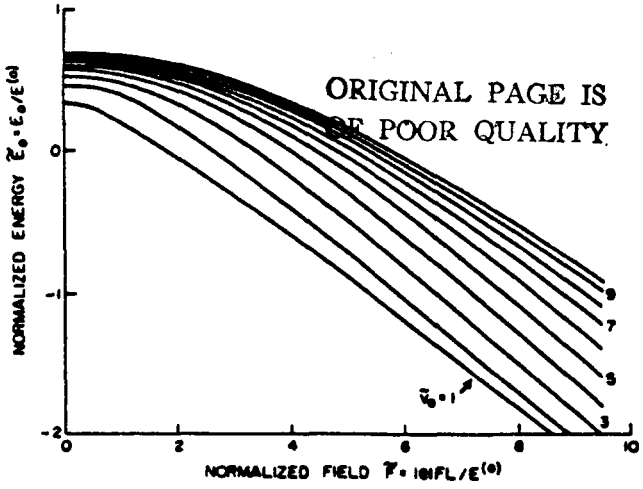

FIG. 3. The real part of the normalized energy $\tilde{E}_0 = E_0/E^{(0)}$ for various normalized well depths $V_0 = V_0/E^{(0)}$ is plotted vs the normalized electric field $\tilde{F} = |e|FL/E^{(0)}$.

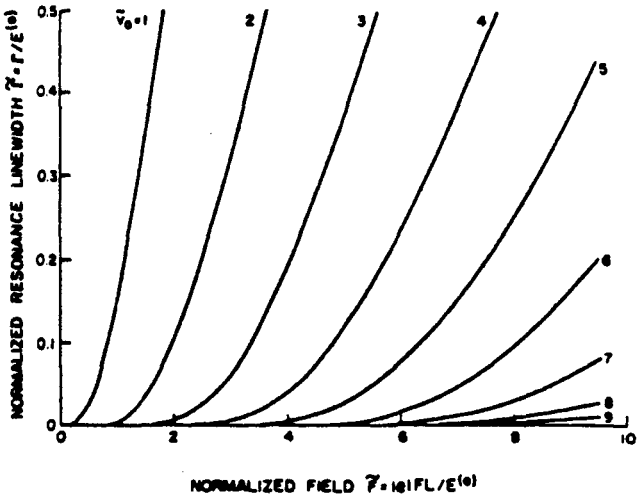

FIG. 4. The normalized resonance width $\tilde{\Gamma} = \Gamma/E^{(0)}$ for various $\tilde{V}_0$ is plotted vs normalized electric field $\tilde{F} = |e|FL/E^{(0)}$.

and Γ for holes, one need only multiply $\tilde{E}$ by E_0 using the effective mass of the hole. We have solved Eq. (6) numerically to the desired accuracy using the series and asymptotic expansions of the Airy functions with complex arguments.[11] To check the validity of our approach, we compared our results with those of the previous methods[7,8] in Table I. The values of V_0, L, and m^* for the heavy holes used in the calculations are, respectively,

$$V_0 = 100 \text{ meV}, \ L = 37 \text{ Å}, \ m^* = 0.45 m_0 , \tag{9}$$

where m_0 is the free-electron mass. It is readily seen that our results agree very well with those of the phase-shift analysis[7,9] and the stabilization method.[8]

In Fig. 2, the real part of the energy E_0 (resonance position–solid line) for the ground-state energy with the values of V_0, L, and m^* for electrons given by $V_0 = 340$ meV, $L = 100$ Å, and $m^* = 0.0665 m_0$ is compared with the results of infinite-well variational calculations[13–15] (dashed lines), where we have used an effective well width $L_{\text{eff}} = 126.5$ Å, chosen to give the same E_0 at zero field for the variational calculations. It can be easily noticed that both calculations gave very similar results even up to 2×10^5 V/cm. However, the variational calculation for the infinite-well model cannot give the resonance width since no tunneling exists for the infinite well. The results of the normalized resonance energy $\tilde{E}_0 = E_0/E^{(0)}$ for various $\tilde{V}_0$ are plotted versus $\tilde{F}$ in Fig. 3. In contrast to the previous results[7] which are still controversial, the resonance position is found to be in the well even at very high field. The behaviors of the resonant position are the same for both electrons and holes with proper $E^{(0)}$ used together with Fig. 3 as discussed before. Thus the turnaround behavior for the holes and electrons in the energy shift shown in Ref. 7 is probably a drawback of that method itself. Using the same numerical values for holes as those in Ref. 7, $L = 30$ Å, $V_0 = 70$ meV, $m^* = 0.45 m_0$, we obtain $E^{(0)} = 92.26$ meV, $\tilde{V}_0 = 0.76$. We do not have any turnaround behavior even up to $\tilde{F} = 10$, or the electric field $F = 3075$ kV/cm, which covers a much wider range of electric field than that of Ref. 7. In Fig. 4, we plot the normalized resonance width $\tilde{\Gamma} = \Gamma/E^{(0)}$ for various $\tilde{V}_0$ vs $\tilde{F}$. Since the lifetime τ is defined by $\tau = \hbar/\Gamma$, the results plotted in Fig. 4 predict a rapid decrease of the carrier lifetime with increasing applied field by field enhanced tunneling.

In conclusion, we have solved the Schrödinger equation for a quantum well with uniform electric field directly. Complex eigenvalues for quantum-well Stark resonance are obtained. Our approach has an advantage over previous analyses[7–9] in that both the resonance position and width can be obtained from a single complex eigenvalue of the problem.

This work was partially supported by the Air Force, Contract No. F33615-84-K-1557 and the NASA Grant No. NAG 1-500. One of the authors (D.A.) would like to acknowledge the support of GTE.

[1] E. Tarucha and H. Okamoto, Appl. Phys. Lett. 48, 1 (1986).
[2] D. A. B. Miller, D. S. Chemla, T. C. Damen, T. H. Wood, C. A. Burrus, A. C. Gossard, and W. Wiegmann, IEEE J. Quantum Electron. 21, 1462 (1985).
[3] R. Tsu and L. Esaki, Appl. Phys. Lett. 22, 562 (1973).
[4] A. R. Bonnefoi, D. H. Chow, and T. C. McGill, Appl. Phys. Lett. 47, 886 (1985).
[5] F. Capasso, K. Mohammed, and A. Y. Cho, IEEE J. Quantum Electron. 22, 1853 (1986).
[6] Y. Nakata, M. Asada, and Y. Suematsu, IEEE J. Quantum Electron. 22, 1880 (1986).
[7] E. J. Austin and M. Jaros, Phys. Rev. B 31, 5569 (1985).
[8] F. Borondo and J. Sánches-Dehesa, Phys. Rev. B 33, 8758 (1986).

[9]E. J. Austin and M. Jaros, Appl. Phys. Lett. 47, 274 (1985).
[10]L. D. Landau and E. M. Lifshitz, *Quantum Mechanics —Nonrelativistic Theory* (Pergamon, New York, 1981), pp. 555–560.
[11]*Handbook of Mathematical Functions*, edited by M. Abramowitz and I. A. Stegun (National Bureau of Standards, Washington, DC, 1964), pp. 446–452.
[12]M. Matsuura and T. Kamizato, Phys. Rev. B 33, 8385 (1986).
[13]G. Bastard, E. E. Mendez, L. L. Chang, and L. Esaki, Phys. Rev. B 28, 3241 (1983).
[14]D. A. B. Miller, D. S. Chemla, T. C. Damen, A. C. Gossard, W. Wiegmann, T. H. Wood, and C. A. Burrus, Phys. Rev. Lett. 53, 2173 (1984).
[15]D. Ahn and S. L. Chuang, Appl. Phys. Lett. 49, 1450 (1986).

Appendix D

D. Ahn and S. L. Chuang, "Intersubband optical absorption in a quantum well with applied electric field," Phys. Rev. B, accepted for publication.

INTRASUBBAND OPTICAL ABSORPTION IN A QUANTUM WELL WITH APPLIED ELECTRIC FIELD

D. Ahn and S. L. Chuang

Department of Electrical and Computer Engineering
University of Illinois at Urbana-Champaign
Urbana, IL 61801

Abstract

We present new results for the electric field dependence of the intrasubband optical absorption within the conduction band of a quantum well. We show that for increasing electric field the absorption peak corresponding to the transition of states $1 \rightarrow 2$ is shifted higher in energy and the peak amplitude is increased. These features are different from those of the exiton absorption. It is also found that the forbidden transition for states $1 \rightarrow 3$ when $F = 0$ is possible when F is nonzero.

Quantum confinement of carriers in a semiconductor quantum well leads to the formation of discrete energy levels and the drastic change of optical absorption spectra.[1] The interband absorptions near the band gap have been extensively studied, and it has been shown that their absorption and luminescence spectra are dominated by excitonic effects.[2, 3] Some more recent studies have concentrated on the electric field dependence of energy levels[4-7] and band edge optical absorption including the exciton effect.[8-10] Very recently, the experimental studies of the intrasubband absorption within the conduction band of a GaAs quantum well without the applied electric field have been reported[11]. A very large dipole strength and a narrow band width were observed. In this paper, we present the theoretical calculations for the electric field dependence of the optical absorption between the discrete subbands within the conduction band of a quantum well based on the infinite potential barrier model. One of the reasons for increased interest in this area is the possibility of practical device application. For example, in 1970, Kazarinov and Suris[12] proposed a new type of infrared laser amplifier using the intrasubband transition and resonant tunneling. Far-infrared photodetector with high wavelength selectivity based on the intrasubband absorption and the sequential resonant tunneling has also been suggested.[13]

The Hamiltonian of the system (for a single quantum well) subject to a uniform electric field perpendicular to the quantum well (the z-direction) in the presence of an optical radiation (Fig. 1) is written as

$$H = H_o + H'_{op} , \qquad (1)$$

where H_o is the unperturbed Hamiltonian for an electron in the quantum well in the presence of perpendicular electric field, and the interaction Hamiltonian H'_{op} is given by[14]

$$H'_{op} = -\frac{e}{m_o}\vec{A}\cdot\vec{p}$$

$$= -\frac{e}{2m_o}A_0\left[e^{i\vec{q}\cdot\vec{r} - i\omega t} + c.c\right]\hat{\varepsilon}\cdot\vec{p} \qquad (2)$$

where $\vec{A}$ is the vector potential, $\hat{\varepsilon}$ is the polarization vector, and $\vec{q}$ is the wave vector for incoming optical radiation, e is the magnitude of the charge of the electron, m_o is the free space electron mass, and $\vec{p}$ is the momentum vector of the electron in the crystal. The first term in (2) gives the absorption, H'^{abs}_{op}, and the second term gives the emission of photon.

Then, for a given interaction potential H'_{op}, the transition rate from the initial state ψ_i to the final state ψ_f for the absorption is given by[14]

$$W_{fi} = \frac{2\pi}{\hbar}\left| < \psi_f \left| H'^{abs}_{op} \right| \psi_i > \right|^2 \delta\left(E_f - E_i - \hbar\omega\right) \qquad (3)$$

where E_i and E_f are the energies of the electron in the initial state and the final state, respectively and ω is the angular frequency of the incident photon. If we neglect the interaction between the electrons in the well, the wave functions for the initial state ψ_i and the final state ψ_f after absorption can be written as[15]

$$\psi_i = u_c(\vec{r})\,\xi_i(\vec{r})$$

$$= A^{-1/2}\,u_c(\vec{r})\,e^{i\vec{k}_t\cdot\vec{r}_t}\,\phi_i(z), \qquad |z| < \frac{L}{2} \qquad (4a)$$

and

$$\psi_f = u_{c'}(\vec{r})\,\xi_f(\vec{r})$$
$$= A^{-1/2}\,u_{c'}(\vec{r})\,e^{i\vec{k}'_t\cdot\vec{r}_t}\,\phi_f(z), \qquad |z| < \frac{L}{2} \tag{4b}$$

where A is the area of the well, L is the width of the well, $\vec{k}_t$, $\vec{k}'_t$ are the wave vectors of the electron in the x-y plane for the initial and the final states, respectively, $\vec{r}_t$ is the position vector in the x-y plane, and u_c and $u_{c'}$ are the cell periodic functions near the conduction band extremum. The envelope functions ϕ_i and ϕ_f satisfy the following Schrödinger's equation in the effective mass approximation,[5, 7]

$$-\frac{\hbar^2}{2m^*}\frac{d^2}{dz^2}\phi(z) + |e|\,Fz\,\phi(z) = E\,\phi(z), \quad |z| \leq \frac{L}{2}\ , \tag{5}$$

and are given by the linear combination of two independent Airy functions Ai(η) and Bi(η), where η is defined by

$$\eta = -\left[\frac{2m^*}{(e\hbar F)^2}\right]^{1/3}(E - |e|\,Fz) \tag{6}$$

In Eqs. (5) and (6), m^* and F denote the effective mass of an electron and the electric field, respectively.

For intrasubband transitions, the matrix element $\langle\psi_f\,|H'^{abs}_{op}|\,\psi_i\rangle$ can be approximated by[16]

$$\langle \psi_f \,|H_{op}^{'abs}|\, \psi_i \rangle \approx \langle \xi_f \,|H_{op}^{'abs}|\, \xi_i \rangle$$

$$= -\frac{eA_o}{2m_o} \langle \xi_f | e^{i\vec{q}\cdot\vec{r}}\, \hat{e}\cdot\vec{p} | \xi_i \rangle$$

$$\approx -\frac{eA_o}{2m_o}\, \hat{e} \cdot \langle \xi_f \,|\vec{p}|\, \xi_i \rangle \qquad (7)$$

$$= -\frac{eA_o}{2i\hbar} (E_i - E_f)\, \hat{e} \cdot \langle \xi_f \,|\vec{r}|\, \xi_i \rangle,$$

where the portion of the cell periodic function has been taken care of following ref. 16, and we have used the dipole approximation. Since $\int_{-L/2}^{L/2} \phi_f^*(z)\, \phi_i(z)\, dz = \delta_{fi}$, we find that the major contribution to the optical matrix element is the z-component of the $\vec{r}$ vector. So the absorption is strongly polarization dependent. The absorption constant α in the well is defined as[17]

$$\alpha = \hbar\omega \frac{\text{number of transitions per unit volume per unit time}}{\text{incident power per unit area}}$$

$$= \frac{1}{V} \sum_i \sum_f \sum_{\vec{k}_t} \sum_{\vec{k}_t'} \frac{\hbar\omega W_{fi}}{\left(\frac{n_r \omega^2 A_o^2}{2\mu c}\right)} \qquad (8)$$

where the summations over i and f are for the quantized initial and final energies respectively for the z-components of the momenta. If we calculate the total transition rate and take into account the line broadening[14], we obtain

$$\alpha = \sum_{if}\sum \frac{\mu c m^* k_B T e^2}{\pi \hbar^2 m_0^2 L n_r \omega} \cos^2\theta \; |M_{fi}|^2 \; \ell n \left[\frac{1+\exp\left(\frac{E_F - E_i^{(z)}}{k_B T}\right)}{1+\exp\left(\frac{E_F - E_f^{(z)}}{k_B T}\right)} \right] \frac{(\Gamma/2)}{(\hbar\omega - E_{fi})^2 + (\Gamma/2)^2} \quad (9)$$

with the matrix element

$$M_{fi} = \frac{m_o (E_i^{(z)} - E_f^{(z)})}{i\hbar} \int_{-L/2}^{L/2} \phi^*_f(z) \; z \; \phi_i(z) \; dz \quad (10)$$

where $E_{fi} = E_f^{(z)} - E_i^{(z)}$, and $E_i^{(z)}$ and $E_f^{(z)}$ denote the quantized energy levels for the initial state and final state, respectively, μ is the permeability, c is the speed of light in free space, k_B is the Boltzmann constant, T is the temperature, θ is the angle between the polarization vector and the normal to the quantum well, n_r is the refractive index, E_F is the Fermi energy which depends on the density of electrons in the well, and Γ is the line width.

The oscillator strength f is given by[11],

$$f = \frac{2m_o (E_f^{(z)} - E_i^{(z)})}{\hbar^2} \langle z \rangle^2$$

$$= \frac{2|M_{fi}|^2}{\hbar m_o (E_f^{(z)} - E_i^{(z)})} \quad (11)$$

In the zero field limit, f = 14.45 for the 1 → 2 transition, which is independent of the width of the well for the infinite potential well model. The experimental result[11] of f for L = 65 Å (or L_{eff} = 101.27 Å) is 12.2 and slightly depends on the well width.

We calculated α for the first three states with field dependence numerically for T = 300 K. In Fig. 2, we plot the absorption coefficient α for the incident photon with polarization perpendicular to the well (θ = 0) taking into account the first three states as a function of the energy of the photon with F = 0 (dashed line) and F = 250 kV/cm (solid line) for an effective well width 101.27 Å, which gives the same ground state energy for F = 0 with the true well width L = 65 Å and the barrier height ΔE_c = 245 meV.[11] We use E_F = 6.49 meV which corresponds to about $2.5 \times 10^{17}/cm^3$ electrons and Γ = 10 meV from the experimental results[11] and is assumed to be independent for the variation of F. One can easily see that the transition 1 → 2 is dominant for both electric fields F = 0 and 250 kV/cm. For F = 250 kV/cm the absorption peak is shifted by 16 meV from 165 meV to 181 meV and the peak amplitude is increased from 315.3 cm^{-1} to 461.9 cm^{-1}. There are two distinct features for the case of the intrasubband absorption compared with the exciton absorption.[9]

(i) The absorption peak for intrasubband optical absorption is increased in energy with increasing electric field over a wide range of the electric field, because for increasing electric fields the energy of the ground state decreases rapidly, while those of the higher subband states increase slightly then decrease slowly as cited in Ref. 6. On the other hand, for the exciton absorption, both the ground states of the electrons and the holes decreases. Thus the absorption peak is decreased in energy with increasing electric field.

(ii) The absorption peak for intrasubband optical absorption is increased in magnitude with increasing electric field because the electrons

are shifted to the same side of the well for both the initial and the final states with increasing electric field, and the energy difference $E_2 - E_1$ also increases for the reason mentioned in (i). As a result, the absolute value of the overlap integral M_{fi} for $1 \rightarrow 2$ transition increases. While for the exciton absorption, increasing electric field causes further separation of electrons and holes in the well and the decrease of the energy difference between the electron and the hole ground states. Thus, the decrease of the absolute value of the overlap integral.[4]

It is also remarkable that the forbidden transition $1 \rightarrow 3$ for $F = 0$ becomes possible when F is nonzero because the parity which prohibits the transition $1 \rightarrow 3$ no longer exists when F is nonzero. In Fig. 3 we plot $(M_{fi}/M_{fi}^{(0)})^2$ as a function of F for the $1 \rightarrow 2$ transition, where $M_{fi}^{(0)}$ is the value of M_{fi} for the $1 \rightarrow 2$ transition with $F = 0$. One can easily see as expected that the ratio increases slightly from 1 as F increases. In our calculation, we assume Γ is constant, however, to account for the effect of the electric field on the absorption completely, further analysis of the electric field dependence of the line broadening is desired.

In conclusion, we have calculated the electric field dependence of the intrasubband absorption within a conduction band of a quantum well. It is found that the absorption peak is shifted in energy and is also increased in magnitude with increasing electric field. The forbidden transition $1 \rightarrow 3$ when $F = 0$ becomes allowable for the nonzero electric field.

This work was partially supported by the NASA Grant No. NAG 1-500 and the Air Force Contract No. F33615-84-K-1557. D. Ahn would also like to thank GTE for financial support.

References

[1] R. Dingle, W. Wiegmann, and C. H. Henry, Phys. Rev. Lett. 33, 827 (1974).

[2] C. Weisbuch, R. C. Miller, R. Dingle, A. C. Gossard, and W. Wiegmann, Solid State Commun. 37, 219 (1981).

[3] J. S. Weiner, D. S. Chemla, D. A. B. Miller, T. H. Wood, D. Sivco, and A. Y. Cho, Appl. Phys. Lett. 46, 619 (1985).

[4] G. Bastard, E. E. Mendez, L. L. Chang, and L. Esaki, Phys. Rev. B28, 3241 (1983).

[5] E. J. Austin and M. Jaros, Phys. Rev. B31, 5569 (1985).

[6] D. Ahn and S. L. Chuang, Appl. Phys. Lett. 49, (1986).

[7] D. Ahn and S. L. Chuang, Phys. Rev B. 34, (1986).

[8] D. A. B. Miller, D. S. Chemla, T. C. Damen, A. C. Gossard, W. Wiegmann, T. H. Wood, and C. A. Burrus, Phys. Rev. Lett. 53, 2173 (1984).

[9] D. A. B. Miller, D. S. Chemla, T. C. Damen, A. C. Gossard, W. Wiegmann, T. H. Wood, and C. A. Burrus, Phys. Rev. B32, 1043 (1985).

[10] Y. C. Chang and J. N. Schulman, Phys. Rev. B31, 2069 (1985).

[11] L. C. West and S. J. Eglash, Appl. Phys. Lett. 46, 1156 (1985).

[12] R. F. Kazarinov and R. A. Suris, Sov. Phys. - semicond 5, 707 (1971).

[13] F. Capasso, K. Mohammed, and A. Y. Cho, IEEE J. Quantum Electron. 22, 1853 (1986).

[14] W. Heitler, The Quantum Theory of Radiation (Dover, New York, 1984).

[15] C. Kittel, Quantum Theory of Solids (John Wiley & Sons, New York, 1963) pp. 286 -290.

[16] D. D. Coon and R. P. G. Karunasiri, Appl. Phys. Lett. 45, 649 (1984).

[17] A. Yariv, Quantum Electronics (John Wiley & Sons, New York, 1975) pp. 222-227.

Figure Captions

Fig. 1. Potential energy profile for an infinite quantum well with width L subject to an external electric field F in the presence of incoming radiation with angular frequency $\hbar\omega$.

Fig. 2. Comparison of the intrasubband absorption coefficient α for infinite well with L = 101.27 Å for the first three states with electron density $2.5 \times 10^{17}/cm^3$ electrons for the zero electric field (dashed line) and for the electric field of 250 kV/cm (solid line).

Fig. 3. The normalized overlap integral $|M_{21}/M_{21}^{(0)}|^2$, where $M_{21}^{(0)}$ is for the zero electric field, is plotted versus electric field F.

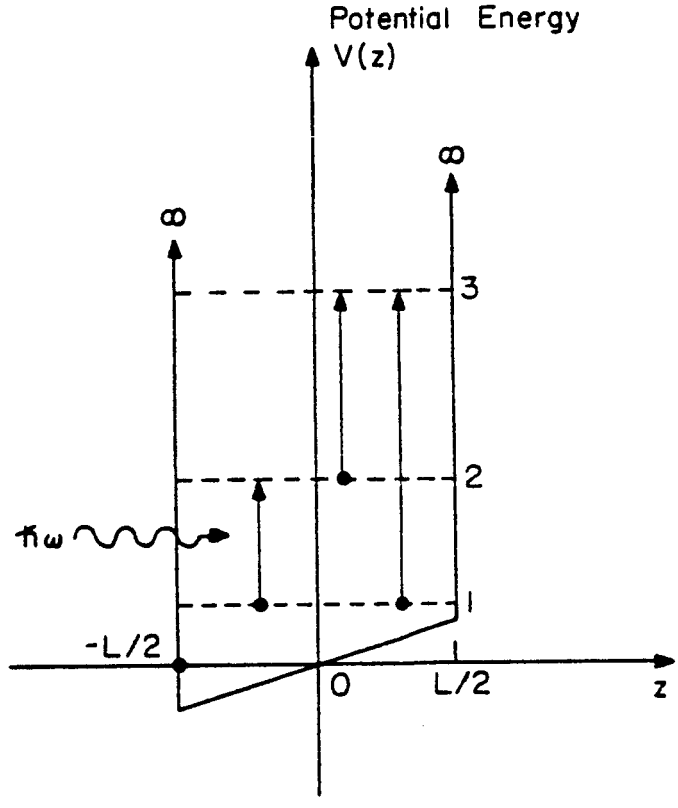

Fig. 1

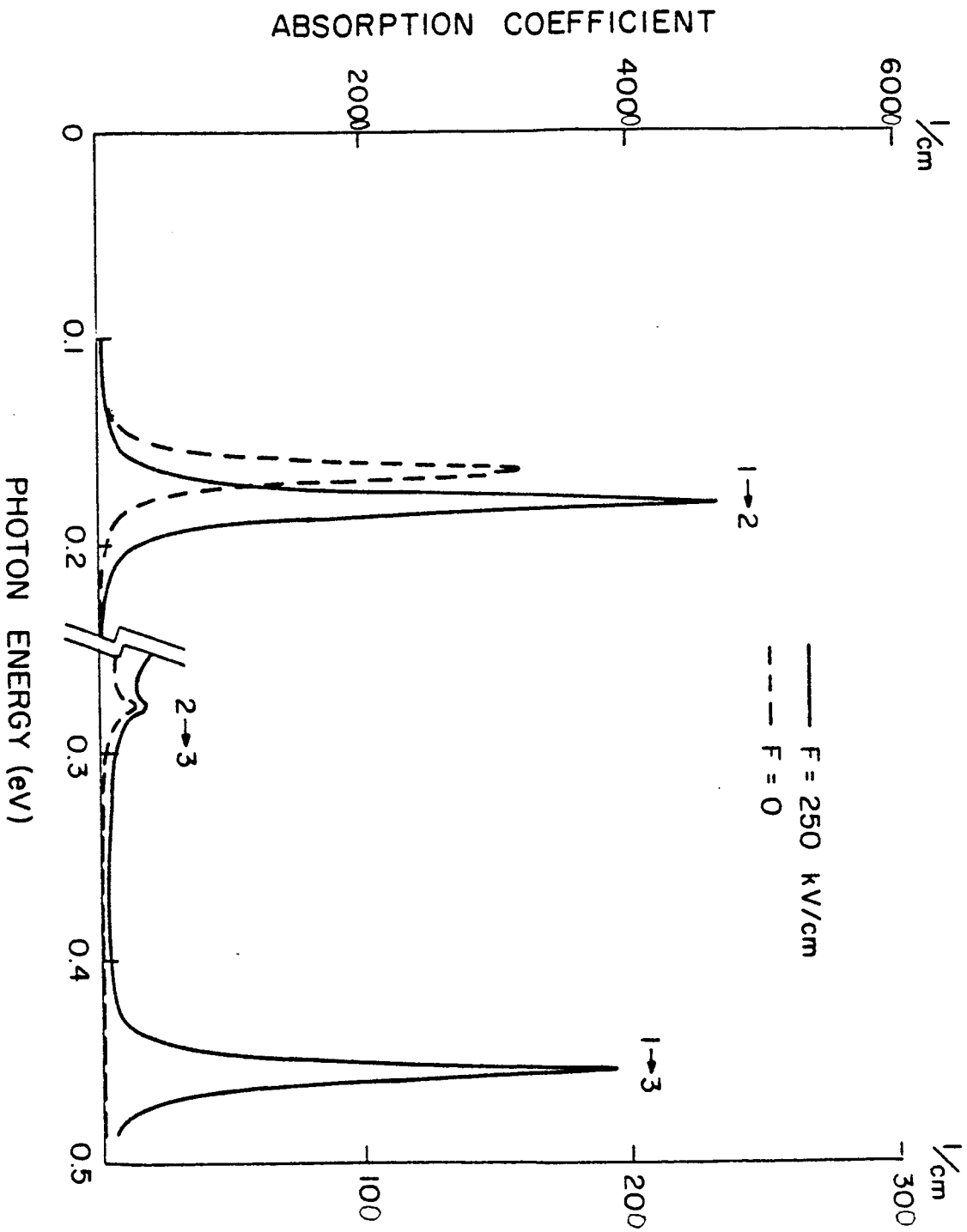
ABSORPTION COEFFICIENT
2000
4000
6000
1/cm
0
0.1
0.2
0.3
0.4
0.5
PHOTON ENERGY (eV)
1→2
2→3
1→3
F = 250 kV/cm
F = 0
100
200
300
1/cm

Fig. 2

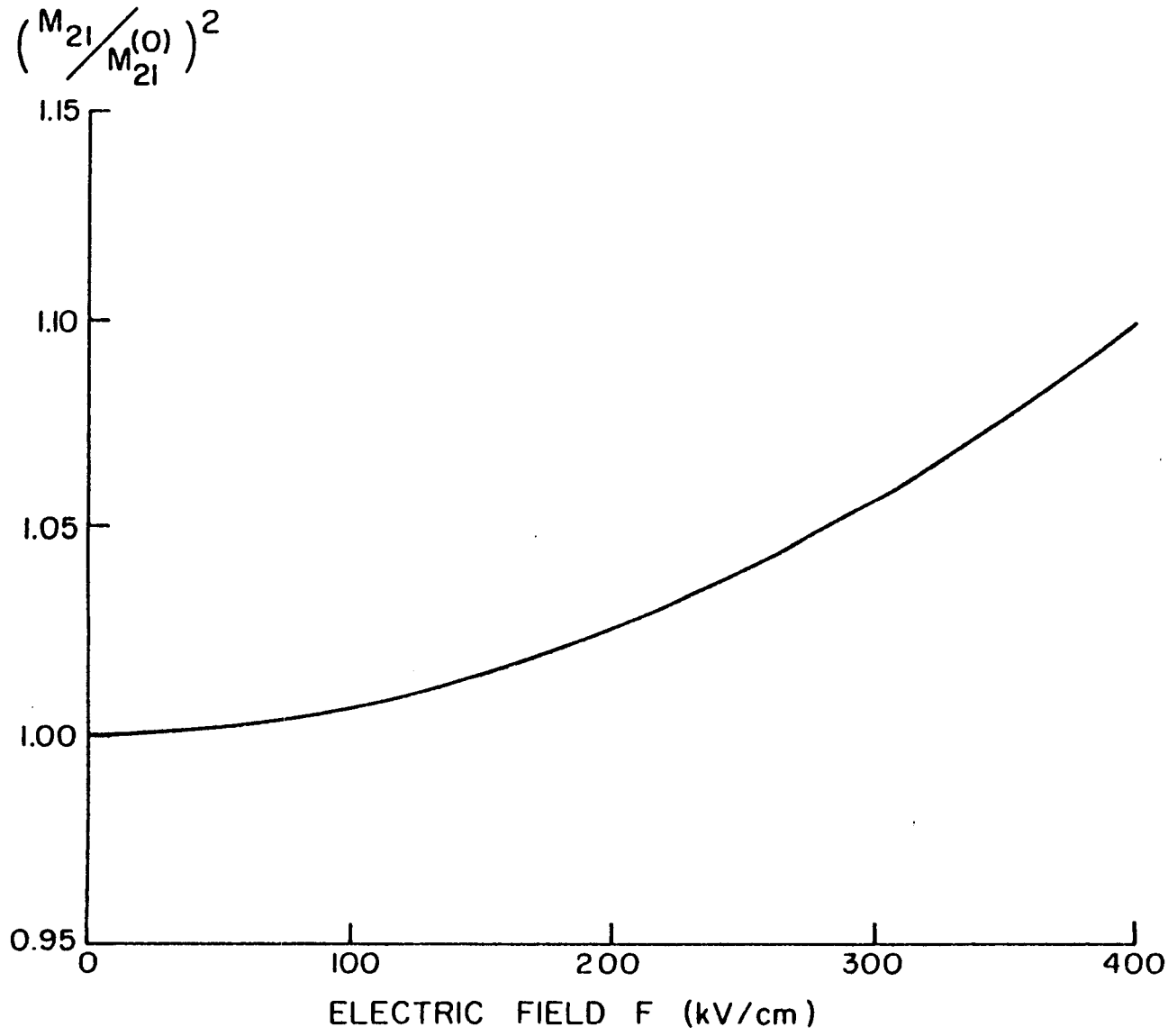
$\left(M_{21}/M_{21}^{(0)}\right)^2$
1.15
1.10
1.05
1.00
0.95
0
100
200
300
400
ELECTRIC FIELD F (kV/cm)

Fig. 3

Appendix E

S. L. Chuang, "A coupled-mode formulation by reciprocity and a variational principle," IEEE J. Lightwave Technology, vol. LT-5, pp.5-15, 1987.

A Coupled Mode Formulation by Reciprocity and a Variational Principle

SHUN-LIEN CHUANG, MEMBER, IEEE

Abstract—A coupled mode formulation for parallel dielectric waveguides is presented via two methods: a reciprocity theorem and a variational principle. In the first method, a generalized reciprocity relation for two sets of field solutions $(E^{(1)}, H^{(1)})$ and $(E^{(2)}, H^{(2)})$ satisfying Maxwell's equations and the boundary conditions in two different media $\epsilon^{(1)}(x, y)$ and $\epsilon^{(2)}(x, y)$, respectively, is derived. Based on the generalized reciprocity theorem, we then formulate the coupled mode equations. The second method using a variational principle is also presented for a general waveguide system which can be lossy. The results of the variational principle can also be shown to be identical to those from the reciprocity theorem. The exact relations governing the "conventional" and the new coupling coefficients are derived. It is shown analytically that our formulation satisfies the reciprocity theorem and power conservation exactly, while the conventional theory violates the power conservation and reciprocity theorem by as much as 55 percent and the Hardy-Streifer theory by 0.033 percent, for example.

I. Introduction

THE COUPLED mode theory has been very useful in the fields of integrated optics, semiconductor laser arrays or microstrip coupled transmission lines. A "conventional" coupled mode theory usually makes use of a perturbation theory to calculate the coupling coefficients [1], [2]. It has been recognized that a simple power conservation argument for the powers in individual waveguides leads to the fact that the two coupling coefficients K_{ab} and K_{ba} are complex conjugate of each other, which is generally not true if the guides are not identical [3]. A more rigorous approach has been recently proposed and very good numerical results have also been presented [3]–[5]. However, there is still considerable ambiguity about the reciprocity and the power conservation in the coupled mode theory. One knows that both the reciprocity relation and the power conservation are the two basic laws which must be obeyed and they are usually used in electromagnetics as necessary conditions to check the numerical accuracy [6], [7] of the results. The reciprocity relation is applied to the fileds and is applicable to a lossy medium. Thus, most results derived from the reciprocity relations do not contain any complex conjugate quantities. If the medium is lossless, the complex conjugate of the permittivity ϵ^* equals to ϵ itself, one then applies the conjugate fields to the reciprocity relation. On the other hand, the power conservation deals with the power and, thus, the complex conjugate quantities are usually used.

Manuscript received April 11, 1986; revised June 4, 1986. This work was partially supported by NASA grant NAG 1-500.

The author is with the Department of Electrical and Computer Engineering, university of Illinois at Urbana-Champaign, Urbana, IL 61801.

IEEE Log Number 8611065.

The goal of this paper is to present new coupled mode equations and analytical relations for the coupling coefficients which follow the reciprocity theorem in a general lossy medium, and then the power conservation law if the medium becomes lossless. This new formulation removes the slight discrepancies of the power conservation encountered in a previous theory presented in [3], [5]. The analytical relation governing the coupling coefficients K_{ab} and K_{ba} is derived from a reciprocity relation for the fields instead of the power conservation law for the intensity. Thus, it is also applicable to any lossy (or gain) waveguide system.

The general reciprocity relation and the derivation of the new coupled mode equations are presented in Section II-A. A variational principle for a general lossy or lossless medium is presented in Section II-B while a previous method is limited to a lossless system [8]. We show that our formulation using the variational principle is identical to that of the formulation based on the reciprocity relation. In Section III, we derive the relation between the coupling coefficients and the propagation constants used in the coupled-mode equations. Note that this derivation is independent of the procedure in which one calculates those coupling coefficients and the propagation constants. We also show that the coupling coefficients and the propagation constants derived in Section II-A and Section II-B for the coupled mode equations do satisfy the reciprocity relation analytically. For a lossless case, the power conservation relation is derived from the reciprocity relation also. Finally, we present some numerical results and compare them with those of the previous theories. It is also demonstrated that an error of 55 percent in the power conservation using a previous theory [2] can occur unless the overlap integrals C_{pq} are taken into account properly. An error of 0.033 percent occurs using the Hardy-Streifer theory [3]–[5]. It is noted that the Hardy-Streifer theory, the theory of Haus *et al.* [8], and the present one give numerical results almost indistinguishable on the plots of propagation constants and coupling coefficients for the examples considered so far, although slight differences exist among the three theories.

II. Formulation

A. Coupled Mode Theory from a Generalized Reciprocity Theorem

In this section, we present a "generalized" reciprocity theorem for two sets of solutions $(E^{(1)}, H^{(1)})$ and $(E^{(2)},$

0733-8724/87/0100-0005$01.00 © 1987 IEEE

$H^{(2)}$) to Maxwell's equations in *two* media $\epsilon^{(1)}$ and $\epsilon^{(2)}$ respectively. Based on the generalized reciprocity theorem, we show by choosing various $\epsilon^{(1)}$ and $\epsilon^{(2)}$, and their corresponding field solutions, two exact relations for the conventional coupling coefficients K_{ab} and K_{ba} for two waveguides a and b can be derived in Cases A1 and A2. We then derive the coupled-mode equations in Cases A3 and A4. A different approach using the variational principle for waveguide systems will be presented in Section II-B, and identical results of the two approaches are also illustrated.

1. A Generalized Reciprocity Theorem for Two Media $\epsilon^{(1)}(x, y)$ and $\epsilon^{(2)}(x, y)$: Consider the first two Maxwell's equations in a medium $\epsilon^{(1)}(x, y)$

$$\nabla \times \boldsymbol{E}^{(1)} = i\omega\mu \boldsymbol{H}^{(1)} \tag{1a}$$

$$\nabla \times \boldsymbol{H}^{(1)} = -i\omega\epsilon^{(1)} \boldsymbol{E}^{(1)} \tag{1b}$$

where the fields $(\boldsymbol{E}^{(1)}, \boldsymbol{H}^{(1)})$ satisfy all the Maxwell's equations and the boundary conditions in the medium $\epsilon^{(1)}(x, y)$. For a different medium $\epsilon^{(2)}(x, y)$, the fields $(\boldsymbol{E}^{(2)}, \boldsymbol{H}^{(2)})$ satisfy a similar set of equations and also the boundary conditions in $\epsilon^{(2)}$. Following similar procedures for the Lorentz reciprocity theorem, we obtain

$$\nabla \cdot (\boldsymbol{E}^{(1)} \times \boldsymbol{H}^{(2)} - \boldsymbol{E}^{(2)} \times \boldsymbol{H}^{(1)}) = i\omega(\epsilon^{(2)} - \epsilon^{(1)}) \boldsymbol{E}^{(1)} \cdot \boldsymbol{E}^{(2)}. \tag{2}$$

If we apply the above relation to an infinitesimal section Δz of a cylindrical geometry which is translational invariant in the z direction, we obtain

$$\frac{\partial}{\partial z} \iint (\boldsymbol{E}^{(1)} \times \boldsymbol{H}^{(2)} - \boldsymbol{E}^{(2)} \times \boldsymbol{H}^{(1)}) \cdot \hat{z}\, dx\, dy = i\omega \iint (\epsilon^{(2)}(x, y) - \epsilon^{(1)}(x, y)) \boldsymbol{E}^{(1)} \cdot \boldsymbol{E}^{(2)}\, dx\, dy \tag{3}$$

where the divergence theorem has been used. A similar equation using the polarization vector has been derived before [1]. However, our interpretation using $\epsilon^{(2)}$ and $\epsilon^{(1)}$ instead of the polarization vector is slightly different and will be shown to be very useful. We note that the above relations are *exact* as long as the fields $(\boldsymbol{E}^{(1)}, \boldsymbol{H}^{(1)})$ satisfy the Maxwell equations and all the boundary conditions in the medium $\epsilon^{(1)}(x, y)$ and $(\boldsymbol{E}^{(2)}, \boldsymbol{H}^{(2)})$ in the medium $\epsilon^{(2)}(x, y)$, respectively. The above reciprocity relation is applicable to any two reciprocal media and is exact, while most reciprocity relations are applied to only one reciprocal medium with a polarization vector introduced and approximated using a perturbation approach. The advantage of using the above exact relation will be shown in the next few cases when applied to a coupled-waveguide system. The time convention $\exp(-i\omega t)$ will be adopted in this paper.

Case A1: We choose first

$$\epsilon^{(1)}(x, y) = \epsilon^{(a)}(x, y) \tag{4}$$

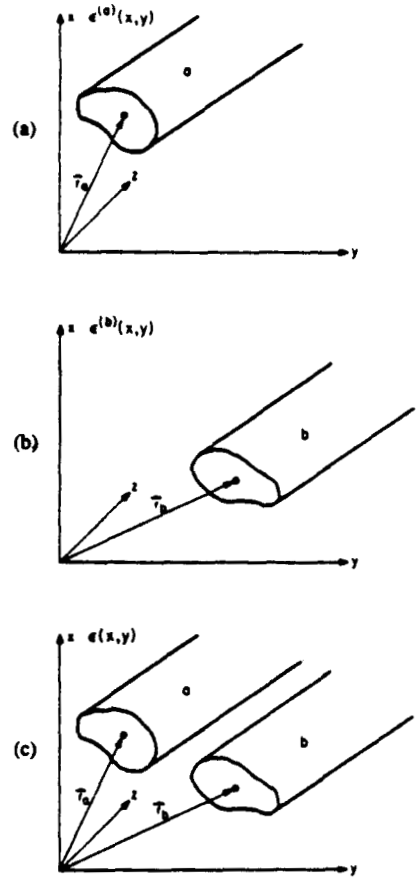

Fig. 1. Schematic diagrams for various media under consideration: (a) $\epsilon^{(a)}(x, y)$ with a single waveguide a. (b) $\epsilon^{(b)}(x, y)$ with a single waveguide b. (c) $\epsilon(x, y)$ with both waveguides a and b.

where $\epsilon^{(a)}(x, y)$ is a single waveguide a as shown in Fig. 1(a), and we choose the solutions to be a guided mode propagating in the $+z$ direction

$$\boldsymbol{E}^{(1)} = \boldsymbol{E}^{(a)+}(x, y)\, e^{i\beta_a z} = (\boldsymbol{E}_t^{(a)} + \hat{z}E_z^{(a)})\, e^{i\beta_a z} \tag{5a}$$

$$\boldsymbol{H}^{(1)} = \boldsymbol{H}^{(a)+}(x, y)\, e^{i\beta_a z} = (\boldsymbol{H}_t^{(a)} + \hat{z}H_z^{(a)})\, e^{i\beta_a z}. \tag{5b}$$

We then choose

$$\epsilon^{(2)}(x, y) = \epsilon^{(b)}(x, y) \tag{6}$$

and

$$\boldsymbol{E}^{(2)} = \boldsymbol{E}^{(b)-}(x, y)\, e^{-i\beta_b z} = (\boldsymbol{E}_t^{(b)} - \hat{z}E_z^{(b)})\, e^{-i\beta_b z} \tag{7a}$$

$$\boldsymbol{H}^{(2)} = \boldsymbol{H}^{(b)-}(x, y)\, e^{-i\beta_b z} = (-\boldsymbol{H}_t^{(b)} + \hat{z}H_z^{(b)})\, e^{-i\beta_b z} \tag{7b}$$

which are the guided modes propagating in the $-z$ direction for another waveguide b as shown in Fig. 1(b). Substituting the above two sets of solutions into the reciprocity relation (3), we obtain

$$\bar{K}_{ba} - \bar{K}_{ab} = \tfrac{1}{2}(C_{ab} + C_{ba})(\beta_b - \beta_a) \tag{8}$$

where

$$\bar{K}_{pq} = \frac{\omega}{4} \int_{-\infty}^{\infty}\int \Delta\epsilon^{(q)}(E_t^{(p)} \cdot E_t^{(q)} - E_z^{(p)}E_z^{(q)})\, dx\, dy \tag{9}$$

$$C_{pq} = \frac{1}{2} \int_{-\infty}^{\infty}\int E_t^{(q)} \times H_t^{(p)} \cdot \hat{z}\, dx\, dy \tag{10}$$

and

$$\Delta\epsilon^{(q)}(x, y) = \epsilon(x, y) - \epsilon^{(q)}(x, y),\ q = a, b \tag{11}$$

which are defined almost identically to those used in [3] except a constant factor of 4. The choice of the background $\epsilon(x, y)$ is not unique (in general). Here, it is chosen to be the coupled waveguide system (Fig. 1(c)) for convenience. One notes that $\bar{K}_{pq}$'s are the "conventional" coupling coefficients except for the z components in the last term of the integrand [2]. Note that Equation (8) is an exact relation as long as the field solutions for each waveguide system $\epsilon^{(a)}(x, y)$ and $\epsilon^{(b)}(x, y)$ are exact. For a slab waveguide structure, the exact solutions are known and the identity (8) can also be proved analytically since all the quantities $\bar{K}_{pq}$ and $\bar{C}_{pq}$ can be derived. That proof is mathematically laborious but straightforward, and will not be shown here. Equation (8) is also a very useful relation in checking the numerical accuracies of the "coupling coefficients" in the computer program. One sees clearly that in general $\bar{K}_{ba} \neq \bar{K}_{ab}$ when $\beta_b \neq \beta_a$. Equation (8) shows the precise relation that the difference between the coupling coefficients is equal to the difference between the two propagation constants multiplied by the average of the overlap integrals C_{ab} and C_{ba}. In the limit of extremely weak coupling C_{ab}, $C_{ba} \ll 1$, we have $\bar{K}_{ba} = \bar{K}_{ab}$, which is the reciprocity relation under the very weak coupling condition in a conventional analysis.

Case A2: We choose

$$\epsilon^{(1)}(x, y) = \epsilon^{(a)}(x, y) \tag{12}$$

$$E^{(1)} = E^{(a)+}(x, y)\, e^{i\beta_a z} \tag{13a}$$

$$H^{(1)} = H^{(a)+}(x, y)\, e^{i\beta_a z} \tag{13b}$$

and

$$\epsilon^{(2)}(x, y) = \epsilon^{(b)}(x, y) \tag{14}$$

$$E^{(2)} = E^{(b)+}(x, y)\, e^{i\beta_b z} \tag{15a}$$

$$H^{(2)} = H^{(b)+}(x, y)\, e^{i\beta_b z}. \tag{15b}$$

Both fields are propagating in the $+z$ direction. We obtain from (3)

$$(\bar{K}_{ba}^t + \bar{K}_{ba}^z) - (\bar{K}_{ab}^t + \bar{K}_{ab}^z) = \tfrac{1}{2}(C_{ba} - C_{ab})(\beta_b + \beta_a) \tag{16}$$

where

$$\bar{K}_{pq}^t = \frac{\omega}{4} \int\int \Delta\epsilon^{(q)} E_t^{(p)} \cdot E_t^{(q)}\, dx\, dy \tag{17a}$$

and

$$\bar{K}_{pq}^z = \frac{\omega}{4} \int\int \Delta\epsilon^{(q)} E_z^{(p)} E_z^{(q)}\, dx\, dy. \tag{17b}$$

Note from (9):

$$\bar{K}_{pq} = \bar{K}_{pq}^t - \bar{K}_{pq}^z. \tag{17c}$$

(If only TE modes are excited, we have $E_z^{(p)} = 0$, $p = a$, b; thus, $\bar{K}_{pq}^z = 0$. Equations (8) and (16) will lead to $C_{ba}\beta_a = C_{ab}\beta_b$.) In general, relations between $\bar{K}_{ab}^t$ and $\bar{K}_{ba}^t$, or $\bar{K}_{ab}^z$ and $\bar{K}_{ba}^z$ can also be derived from (8) and (16). In the following cases, we apply the reciprocity relation to the coupled waveguide medium $\epsilon(x, y)$ as shown in Fig. 1(c), and derive the new coupled mode equations.

Case A3: We choose

$$\epsilon^{(1)}(x, y) = \epsilon(x, y) \tag{18}$$

and

$$E_t^{(1)} \simeq a(z)\, E_t^{(a)+}(x, y) + b(z)\, E_t^{(b)+}(x, y) \tag{19a}$$

$$H_t^{(1)} \simeq a(z)\, H_t^{(a)+}(x, y) + b(z)\, H_t^{(b)+}(x, y) \tag{19b}$$

for the transverse components. The above relations are just the modal expansions in terms of the two guided modes in waveguides a and b. We also note that the above expansion is only an approximate set of solutions to the Maxwell equations in the coupled-waveguide medium $\epsilon(x, y)$ and the radiation mode has been neglected. Both waveguides a and b are assumed to support only a single TE (or TM) mode. The extension to a multiple mode waveguide is straightforward by including a summation over all the guided modes in each waveguide. The longitudinal components of the fields follow from Maxwell's equations for the waveguides

$$E_z^{(1)} \simeq a(z)\frac{\epsilon^{(a)}}{\epsilon} E_z^{(a)}(x, y) + b(z)\frac{\epsilon^{(b)}}{\epsilon} E_z^{(b)}(x, y) \tag{20a}$$

$$H_z^{(1)} \simeq a(z)H_z^{(a)}(x, y) + b(z)H_z^{(b)}(x, y). \tag{20b}$$

A derivation of the above two components in (20a) and (20b) is given in Appendix A. A similar relation has been given for the z-component of the polarization vector in [1], and used in [3]–[5]. The factors $\epsilon^{(a)}/\epsilon$ and $\epsilon^{(b)}/\epsilon$ in (20a) have been ignored in [8]. We think they should be kept for consistency with the Maxwell equations as shown in Appendix A.

For the second set of solutions, we choose the medium for a single waveguide a

$$\epsilon^{(2)}(x, y) = \epsilon^{(a)}(x, y) \tag{21}$$

and the guided mode solutions in the $-z$ direction

$$E^{(2)} = E^{(a)-}(x, y)\, e^{-i\beta_a z} \tag{22a}$$

$$H^{(2)} = H^{(a)-}(x, y)\, e^{-i\beta_a z}. \tag{22b}$$

We obtain from (3)

$$\frac{da(z)}{dz} + \frac{C_{ab} + C_{ba}}{2}\frac{db(z)}{dz} = i(\beta_a + \bar{K}_{aa})\, a(z) + i\left(\beta_a \frac{C_{ab} + C_{ba}}{2} + \bar{K}_{ba}\right) b(z) \tag{23}$$

where

$$\bar{K}_{pq} = \frac{\omega}{4}\iint \Delta\epsilon^{(q)}(E_t^{(p)} \cdot E_t^{(q)} - \frac{\epsilon^{(p)}}{\epsilon} E_z^{(p)} E_z^{(q)})\, dx\, dy. \tag{24}$$

To keep the same convention as in $\overline{K}_{pq}$, the order p, q for the definition of $\bar{K}_{pq}$ is reversed from that in [3], and for later use. It is straightforward to show that $\bar{K}_{pq}$ satisfies the same relation (8) as $\overline{K}_{pq}$ by observing that

$$\bar{K}_{pq} = \overline{K}_{pq} + \frac{\omega}{4}\iint \Delta\epsilon^{(q)} \frac{\Delta\epsilon^{(p)}}{\epsilon} E_z^{(p)} E_z^{(q)}\, dx\, dy \tag{25}$$

where the second term is symmetrical when we exchange p and q. Thus.

$$\bar{K}_{pq} - \bar{K}_{qp} = \overline{K}_{pq} - \overline{K}_{qp} = \tfrac{1}{2}(C_{pq} + C_{qp})(\beta_p - \beta_q) \tag{26}$$

which are exact relations.

Case A4: We choose

$$\epsilon^{(1)}(x, y) = \epsilon(x, y)$$

and $(E_t^{(1)}, H_t^{(1)})$ and $(E_z^{(1)}, H_z^{(1)})$ to be the same as in the first set of solutions (19)–(20) in Case A3. We use for the second set of solutions

$$\epsilon^{(2)}(x, y) = \epsilon^{(b)}(x, y) \tag{27}$$

$$E^{(2)} = E^{(b)-}(x, y)\, e^{-i\beta_b z} \tag{28a}$$

$$H^{(2)} = H^{(b)-}(x, y)\, e^{-i\beta_b z}. \tag{28b}$$

We obtain again from (3)

$$\frac{C_{ab} + C_{ba}}{2}\frac{da(z)}{dz} + \frac{db(z)}{dz} = i\left(\beta_b \frac{C_{ab} + C_{ba}}{2} + \bar{K}_{ab}\right) a(z) + i(\beta_b + \bar{K}_{bb})\, b(z). \tag{29}$$

2. *Coupled Mode Equations:* Based on the results in Cases A3 and A4, we obtain the coupled mode equations

$$\overline{C}\frac{d}{dz}\begin{bmatrix} a(z) \\ b(z) \end{bmatrix} = iS\begin{bmatrix} a(z) \\ b(z) \end{bmatrix} \tag{30}$$

where the matrix elements for $\overline{C}$ and S are

$$\overline{C}_{pq} = \overline{C}_{qp} = \frac{C_{pq} + C_{qp}}{2}$$

where

$$p, q = a, b \text{ (or } 1, 2) \tag{31}$$

$$S_{pq} = \bar{K}_{qp} + \beta_p\left(\frac{C_{pq} + C_{qp}}{2}\right) \tag{32a}$$

$$= \bar{K}_{pq} + \overline{C}_{pq}\beta_q \tag{32b}$$

and where C_{pq} and $\bar{K}_{pq}$ are defined in (10) and (24), respectively, and (26) has been used in (32). We note that $\overline{C}_{11} = \overline{C}_{22} = C_{11} = C_{22} = 1$, and the matrix $\overline{C}$ is symmetric. The matrix S_{pq} is obviously symmetric following (32).

Let

$$\bar{c} = \frac{C_{ab} + C_{ba}}{2}.$$

We invert the matrix $\overline{C}$ and obtain the coupled mode equations

$$\frac{da}{dz} = i\gamma_a a + iK_{ab} b \tag{33a}$$

$$\frac{db}{dz} = i\gamma_b b + iK_{ba} a \tag{33b}$$

where

$$\gamma_a = \beta_a + [\bar{K}_{aa} + (\beta_a - \beta_b)\bar{c}^2 - \bar{K}_{ab}\bar{c}]/(1 - \bar{c}^2)$$
$$= \beta_a + [\bar{K}_{aa} - \bar{K}_{ba}\bar{c}]/(1 - \bar{c}^2) \tag{34a}$$

$$\gamma_b = \beta_b + [\bar{K}_{bb} + (\beta_b - \beta_a)\bar{c}^2 - \bar{K}_{ba}\bar{c}]/(1 - \bar{c}^2)$$
$$= \beta_b + [\bar{K}_{bb} - \bar{K}_{ab}\bar{c}]/(1 - \bar{c}^2) \tag{34b}$$

$$K_{ab} = [\bar{K}_{ba} + (\beta_a - \beta_b - \bar{K}_{bb})\bar{c}]/(1 - \bar{c}^2)$$
$$= (\bar{K}_{ab} - \bar{K}_{bb}\bar{c})/(1 - \bar{c}^2) \tag{34c}$$

$$K_{ba} = [\bar{K}_{ab} + (\beta_b - \beta_a - \bar{K}_{aa})\bar{c}]/(1 - \bar{c}^2)$$
$$= (\bar{K}_{ba} - \bar{K}_{aa}\bar{c})/(1 - \bar{c}^2) \tag{34d}$$

where the first form in each equation is to compare with that in [3], and the second form is simplified after making use of (26) or (32b). One should know that although the matrices $\overline{C}$ and S are both symmetric, $\overline{C}^{-1}S$ is not symmetric in general. That is, $K_{ab} \neq K_{ba}$, unless we have two identical waveguides. This does not violate the reciprocity theorem or the power conservation law as will be presented rigorously later.

B. Coupled Mode Theory From a Variational Principle Applicable to a Lossy Medium

Variational principle has been widely used to study the resonators, the waveguides or scattering from objects [9], [10]. A general variational formula for the propagation

constant γ of the coupled waveguide system $\epsilon(x, y)$ can be derived from two oppositely traveling modes of the system

$$\nabla_t \times E^+ - i\omega\mu H^+ = -i\gamma \hat{z} \times E^+ \tag{35a}$$

$$\nabla_t \times H^+ + i\omega\epsilon E^+ = -i\gamma \hat{z} \times H^+ \tag{35b}$$

$$\nabla_t \times E^- - i\omega\mu H^- = i\gamma \hat{z} \times E^- \tag{36a}$$

$$\nabla_t \times H^- + i\omega\epsilon E^- = i\gamma \hat{z} \times H^-. \tag{36b}$$

Dot multiplying (35a) by H^- and (35b) by E^-, and adding the results, we obtain

$$\gamma = \frac{\frac{1}{4i}\iint [E^- \cdot (\nabla_t \times H^+ + i\omega\epsilon E^+) + H^- \cdot (\nabla_t \times E^+ - i\omega\mu H^+)]\, dx\, dy}{\frac{1}{4}\iint (H^- \times E^+ + E^- \times H^+) \cdot \hat{z}\, dx\, dy} = \frac{N}{D} \tag{37}$$

where N and D denote, respectively, the numerator and the denominator in (37). A similar form to (37) has been derived in [8], [10]–[12], except that we keep H^-, E^+, etc., in the denominator which will be shown to be necessary in the following case.

It is straightforward to show that (37) is a variational formula for the propagation constant γ by taking the first variation in γ, $\delta\gamma$, from the trial fields

$$E^\pm = E_0^\pm + \delta E^\pm \tag{38a}$$

$$H^\pm = H_0^\pm + \delta H^\pm \tag{38b}$$

where $E_0^\pm$ and $H_0^\pm$ are assumed to be the exact solutions. That is, using (35) and (36) for $E_0^\pm$, $H_0^\pm$ and γ_0, one finds

$$\delta\gamma = \frac{1}{D_0}\left[\delta N - \frac{N_0}{D_0}\delta D\right] = \frac{1}{D_0}[\delta N - \gamma_0 \delta D] = 0 \tag{39}$$

where N_0 and D_0 are the expressions in (37) evaluated using $E_0^\pm$ and $H_0^\pm$. Thus any deviations of first order in $\delta E^\pm$ and $\delta H^\pm$ only result in errors of second order $(\delta E^\pm)^2$ and $(\delta H^\pm)^2$ in γ.

We choose the trial functions to be

$$E_t^+ \simeq a_1^+ E_t^{(a)+} + a_2^+ E_t^{(b)+} \tag{40a}$$

$$H_t^+ \simeq a_1^+ H_t^{(a)+} + a_2^+ H_t^{(b)+} \tag{40b}$$

for the transverse components of the fields propagating in the $+z$ direction. Here the subscript 1 refers to a, or waveguide a, and 2 for b for convenience. We also choose

$$E_t^- \simeq a_1^- E_t^{(a)-} + a_2^- E_t^{(b)-} \tag{41a}$$

$$H_t^- \simeq a_1^- H_t^{(a)-} + a_2^- H_t^{(b)-} \tag{41b}$$

for the transverse components of the fields propagating in the $-z$ direction. The longitudinal components are found to be (Appendix A):

$$E_z^\pm = a_1^\pm \frac{\epsilon^{(a)}}{\epsilon} E_z^{(a)\pm} + a_2^\pm \frac{\epsilon^{(b)}}{\epsilon} E_z^{(b)\pm} \tag{42a}$$

$$H_z^\pm = a_1^\pm H_z^{(a)\pm} + a_2^\pm H_z^{(b)\pm} \tag{42b}$$

where a_1^+, a_2^+ are, in general, independent of a_1^- and a_2^-. The variational formula can be put in a quotient of two quadratic forms

$$\gamma = \frac{\sum_{p,q} Q_{pq} a_p^- a_q^+}{\sum_{p,q} \bar{C}_{pq} a_p^- a_q^+} \tag{43}$$

where $p, q = 1, 2$ or a, b in a two-waveguide system. The matrix elements $\bar{C}_{pq}$ are defined as (31). The derivation of the matrix elements Q_{pq}'s is more complicated and is given by

$$\begin{aligned} Q_{pq} = \frac{1}{4}\iint \Big[& \omega\Delta\epsilon^{(q)} \mathbf{E}_t^{(p)-} \cdot \mathbf{E}_t^{(q)+} \\ & - \beta_q \mathbf{E}_t^{(p)-} \cdot \hat{z} \times \mathbf{H}_t^{(q)+} \\ & - \beta_q H^{(p)-} \cdot \hat{z} \times E_t^{(q)+} \\ & + iH^{(p)-} \cdot \nabla_t \times \left(\frac{\Delta\epsilon^{(q)}}{\epsilon} E_z^{(q)+}\right)\Big] dx\, dy \end{aligned} \tag{44}$$

where various relations such as those in Appendix A have been used. Using some vector identity and integration by parts for the last term in (44):

$$\begin{aligned} \iint iH^{(p)-} \cdot \nabla_t \times \left(\hat{z}\frac{\Delta\epsilon^{(q)}}{\epsilon} E_z^{(q)+}\right) dx\, dy \\ = \iint \omega\epsilon^{(p)} \frac{\Delta\epsilon^{(q)}}{\epsilon} E_z^{(p)-} E_z^{(q)+}\, dx\, dy. \end{aligned} \tag{45}$$

We simplify Q_{pq}

$$\begin{aligned} Q_{pq} &= \frac{1}{4}\iint \left[\omega\Delta\epsilon^{(q)} \mathbf{E}_t^{(p)} \cdot \mathbf{E}_t^{(q)} - \omega\Delta\epsilon^{(q)} \frac{\epsilon^{(p)}}{\epsilon} E_z^{(p)} E_z^{(q)}\right] \cdot dx\, dy + \left(\frac{C_{pq} + C_{qp}}{2}\right)\beta_q \\ &= \bar{K}_{pq} + \bar{C}_{pq}\beta_q \\ &= S_{pq}. \end{aligned} \tag{46}$$

Thus it is clear that Q_{pq} is identical to S_{pq}.

The propagation constant γ of the supermode is determined from the variational formula (37). We thus take the partial derivative with respect to a_p^- regarding the amplitudes of the positive traveling waves a_q^+ to be independent of a_p^-

$$\frac{\partial \gamma(a_p^-, a_q^+)}{\partial a_p^-} = 0 \tag{47}$$

and obtain

$$\gamma \sum_q \bar{C}_{pq} a_q^+ = \sum_q Q_{pq} a_q^+ \tag{48}$$

where we have made use of (43) again.

Noting that

$$\frac{d}{dz} \to i\gamma$$

for the system mode, we obtain the coupled-mode equation

$$\bar{C} \frac{d}{dz} \begin{bmatrix} a_1 \\ a_2 \end{bmatrix} = iQ \begin{bmatrix} a_1 \\ a_2 \end{bmatrix} \tag{49}$$

which is identical to the coupled-mode equation (30) derived in Section II-A since $Q = S$. If one takes partial derivative with respect to a_q^+ in (47), one obtains identical results as (49) since both $\bar{C}$ and Q are symmetric.

III. Reciprocity and Power Conservation

Almost all the previous theories use the power conservation to find the relation between the two coupling coefficients K_{ab} and K_{ba}. That would lead to erroneous results since $K_{ab} \neq K_{ba}^*$, in general, if two waveguides are not identical. An approximate theory from a more rigorous approach indicates some clue to the reciprocity relation by a power conservation argument but the results still contain some small discrepancies [3]. The explanation given in [3] was that they are due to the neglect of the radiation modes. In this section, we show that reciprocal relations can indeed be satisfied *analytically* and the precise analytical relation of K_{ab} to K_{ba} can be obtained, and the radiation field can be ignored from the beginning. The relation derived here should be obeyed and our coupled mode theory does satisfy this analytical relation.

A. Reciprocity Relations

Let us apply the reciprocity relation (2) to the two waveguide system described by $\epsilon(x, y)$ (Fig. 2). We choose $\epsilon^{(1)}(x, y) = \epsilon^{(2)}(x, y) = \epsilon(x, y)$, and the two sets of solutions

$$E_t^{(1)} = a^{(1)}(z)\, E_t^{(a)+}(x, y) + b^{(1)}(z)\, E_t^{(b)+}(x, y) \tag{50a}$$

$$H_t^{(1)} = a^{(1)}(z)\, H_t^{(a)+}(x, y) + b^{(1)}(z)\, H_t^{(b)+}(x, y) \tag{50b}$$

and

$$E_t^{(2)} = a^{(2)}(z)\, E_t^{(a)-}(x, y) + b^{(2)}(z)\, E_t^{(b)-}(x, y) \tag{51a}$$

$$H_t^{(2)} = a^{(2)}(z)\, H_t^{(a)-}(x, y) + b^{(2)}(z)\, H_t^{(b)-}(x, y) \tag{51b}$$

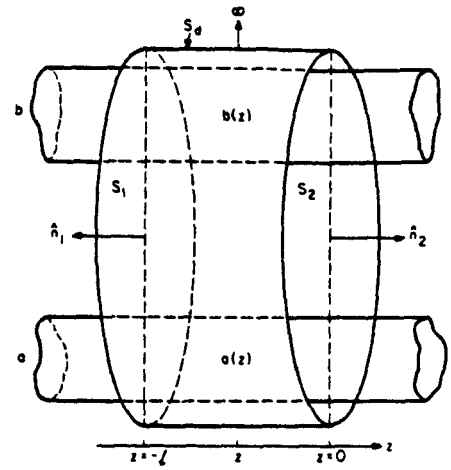

Fig. 2. Two parallel dielectric waveguides applied to the reciprocity relation. The surfaces S_1 and S_2 are normal to the z-direction. The side surface S_d expands to infinity. The two sets of solutiosn used are: 1) $a^{(1)}(-l) = 0$, $b^{(1)}(-l) = V_0$, $a^{(1)}(0)$ = equation (55a), $b^{(1)}(0)$ = equation (55b). 2) $a^{(2)}(-l)$ = equation (60a), $b^{(2)}(-l)$ = equation (60b), $a^{(2)}(0) = U_0$, $b^{(2)}(0) = 0$.

for the transverse components where the radiation mode has been neglected.

The volume of integration is chosen to be bound by S_1, S_2, and S_d as shown in Fig. 2. Using the divergence theorem and the fact that the surface integral on the side S_d goes to zero because of the radiation condition, we obtain

$$\iint_{\substack{z=-l \\ S_1}} (E_t^{(1)} \times H_t^{(2)} - E_t^{(2)} \times H_t^{(1)}) \cdot \hat{z}\, dx\, dy = \iint_{\substack{z=0 \\ S_2}} (E_t^{(1)} \times H_t^{(2)} - E_t^{(2)} \times H_t^{(1)}) \cdot \hat{z}\, dx\, dy \tag{52}$$

which leads to

$$\begin{aligned} a^{(1)}(0)\, a^{(2)}(0) + \frac{C_{ab} + C_{ba}}{2} [a^{(1)}(0)\, b^{(2)}(0) + a^{(2)}(0)\, b^{(1)}(0)] \\ + b^{(1)}(0)\, b^{(2)}(0) \\ = a^{(1)}(-l)\, a^{(2)}(-l) + \frac{C_{ab} + C_{ba}}{2} [a^{(1)}(-l)\, b^{(2)}(-l) \\ + a^{(2)}(-l)\, b^{(1)}(-l)] + b^{(1)}(-l)\, b^{(2)}(-l). \end{aligned} \tag{53}$$

We next consider these two sets of solutions to be the coupled mode equations with two boundary conditions satisfied respectively. One starts at $z = -l$ with the boundary conditions

(1)

$$a^{(1)}(-l) = 0 \tag{54a}$$

$$b^{(1)}(-l) = V_0 \tag{54b}$$

and the solutions of the mode amplitudes when propagating to $z = 0$ are

$$a^{(1)}(0) = V_0 i \frac{K_{ab}}{\psi} \sin \psi l \, e^{i\phi l} \tag{55a}$$

$$b^{(1)}(0) = V_0 \left[\cos \psi l + i \frac{\Delta}{\psi} \sin \psi l \right] e^{i\phi l} \tag{55b}$$

where

$$\Delta = \frac{\gamma_b - \gamma_a}{2} \tag{56}$$

$$\psi = \sqrt{\Delta^2 + K_{ab} K_{ba}} \tag{57}$$

$$\phi = \frac{\gamma_b + \gamma_a}{2}. \tag{58}$$

The next set of solutions are the propagating modes in the $-z$ direction with the boundary conditions

$$a^{(2)}(0) = U_0 \tag{59a}$$

$$b^{(2)}(0) = 0 \tag{59b}$$

and the solutions when the mode propagates to $z = -l$ are

$$a^{(2)}(-l) = U_0 \left[\cos \psi l - i \frac{\Delta}{\psi} \sin \psi l \right] e^{i\phi l} \tag{60a}$$

$$b^{(2)}(-l) = U_0 \frac{iK_{ba}}{\psi} \sin \psi l \, e^{i\phi l}. \tag{60b}$$

Substituting these field amplitudes (54), (55), (59), and (60) into the reciprocal relation (53), we obtain immediately the relation

$$K_{ba} - K_{ab} = \Delta(C_{ab} + C_{ba}) \tag{61}$$

which is the reciprocal relation that must be obeyed. Note that the above relation is exact and there is no complex conjugate operation involved here. It is applicable to lossy as well as lossless systems. Each quantity in (61) can be complex in general. Using our theory as derived in Section II, the quantities given by (34a)–(34d) do indeed satisfy the above reciprocal relation (61) analytically! The proof is straightforward by substitutions and making use of (26) for $\bar{K}_{ba}$ and $\bar{K}_{ab}$. Interestingly, the above relation (61) is of the same form as (26) except that the propagation constants are the modified γ_a and γ_b instead of β_a and β_b for individual waveguides.

I. Power Conservations

We choose the first set of solutions to be

$$E_t^{(1)}(x, y) = a(z) \, E_t^{(a)+}(x, y) + b(z) \, E_t^{(b)+}(x, y) \tag{62a}$$

$$H_t^{(1)}(x, y) = a(z) \, H_t^{(a)+}(x, y) + b(z) \, H_t^{(b)+}(x, y) \tag{62b}$$

or $\epsilon^{(1)}(x, y) = \epsilon(x, y)$.

For the second set of solutions, we choose $\epsilon^{(2)}(x, y) = \epsilon^*(x, y)$. Since the medium is lossless, $\epsilon^* = \epsilon$, the complex conjugate fields are also solutions. We choose

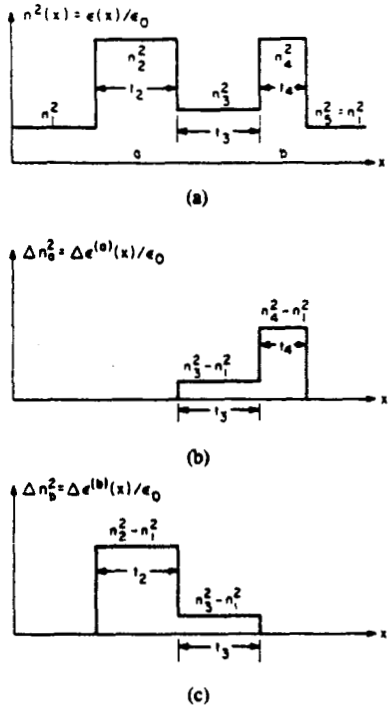

Fig. 3. (a) (b) (c) An illustrative example to show the two coupled waveguides under consideration. There also exists an external perturbation between the two waveguides.

$$E_t^{(2)}(x, y) = a^*(z) \, E_t^{(a)-}(x, y) + b^*(z) \, E_t^{(b)-}(x, y) \tag{63a}$$

$$H_t^{(2)}(x, y) = a^*(z) \, H_t^{(a)-}(x, y) + b^*(z) \, H_t^{(b)-}(x, y) \tag{63b}$$

making use of the z-inversion symmetry also. Substituting (62) and (63) into (52), we obtain

$$P(z = -l) = P(z = 0) \tag{64a}$$

where

$$P(z) = |a(z)|^2 + |b(z)|^2 + (C_{ab} + C_{ba}) \operatorname{Re}(a(z) \, b^*(z)) \tag{64b}$$

turns out to be the power guided by the two waveguides, where we have used relations such as

$$C_{ab} = \tfrac{1}{2} \iint E_t^{(b)} \times H_t^{(a)} \cdot \hat{z} \, dx \, dy = \tfrac{1}{2} \iint E_t^{(b)} \times H_t^{(a)*} \cdot \hat{z} \, dx \, dy \tag{65}$$

for a lossless system assuming one chooses E_t and H_t to be real, which is possible [13]. We note that since the distance l between the two surfaces S_1 and S_2 is arbitrary, (64a) leads to the fact that $P(z)$ should be constant independent of z, which is also obvious from the power conservation point of view. Using the boundary conditions

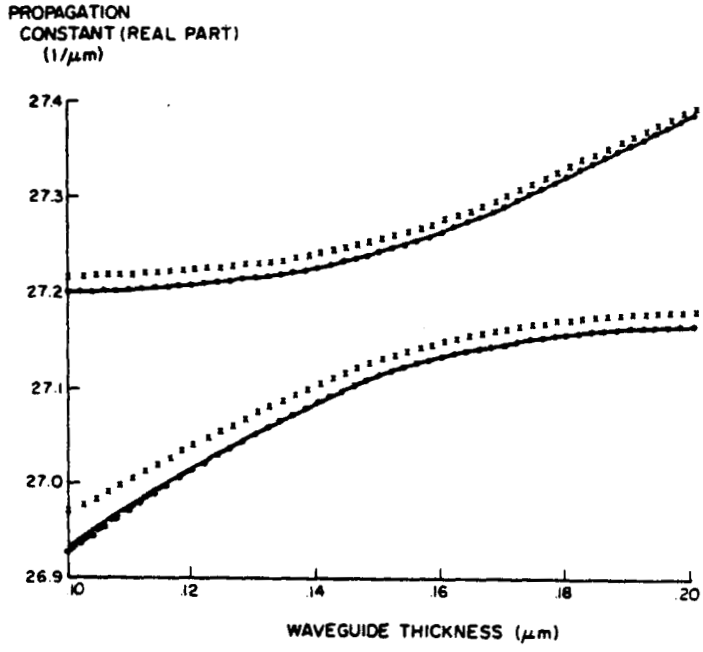

(a)

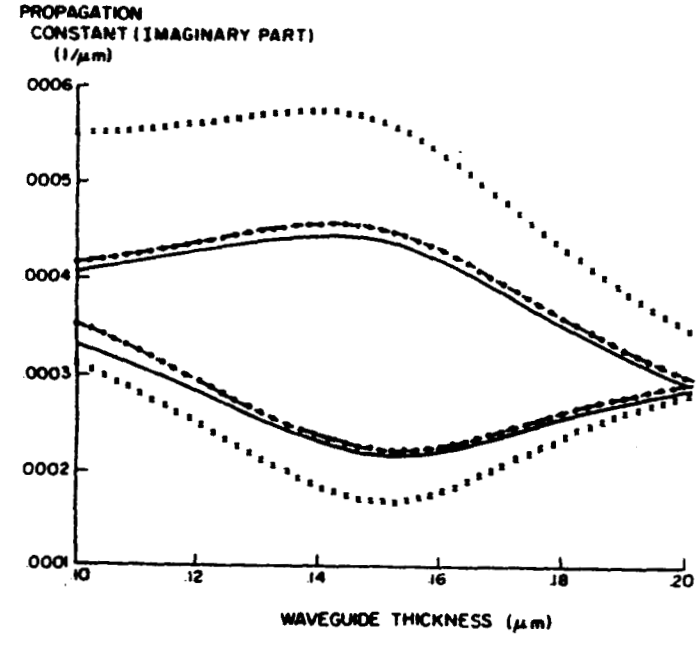

(b)

Fig. 4. The propagation constants for the coupled waveguides in Fig. 3: (a) the real parts, and (b) the imaginary parts of the propagation constants ($1/\mu m$) are plotted versus the thickness (μm) of waveguide b. The exact solution (solid line), our results (dashed line), and the results using [3] (dotted line) are almost on top of each other. The crosses are results using [2].

that $a(0) = 0$ and $b(0) = V_0$, we find [3]

$$P(z) = |V_0|^2 \left\{ 1 + \frac{K_{ab}}{\psi^2} [(K_{ab} - K_{ba}) + \Delta(C_{ab} + C_{ba})] \sin^2 \psi z \right\} = \text{constant.} \quad (66)$$

Thus the "power conservation violation factor" for excitation in waveguide b at $z = 0$

$$F_{b \to a} = \frac{K_{ab}}{\psi^2} [(K_{ab} - K_{ba}) + \Delta(C_{ab} + C_{ba})] \quad (67)$$

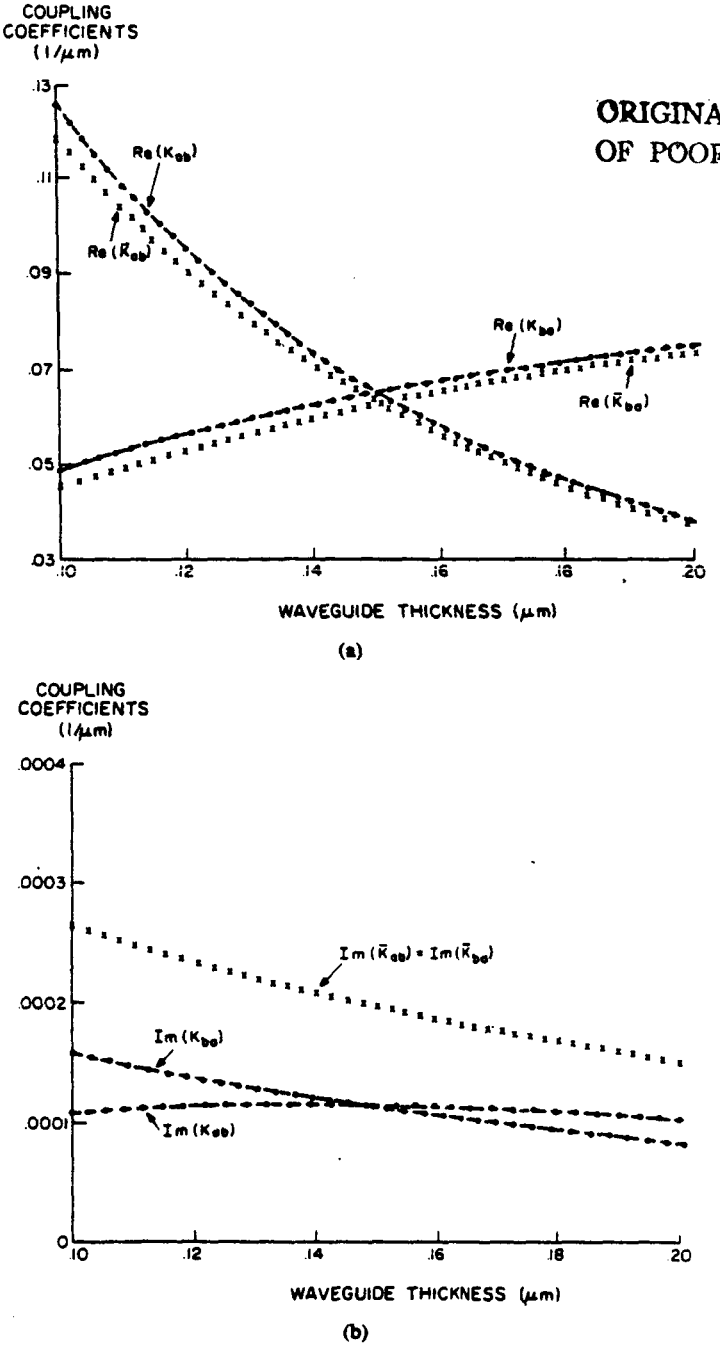

Fig. 5. (a) The real parts, and (b) the imaginary parts of the coupling coefficients K_{aa} and K_{ba} for the waveguide system in Fig. 3 are plotted versus the thickness (μm) of waveguide b. Our results (dashed lines) and the results using [3] (dotted lines) are on top of each other. The crosses are the results using [2].

should be zero. One sees clearly that this condition has been derived in the previous section using the reciprocity theorem which is more general for lossy as well as lossless cases. In deriving (67), one needs to restrict every quantity in (67) to be real for a lossless medium. Our new formulation presented in the previous sections does satisfy exactly these reciprocity conditions and power conservation, since the factor F is zero if we substitute all quantities in (34a)–(34d) into (67) and use (26). The factor F is an indication of the power conservation and the reciprocity relation. It can be used for the final numerical check of the consistency of the theory. Similarly, for an initial excitation in waveguide a at $z = 0$, one can define another factor

$$F_{a\to b} = \frac{K_{ba}}{\psi^2}\left[(K_{ba} - K_{ab}) - \Delta(C_{ab} + C_{ba})\right] \quad (68)$$

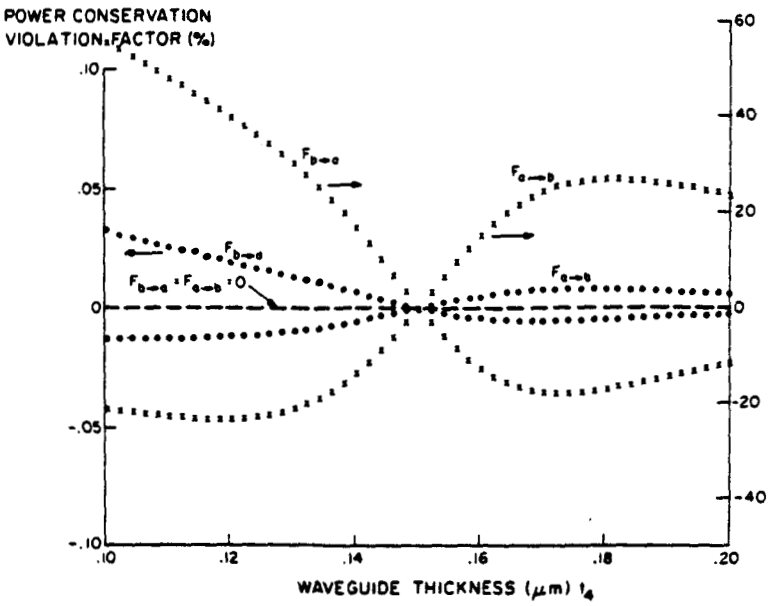

Fig. 6. The power conservation violator factors $F_{b\to a}$ and $F_{a\to b}$ for the three methods; our results (dashed line), the results using [3] (dotted lines) are shown using the left scale. The results using [2] (crosses) are shown using the right scale.

to check the numerical accuracy. The numerical results of these two factors in (67) and (68) using various methods will be presented in the next section.

IV. Numerical Results and Discussions

In this section, we consider an example from [3]. The coupled mode equations (33a) and (33b) with the expressions in (34a)–(34d) are used in the numerical calculations in this paper. The refractive index profile is shown in Fig. 3 where an external perturbation between the two planar waveguides also exists. We choose the index variation to be along the x direction, and for TE polarized waves, the electric field has only the y-component. The refractive indices are $n_1 = n_5 = \text{Re}\,(n_3) = 3.4$, $n_2 = n_4 = 3.6$ and an additional loss exists between two guides such that $n_3^2 - n_1^2 = \text{il.}\,299 \times 10^{-3}$. The other parameters are $t_2 = 0.15$ μm, $t_3 = 0.4$ μm, $\lambda = 0.8$ μm, and t_4 varies from 0.1 μm to 0.2 μm. The numerical results using an exact root-searching approach have also been shown as the solid lines in Fig. 4(a) and 4(b) for the real and imaginary parts of the propagation constants. (In [3], the "exact" numerical method combines a root searching approach assuming a lossless system to find the real parts of the propagation constants, and a perturbational approach for the imaginary parts when the loss is added. The final "exact" results in [3] are indeed very good compared with our exact root searching approach.) The results of the theory in this paper are shown as the dashed lines, and the results using that in [3] are shown as the dotted lines. We see clearly that all three methods agree very well with each other. The results of a conventional method [2] are also shown as the crosses which deviate more from the exact solutions especially for the imaginary parts of the propagation constants.

In Fig. 5(a) and 5(b) we compare both the real and the imaginary parts of the coupling coefficients using our method and the methods in [2] and [3]. It is clear that our results do agree very well with those using the method in [3] with a different approach, which has been checked with the "exact" numerical results presented in [3]. We note that our results satisfy the reciprocity and power conservation analytically and, thus, the factors $F_{b\to a}$ and $F_{a\to b}$ in (67) and (68) are zero while the F's of the method in [3] still contain a small discrepancy which is around 0.033 percent at a maximum value at $t_4 = 0.1$ μm, and the F's of the method in [2] yield a maximum power discrepancy of 55 percent at $t_4 = 0.1$ μm (instead of only about 20 percent as claimed in [3]). Detailed calculations of the two power conservation violation factors are shown in Fig. 6 (assuming the lossless case, i.e., Im $[n_3^2 - n_1^2] = 0$) where $F_{b\to a}$ and $F_{a\to b}$ for the method in [3] are shown (the dotted lines) in the left scale. The results are within 0.033 percent. The results using [2] (crosses) show in the right scale that $F_{a\to b}$ for excitation in waveguide a has an error of power conservation of 21 percent at $t_4 = 0.1$ μm, and $F_{b\to a}$ for excitation in waveguide b has a value of 55 percent. Our results (the dashed line) for $F_{b\to a}$ and $F_{a\to b}$ are always zero or within the round off errors in the computer, and the power conservation is indeed satisfied.

One should also note that the relations using the reciprocity and power conservation laws are necessary conditions, not sufficient conditions, for the accuracy of the numerical results [7]. They usually serve as checks, not direct proofs, of the numerical solutions to the Maxwell equations.

V. Conclusions

A new coupled mode formulation has been described via two methods: a generalized reciprocity relation and a

variational principle. Both give the same results. Exact analytical relations governing the coupling coefficients $\hat{K}_{ab}$ and $\hat{K}_{ba}$ (also K_{ab} and K_{ba}) and the propagation constants of individual waveguide β_a and β_b (γ_a and γ_b) are derived. These relations are used to show that our formulation does satisfy the reciprocity theorem and the power conservation analytically. Numerical results compared with the exact solutions and a previous method [3] which contains a slight discrepancy show that our new formulation should be very useful and self-consistent. We hope this paper will also clarify the reciprocity relation for the coupled waveguides.

Appendix A
Derivation of (20a) and (20b)

For the guided modes, we have

$$\nabla_t \times \boldsymbol{E}^{(a)+} - i\omega\mu \boldsymbol{H}^{(a)+} = -i\beta_a \hat{z} \times \boldsymbol{E}^{(a)+} \quad \text{(A1)}$$

$$\nabla_t \times \boldsymbol{H}^{(a)+} + i\omega\epsilon^{(a)} \boldsymbol{E}^{(a)+} = -i\beta_a \hat{z} \times \boldsymbol{H}^{(a)+} \quad \text{(A2)}$$

and a similar set of equations for $\epsilon^{(b)}$, $\boldsymbol{E}^{(b)+}$, $\boldsymbol{H}^{(b)+}$, and β_b. For the coupled-waveguide medium, we have

$$\nabla_t \times \boldsymbol{E} - i\omega\mu \boldsymbol{H} = -i\gamma \hat{z} \times \boldsymbol{E} \quad \text{(A3)}$$

$$\nabla_t \times \boldsymbol{H} + i\omega\epsilon \boldsymbol{E} = -i\gamma \hat{z} \times \boldsymbol{H}. \quad \text{(A4)}$$

Breaking the equation into the transverse and longitudinal components, we have

$$\begin{aligned} E_z &= \frac{1}{-i\omega\epsilon} \nabla_t \times \boldsymbol{H}_t = \frac{1}{-i\omega\epsilon} (a(z)\nabla_t \times \boldsymbol{H}_t^{(a)+} \\ &\quad + b(z)\nabla_t \times \boldsymbol{H}_t^{(b)+}) \\ &= a(z) \frac{\epsilon^{(a)}}{\epsilon} E_z^{(a)+} + b(z) \frac{\epsilon^{(b)}}{\epsilon} E_z^{(b)+} \end{aligned} \quad \text{(A5)}$$

which is (20a) in the text. A similar procedure can be applied to H_z and leads to (20b).

References

[1] H. Kogelnik, "Theory of dielectric waveguides," in *Integrated Optics*, T. Tamir, Ed., 2nd ed. New York: Springer-Verlag, 1979, ch. 2.

[2] H. F. Taylor and A. Yariv, "Guided wave optics," *Proc. IEEE*, vol. 62, pp. 1044–1060, 1974.

[3] A. Hardy and W. Streifer, "Coupled mode theory of parallel waveguides," *J. Lightwave Technol.*, vol. LT-3, pp. 1135–1146, 1985.

[4] A. Hardy and W. Streifer, "Coupled modes of multiwaveguide systems and phase arrays," *J. Lightwave Technol.*, vol. LT-4, pp. 90–99, 1986.

[5] A. Hardy and W. Streifer, "Coupled mode solutions of multiwaveguide systems," *IEEE J. Quantum Electron.*, vol. QE-22, pp. 528–534, 1986.

[6] S. L. Chuang and J. A. Kong, "Wave scattering and guidance by dielectric waveguides with periodic surfaces," *J. Opt. Soc. Amer.*, vol. 73, pp. 669–679, 1983, and Addendum, *J. Opt. Soc. Amer.*, vol. 73, pp. 1823–1824, 1983.

[7] S. L. Chuang and J. A. Kong, "Wave scattering from a periodic dielectric surface for a general angle of incidence," *Radio Sci.*, vol. 17, pp. 545–557, 1982.

[8] H. A. Haus, W. P. Huang, S. Kawakami, and N. A. Whitaker, "Coupled-mode theory of optical waveguides," *J. Lightwave Technol.*, this issue, pp. 16–23.

[9] H. A. Haus and M. N. Islam, "Application of a variational principle to systems with radiation loss," *IEEE J. Quantum Electronics*, vol. QE-19, pp. 106–117, 1983.

[10] L. Cairo and T. Kahan, *Variational Techniques in Electromagnetism*. London, England: Blackie and Son, 1965.

[11] R. F. Harrington, *Time-Harmonic Electromagnetic Fields*. New York: McGraw-Hill, 1961.

[12] H. Haus, "Electron beam waves in microwave tubes," in *Proc. Symp. Electronic Waveguides*, Apr. 8–10, 1958, pp. 89–132.

[13] R. E. Collin, *Foundations for Microwave Engineering*. New York: McGraw-Hill, 1966, sect. 3.9.

Shun-Lien Chuang (M'82) was born in Taiwan in 1954. He received the B.S. degree in electrical engineering from National Taiwan University in 1976, and the M.S., E.E., and Ph.D. degrees in electrical engineering from the Massachusetts Institute of Technology in 1980, 1981, and 1983, respectively.

While in graduate school, he held research and teaching assistantships, and also served as a recitation instructor. He conducted research at Schlumberger-Doll Research in Ridgefield, CT, during the summers of 1981 and 1982 and also in 1983 as a member of the professional staff. He is now an Assistant Professor in the Department of Electrical and Computer Engineering at the University of Illinois at Urbana-Champaign. He is conducting research in electromagnetics, integrated optics, and semiconductor devices including superlattice photodetectors and microwave transistors. He teaches courses on Electromagnetics and Solid State Electronic Devices. He has been cited several times in the list for Excellence in Teaching. He recently developed a new graduate course on Integrated Optics and Optoelectronics.

Dr. Chuang is a member of the Optical Society of America, Sigma Xi, and the American Physical Society.

Appendix F

S. L. Chuang, "A coupled-mode theory for multiwaveguide system satisfying the reciprocity theorem and power conservation," IEEE J. Lightwave Technology, vol. LT-5, pp.174-183, 1987.

A Coupled-Mode Theory for Multiwaveguide Systems Satisfying the Reciprocity Theorem and Power Conservation

SHUN-LIEN CHUANG

Abstract—**Two sets of coupled-mode equations for multiwaveguide systems are derived using a generalized reciprocity relation; one set for a lossless system and the other for a general lossy or lossless system. The second set of equations also reduces to those of the first set in the lossless case under the condition that the transverse field components are chosen to be real.**

Analytical relations between the coupling coefficients are shown and applied to the coupling of mode equations. It is shown analytically that our results satisfy exactly both the reciprocity theorem and power conservation. New orthogonal relations between the supermodes are derived in matrix form with the overlap integrals taken into account.

I. Introduction

THE COUPLING of mode theory in parallel waveguide systems has been of great interest in applications to directional couplers, laser arrays, waveguide switches, etc. [1], [2]. Although it has long been recognized that the previous coupled-mode theory is only applicable to very weakly coupled systems [3]–[8], significant improvements for strongly coupled waveguides have only been presented recently in series of papers [5], [8]–[11].

The major improvement is probably the inclusion of the overlap integrals C_{pq} defined in [8], when evaluating the power, and its resultant corrections to the various parameters such as the propagation constants and the coupling coefficients in the coupled-mode equations. Using two different methods, one based on a generalized reciprocity theorem and the other based on the variational principle, a new set of coupled-mode equations has been derived for a general (lossy or lossless) system [12]. Both methods give the same results.

In this paper, we apply the generalized reciprocity theorem [12] to a multiwaveguide system. The lossless case is treated here separately from the general lossy case, since in a lossless system, one may prefer to deal directly with powers for which the complex conjugates of the fields are needed, while for the general lossy case, one may not require any complex conjugate operations in the formulation [8]–[12]. Thus, the definitions for the overlap integrals and the coupling coefficients presented in Section III will be different from those for the general lossy case presented in Section IV. As will be shown in this paper, only when one chooses the *transverse* electric and magnetic field components to be real functions, the two formulations will be identical in the lossless limit. New properties of our coupled-mode equations are also presented analytically with the overlap integrals properly included.

Manuscript received May 12, 1986; revised July 3, 1986. This work was partially supported by NASA grant NAG 1-500.

The author is with the Department of Electrical and Computer Engineering, University of Illinois at Urbana-Champaign, Urbana, IL 61801.

IEEE Log Number 8611417.

II. Generalized Reciprocity Relation

Assuming that the electric and the magnetic fields $\boldsymbol{E}^{(1)}$, $\boldsymbol{H}^{(1)}$ satisfy the Maxwell equations in a medium $\epsilon^{(1)}(x, y)$ (for the whole space) and the corresponding boundary conditions and that $\boldsymbol{E}^{(2)}$ and $\boldsymbol{H}^{(2)}$ satisfy the Maxwell equations in another medium $\epsilon^{(2)}(x, y)$ and the corresponding boundary conditions, it is straightforward to show that [12], [13]

$$\nabla \cdot (\boldsymbol{E}^{(1)} \times \boldsymbol{H}^{(2)} - \boldsymbol{E}^{(2)} \times \boldsymbol{H}^{(1)}) = i\omega(\epsilon^{(2)} - \epsilon^{(1)})\boldsymbol{E}^{(1)} \cdot \boldsymbol{E}^{(2)} \tag{1}$$

with the same procedure used for deriving the Lorentz reciprocity relation [14]. When applied to a cylindrical geometry with an infinitesimal distance in the z-direction, (1) reduces to

$$\frac{\partial}{\partial z}\iint (\boldsymbol{E}^{(1)} \times \boldsymbol{H}^{(2)} - \boldsymbol{E}^{(2)} \times \boldsymbol{H}^{(1)}) \cdot \hat{z}\, dx\, dy = i\omega \iint (\epsilon^{(2)}(x, y) - \epsilon^{(1)}(x, y))\boldsymbol{E}^{(1)} \cdot \boldsymbol{E}^{(2)}\, dx\, dy. \tag{2}$$

Here $\epsilon^{(1)}(x, y)$ and $\epsilon^{(2)}(x, y)$ can be general media such as a single waveguide or a multiple waveguide system as long as they are translational invariant in the z-direction. The time convention $\exp(-i\omega t)$ will be used in this paper. One notes that the two reciprocal relations (1) and (2) are exact as long as the two sets of field expressions $(\boldsymbol{E}^{(1)}, \boldsymbol{H}^{(1)})$ and $(\boldsymbol{E}^{(2)}, \boldsymbol{H}^{(2)})$ are exact solutions to the Maxwell equations in medium $\epsilon^{(1)}(x, y)$ and $\epsilon^{(2)}(x, y)$ respectively.

III. Coupled-Mode Theory for a Lossless Multiwaveguide System

In this section, we derive the coupled-mode equations for a lossless multiwaveguide system.

0733-8724/87/0100-0174$01.00

A. General Properties of the Fields of the Guided Modes

When the medium $\epsilon(x, y)$ is lossless and translational invariant in the z-direction, one knows that the field solutions of the form exist

$$\text{a)} \quad (\boldsymbol{E}_t + \boldsymbol{E}_z)\, e^{i\beta z}$$
$$(\boldsymbol{H}_t + \boldsymbol{H}_z)\, e^{i\beta z}$$

which correspond to the fields propagating in the $+z$ direction. Here, we assume the above set of solutions to be the guided mode of the system. Based on inversion symmetry in the $-z$-direction, the following set of fields will also be solutions to the Maxwell equations [8], [13]–[15]

$$\text{b)} \quad (\boldsymbol{E}_t - \boldsymbol{E}_z)\, e^{-i\beta z}$$
$$(-\boldsymbol{H}_t + \boldsymbol{H}_z)\, e^{-i\beta z}$$

which correspond to the fields propagating in the $-z$-direction. If the medium is lossless $\epsilon^*(x, y) = \epsilon(x, y)$, by taking the complex conjugate of the Maxwell equations or applying the time-reversal concept, it is easy to show that the following two sets of solutions also exist:

$$\text{c)} \quad (\boldsymbol{E}_t^* + \boldsymbol{E}_z^*)\, e^{-i\beta^* z}$$
$$(-\boldsymbol{H}_t^* - \boldsymbol{H}_z^*)\, e^{-i\beta^* z}$$
$$\text{d)} \quad (\boldsymbol{E}_t^* - \boldsymbol{E}_z^*)\, e^{i\beta^* z}$$
$$(\boldsymbol{H}_t^* - \boldsymbol{H}_z^*)\, e^{i\beta^* z}$$

where the * sign means complex conjugate. Since we consider the guided modes of the lossless system (excluding the leaky modes, cutoff modes, etc.), the propagation constant β^* is real. It is thus clear from a) and d) that one can choose the transverse field $\boldsymbol{E}_t$ to be real, and find immediately that $\boldsymbol{H}_t$ is real; $\boldsymbol{E}_z$ and $\boldsymbol{H}_z$ are purely imaginary. However, if one uses complex $\boldsymbol{E}_t$ (e.g., in an optical fiber with a circular cross section, $\boldsymbol{E}_t(\rho, \phi)$ can be of the form $J_m(k_\rho \rho)\, e^{im\phi}$), one finds that $\boldsymbol{H}_t$, $\boldsymbol{E}_z$ and $\boldsymbol{H}_z$ will also be complex. From these general properties of the field solutions, we next derive the coupled-mode equations for a lossless system and some analytical relations between the coupling coefficients and the overlap integrals.

B. The Derivation of the Coupled-Mode Equations

CASE (1): Suppose we choose

$$\epsilon^{\langle 1\rangle}(x, y) = \epsilon^{(q)}(x, y) \tag{3}$$
$$\boldsymbol{E}^{\langle 1\rangle} = (\boldsymbol{E}_t^{(q)} + \boldsymbol{E}_z^{(q)})\, e^{i\beta_q z} \tag{4a}$$
$$\boldsymbol{H}^{\langle 1\rangle} = (\boldsymbol{H}_t^{(q)} + \boldsymbol{H}_z^{(q)})\, e^{i\beta_q z} \tag{4b}$$

to be the guided mode propagating in the $+z$-direction in a medium $\epsilon^{(q)}(x, y)$ with a single waveguide q. We also choose for the second set

$$\epsilon^{\langle 2\rangle}(x, y) = \epsilon^{(p)*}(x, y) = \epsilon^{(p)}(x, y) \tag{5}$$

and

$$\boldsymbol{E}^{\langle 2\rangle} = (\boldsymbol{E}_t^{(p)*} + \boldsymbol{E}_z^{(p)*})\, e^{-i\beta_p z} \tag{6a}$$
$$\boldsymbol{H}^{\langle 2\rangle} = (-\boldsymbol{H}_t^{(p)*} - \boldsymbol{H}_z^{(p)*})\, e^{-i\beta_p z} \tag{6b}$$

which are also solutions as discussed before. They correspond to the fields propagating in the $-z$-direction. Substituting the two sets of expressions into the generalized reciprocity relation (2), we obtain

$$\overline{\overline{K}}_{pq} - \overline{\overline{K}}_{pq}^* = (\beta_p - \beta_q)\left(\frac{\overline{\overline{C}}_{pq} + \overline{\overline{C}}_{qp}^*}{2}\right) \tag{7}$$

where

$$\overline{\overline{K}}_{pq} = \frac{\omega}{4}\int_{-\infty}^{\infty}\int \Delta\epsilon^{(q)}(\boldsymbol{E}_t^{(p)*} \cdot \boldsymbol{E}_t^{(q)} + \boldsymbol{E}_z^{(p)*}\boldsymbol{E}_z^{(q)})\, dx\, dy \tag{8}$$

and

$$\overline{\overline{C}}_{pq} = \frac{1}{2}\int_{-\infty}^{\infty}\int \boldsymbol{E}_t^{(q)} \times \boldsymbol{H}_t^{(p)*} \cdot \hat{z}\, dx\, dy. \tag{9}$$

We note that (7) is an exact relation since the fields ($\boldsymbol{E}^{\langle 1\rangle}$, $\boldsymbol{H}^{\langle 1\rangle}$) and ($\boldsymbol{E}^{\langle 2\rangle}$, $\boldsymbol{H}^{\langle 2\rangle}$) are exact solutions to Maxwell's equations in $\epsilon^{\langle 1\rangle}(x, y)$ and $\epsilon^{\langle 2\rangle}(x, y)$, respectively.

CASE (2): In this case, we choose $\epsilon^{\langle 1\rangle}(x, y)$ to be the medium of the multiwaveguide system $\epsilon(x, y)$

$$\epsilon^{\langle 1\rangle}(x, y) = \epsilon(x, y). \tag{10}$$

The solutions to the system are given approximately by

$$\boldsymbol{E}_t^{\langle 1\rangle} \simeq \sum_{p=1}^{N} a_q(z)\, \boldsymbol{E}_t^{(q)}(x, y) \tag{11a}$$
$$\boldsymbol{H}_t^{\langle 1\rangle} \simeq \sum_{p=1}^{N} a_q(z)\, \boldsymbol{H}_t^{(q)}(x, y) \tag{11b}$$

for the transverse field components. The z-components are given by

$$\boldsymbol{E}_z^{\langle 1\rangle} \simeq \sum_{p=1}^{N} \frac{\epsilon^{(q)}(x, y)}{\epsilon(x, y)}\, a_p(z)\, \boldsymbol{E}_z^{(q)}(x, y) \tag{11c}$$
$$\boldsymbol{H}_z^{\langle 1\rangle} \simeq \sum_{p=1}^{N} a_q(z)\, \boldsymbol{H}_z^{(q)}(x, y). \tag{11d}$$

A similar derivation for the above relations has been given in [13] for the polarization vector or in [12]. One notes that $\boldsymbol{E}_t^{(q)}(x, y)$, $q = 1, \cdots, N$ are not orthogonal functions, and the overlap integrals $C_{pq} \neq 0$. The second set of solutions is chosen as

$$\epsilon^{\langle 2\rangle}(x, y) = \epsilon^{(p)*}(x, y) = \epsilon^{(p)}(x, y) \tag{12}$$
$$\boldsymbol{E}^{\langle 2\rangle} = (\boldsymbol{E}_t^{(p)*} + \boldsymbol{E}_z^{(p)*})\, e^{-i\beta_p z} \tag{13a}$$
$$\boldsymbol{H}^{\langle 2\rangle} = (-\boldsymbol{H}_t^{(p)*} - \boldsymbol{H}_z^{(p)*})\, e^{-i\beta_p z}. \tag{13b}$$

Substituting the two sets of expressions (10)–(13) into the

generalized reciprocity relation (2), we obtain

$$\sum_q \bar{\bar{C}}_{pq} \frac{d}{dz} a_q(z) = i \sum_q (\bar{\bar{K}}^*_{pq} + \beta_p \bar{\bar{C}}_{pq}) a_q(z) \quad (14)$$

where

$$\bar{\bar{K}}_{pq} = \frac{\omega}{4} \int_{-\infty}^{\infty} \int \Delta\epsilon^{(q)} \left(E_t^{(p)*} \cdot E_t^{(q)} + \frac{\epsilon^{(p)}}{\epsilon} E_z^{(p)*} E_z^{(q)} \right) dx\, dy \quad (15)$$

and

$$\bar{\bar{C}}_{pq} = \frac{1}{2} (\bar{\bar{C}}_{pq} + \bar{\bar{C}}^*_{qp}). \quad (16)$$

One notes that $\bar{\bar{C}}_{pq}$ is a hermitian matrix, $\bar{\bar{C}}_{pq} = \bar{\bar{C}}^*_{qp}$. It is straightforward to show that $\bar{\bar{K}}_{pq}$ satisfies the same relation (7) as $\bar{\bar{K}}_{pq}$ because

$$\bar{\bar{K}}_{pq} = \bar{\bar{K}}_{pq} + \frac{\omega}{4} \int\int \Delta\epsilon^{(q)} \Delta\epsilon^{(p)} E_z^{(p)*} E_z^{(q)}\, dx\, dy \quad (17)$$

where the second term is equal to its complex conjugate quantity if one exchanges p and q where both $\Delta\epsilon^{(p)}$ and $\Delta\epsilon^{(q)}$ are real (lossless). Thus

$$\bar{\bar{K}}_{pq} - \bar{\bar{K}}^*_{qp} = \bar{\bar{K}}_{pq} - \bar{\bar{K}}^*_{qp} = (\beta_p - \beta_q) \left(\frac{\bar{\bar{C}}_{pq} + \bar{\bar{C}}^*_{qp}}{2} \right) = (\beta_p - \beta_q) \bar{\bar{C}}_{pq} \quad (18)$$

which is an exact relation. It is seen clearly that only if $\beta_p = \beta_q$, one has $\bar{\bar{K}}_{pq} = \bar{\bar{K}}^*_{qp}$ (or if the overlap integrals are very small in the extremely weak coupling case, $\bar{\bar{K}}_{pq} = \bar{\bar{K}}^*_{qp}$). Otherwise one should treat $\bar{\bar{K}}_{pq}$ and $\bar{\bar{K}}^*_{qp}$ as different quantities in general. One defines the matrix elements:

$$\bar{\bar{Q}}_{pq} = \bar{\bar{K}}^*_{qp} + \beta_p \bar{\bar{C}}_{pq} = \bar{\bar{K}}_{pq} + \bar{\bar{C}}_{pq} \beta_q. \quad (19)$$

Thus, the coupling of mode equations can be written as

$$\bar{\bar{C}} \frac{da}{dz} = i \bar{\bar{Q}} a \quad (20)$$

where $\bar{\bar{Q}}$ is clearly hermitian since

$$\bar{\bar{Q}}_{pq} = \bar{\bar{Q}}^*_{qp} \quad (21)$$

which can be shown from (19) and a is a vector with its elements given by $a_q(z)$, $q = 1, 2, \cdots, N$. Another way to write the above equation is either

$$\bar{\bar{C}} \frac{da}{dz} = i(\bar{\bar{K}}^+ + B\bar{\bar{C}}) a \quad (22)$$

or

$$\bar{\bar{C}} \frac{da}{dz} = i(\bar{\bar{K}} + \bar{\bar{C}} B) a \quad (23)$$

where B is a diagonal matrix with the elements given by the propagation constants of individual waveguides β_p. Here the superscript $^+$ means complex conjugate and transpose of the matrix. The second form (23) is useful since

$$\frac{da}{dz} = i(B + \bar{\bar{C}}^{-1} \bar{\bar{K}}) a \quad (24)$$

while the first form (22), which is similar (but not identical) to that of [10], [11], requires more algebraic manipulations in evaluating $(\bar{\bar{C}}^{-1} B \bar{\bar{C}} + \bar{\bar{C}}^{-1} \bar{\bar{K}}^+)$.

C. Power Conservation

In Section III-B, we derived the coupled-mode equations in matrix form (20), where $\bar{\bar{C}}$ is related to the overlap integrals C_{pq} and C^*_{qp}, and $\bar{\bar{Q}}$ is defined in (19). Both $\bar{\bar{C}}$ and $\bar{\bar{Q}}$ are proved to be hermitian without any approximation in the matrix elements. Let us look at the power guided along the multiwaveguide system

$$P(z) = \frac{1}{2} \mathrm{Re} \int\int E_t \times H_t^* \cdot \hat{z}\, dx\, dy = \mathrm{Re} \left[\sum_{p,q} a_p^*(z) \bar{\bar{C}}_{pq} a_q(z) \right] = \sum_{p,q} a_p^*(z) \left(\frac{\bar{\bar{C}}_{pq} + \bar{\bar{C}}^*_{qp}}{2} \right) a_q(z) = a^+(z) \bar{\bar{C}} a(z) \quad (25)$$

where $\bar{\bar{C}}$ is defined in (16). If the medium is lossless, the power of the guided mode must be independent of the position z, i.e., $dP/dz = 0$. We have the lossless condition

$$\sum_{p,q} \left(\frac{da_p^*(z)}{dz} \right) \bar{\bar{C}}_{pq} a_q(z) + \sum_{i,j} a_p^*(z) \bar{\bar{C}}_{pq} \frac{da_q(z)}{dz} = 0. \quad (26)$$

Using the coupled-mode equation (20), one finds immediately that the *lossless condition* is equivalent to

$$i \sum_{p,q} a_p^* (\bar{\bar{Q}}_{pq} - \bar{\bar{Q}}^*_{qp}) a_q = 0 \quad (27)$$

where we have used the fact that $\bar{\bar{C}}_{pq}$ is hermitian. Since a_p^* and a_q can be arbitrary values, we obtain

$$\bar{\bar{Q}}_{pq} - \bar{\bar{Q}}^*_{qp} = 0. \quad (28)$$

That is, $\bar{\bar{Q}}_{pq}$ must be hermitian, which is true, since we have shown that $\bar{\bar{Q}}_{pq}$ is indeed hermitian in (21) from the definition (19). Thus our formulation satisfies exactly the power conservation. An example will be shown later which illustrates this power conservation criterion.

D. Power Orthogonality of the Supermodes

Let us choose two sets of solutions to be two distinct supermodes in the multiwaveguide system $\epsilon(x, y)$

$$\epsilon^{(1)}(x, y) = \epsilon(x, y) \quad (29)$$

$$E_t^{(1)} = \left(\sum_{q=1}^{N} a_q^{(i)} E_t^{(q)} \right) e^{i\gamma_i z} \tag{30a}$$

$$H_t^{(1)} = \left(\sum_{q=1}^{N} a_q^{(i)} H_t^{(q)} \right) e^{i\gamma_i z} \tag{30b}$$

where $a^{(i)}$ with elements $a_q^{(i)}$, $q = 1, 2, \cdots, N$, is the eigenvector for the first supermode with a propagation constant γ_i

$$\epsilon^{(2)}(x, y) = \epsilon(x, y) = \epsilon^*(x, y) \tag{31}$$

$$E_t^{(2)} = \left(\sum_{p=1}^{N} a_p^{(j)*} E_t^{(p)*} \right) e^{-i\gamma_j z} \tag{32a}$$

$$H_t^{(2)} = \left(-\sum_{p=1}^{N} a_p^{(j)*} H_t^{(p)*} \right) e^{-i\gamma_j z} \tag{32b}$$

and $a^{(j)}$ with elements $a_p^{(j)}$, $p = 1, 2, \cdots, N$, is the eigenvector for the second supermode with a propagation constant γ_j. The reciprocity relation (2) gives

$$(\gamma_i - \gamma_j) \sum_{p,q} \sum a_q^{(i)} a_p^{(j)*} (\bar{\bar{C}}_{pq} + \bar{\bar{C}}_{qp}^*) = 0. \tag{33}$$

Since $\gamma_i \neq \gamma_j$ we obtain the general orthogonality condition:

$$a^{(j)+} \bar{\bar{C}} a^{(i)} = 0, \qquad i \neq j. \tag{34}$$

That is, any two eigenvectors corresponding to different propagation constants are orthogonal to each other with a weighting matrix given by $\bar{\bar{C}}$.

An alternative way of deriving (34) is simply by looking at the coupled-mode equation (20). The supermode solution $a(z)$ is given by the form

$$a(z) = a e^{i\gamma z}. \tag{35}$$

Thus, the matrix equation (20) for the coupled-mode equations reduces to the eigenequation

$$\gamma \bar{\bar{C}} a = \bar{\bar{Q}} a. \tag{36}$$

The eigenvalue γ satisfies

$$\det \left| \bar{\bar{Q}} - \gamma \bar{\bar{C}} \right| = 0. \tag{37}$$

Since both $\bar{\bar{C}}$ and $\bar{\bar{Q}}$ are hermitian, the eigenvalues for (36) must be real, that can be shown from elementary matrix theory [16]. It is also obviously true from the fact that the medium is lossless. Another property of the matrix equation (36) is that two distinct eigenvectors $a^{(i)}$ and $a^{(j)}$ are orthogonal to each other with the "weighting matrix" $\bar{\bar{C}}$

$$a^{(j)+} \bar{\bar{C}} a^{(i)} = 0, \qquad i \neq j. \tag{38}$$

One notes that in the extremely weak coupling case, the coupling of mode equations have the same form as (20) except that $\bar{\bar{C}}$ should be replaced by I, the identity matrix. Thus, the orthogonality relation (38) reduces to the well-known results: $a^{(j)+} a^{(i)} = 0$ for $i \neq j$ in conventional theory.

IV. Coupled-Mode Theory for a General (Lossy or Lossless) Multiwaveguide System

In general, a multiwaveguide system can be lossy. The previous formulation will not be applicable anymore. Actually, the formulation for a lossy medium is very similar to the formulation in the previous section, except one does not have any complex conjugate operation, and special care is taken for the z-components of the fields as can be seen from Section III-A. A derivation has been presented in [12] which is similar to that in the previous section. Therefore, we briefly give the results below.

A. The Derivation of the Coupled Mode Equations for a Lossy System

CASE (1): Following the procedure in Case (1) of Section III-B, except that we choose the second set of solutions to be the form b) in Section III-A, it is easy to derive [12]

$$\bar{K}_{pq} - \bar{K}_{qp} = (\beta_p - \beta_q) \frac{C_{pq} + C_{qp}}{2} \tag{39}$$

where

$$\bar{K}_{pq} = \frac{\omega}{4} \int_{-\infty}^{\infty} \int \Delta\epsilon^{(q)} (E_t^{(p)} \cdot E_t^{(q)} - E_z^{(p)} E_z^{(q)}) \, dx \, dy \tag{40}$$

and

$$C_{pq} = \frac{1}{2} \int_{-\infty}^{\infty} \int E_t^{(q)} \times H_t^{(p)} \cdot \hat{z} \, dx \, dy \tag{41}$$

where no complex conjugate operation is involved, and there is a negative sign in the integrand of (40). The above definitions (40) and (41) are the same as those used in [8] except for the constant factor of 4. The difference is only apparent because once we choose the normalization condition $C_{11} = C_{22} = \cdots C_{NN} = 1$, the factor of 4 is absorbed in E_t and H_t. Thus, numerically, $\bar{K}_{pq}$ is identical to that in [8].

CASE (2): Following the procedures in Case (2) of Section III-B, we choose the first medium and the field solutions to be the same as (10) and (11), and the second medium and the field solutions to be

$$\epsilon^{(2)}(x, y) = \epsilon^{(p)}(x, y) \tag{42}$$

$$E^{(2)} = (E_t^{(p)} - E_z^{(p)}) e^{-i\beta_p z} \tag{43a}$$

$$H^{(2)} = (-H_t^{(p)} + H_z^{(p)}) e^{-i\beta_p z}. \tag{43b}$$

We obtain again from the generalized reciprocity relation 2)

$$\sum_q \frac{C_{pq} + C_{qp}}{2} \frac{d}{dz} a_q(z) = i \sum_q \left(K_{pq} + \beta_p \frac{C_{pq} + C_{qp}}{2} \right) a_q(z) \tag{44}$$

where

$$K_{pq} = \frac{\omega}{4}\iint \Delta\epsilon^{(q)}\left(\boldsymbol{E}_t^{(p)} \cdot \boldsymbol{E}_t^{(q)} - \frac{\epsilon^{(p)}}{\epsilon} E_z^{(p)} E_z^{(q)}\right) \quad (45)$$

and C_{pq} has been defined in (41). One can also show that K_{pq} satisfies the same equation as $\bar{K}_{pq}$ in (39) by recognizing that

$$K_{pq} = \bar{K}_{qp} + \frac{\omega}{4}\iint \Delta\epsilon^{(q)} \frac{\Delta\epsilon^{(p)}}{\epsilon} E_z^{(p)} E_z^{(q)}\, dx\, dy \quad (46)$$

where the second term is symmetric with respect to p and q. Thus

$$K_{pq} - K_{qp} = (\beta_p - \beta_q)\frac{C_{pq} + C_{qp}}{2} \quad (47)$$

which is also an exact relation.

The coupled-mode equation can be written in a matrix form

$$\bar{C}\frac{d}{dz}a(z) = iQa \quad (48)$$

where

$$\bar{C}_{pq} = \frac{C_{pq} + C_{qp}}{2} = \bar{C}_{qp} \quad (49)$$

is symmetric, and

$$\begin{aligned} Q_{pq} &= K_{qp} + \beta_p \frac{C_{pq} + C_{qp}}{2} \\ &= K_{pq} + \frac{C_{pq} + C_{qp}}{2}\beta_q = Q_{qp} \end{aligned} \quad (50)$$

is also symmetric. The matrix equation can also be written as

$$\frac{d}{dz}a(z) = iMa \quad (51)$$

$$M = \bar{C}^{-1}Q \quad (52)$$

or

$$M = \bar{C}^{-1}B\bar{C} + \bar{C}^{-1}K^T \quad (53)$$

or

$$M = B + \bar{C}^{-1}K \quad (54)$$

where B is again a diagonal matrix with the propagation constants β_p as the elements, and the superscript T means transpose of the matrix. Equation (53) is compared with the form in [10], [11]. One sees that the only difference is that the matrix $\bar{C}$ is used here while the matrix C is used in [8]–[11]. K^T used in this paper is the same as K in [10], [11] from the definition (40) except for the factor of 4. The final form (54) is simpler than (53) since B is used instead of $\bar{C}^{-1}B\bar{C}$. Thus, our coupled-mode equation looks simpler using the form (51) with M given by (54), than that in [10], [11]. The coupling coefficients $\bar{K}_{pq}$ defined in (15) for the lossless case or K_{pq} defined in (45) for the general case differ from $\bar{\bar{K}}_{pq}$ (defined in (8)) or $\bar{K}_{pq}$ (defined in (40)) by the factor $\epsilon^{(p)}/\epsilon$ in the second part of the integrand. This factor is also taken as one in [17]. We believe that it should be more self-consistent to keep the factor since it was derived from (11c) making use of Maxwell's equation as shown in [12, appendix A].

B. General Orthogonality Property of the Supermodes

Following a similar procedure to that in Section III-D, one applies the reciprocity relation (2) to any two supermodes

$$\boldsymbol{E}_t^{(1)} = \left(\sum_{q=1}^{N} a_q^{(i)}\boldsymbol{E}_t^{(q)}\right)e^{i\gamma_i z} \quad (55a)$$

$$\boldsymbol{H}_t^{(1)} = \left(\sum_{q=1}^{N} a_q^{(i)}\boldsymbol{H}_t^{(q)}\right)e^{i\gamma_i z} \quad (55b)$$

and

$$\boldsymbol{E}_t^{(2)} = \left(\sum_{p=1}^{N} a_p^{(j)}\boldsymbol{E}_t^{(p)}\right)e^{-i\gamma_j z} \quad (56a)$$

$$\boldsymbol{H}_t^{(2)} = \left(-\sum_{p=1}^{N} a_p^{(j)}\boldsymbol{H}_t^{(p)}\right)e^{-i\gamma_j z}. \quad (56b)$$

Using the eigenvector $a^{(i)}$ = column $(a_1^{(i)}, a_2^{(i)}, \cdots, a_N^{(i)})$ and a similar form for $a^{(j)}$, one obtains

$$a^{(j)T}\bar{C}a^{(i)} = 0, \qquad \text{for } \gamma_i \neq \gamma_j \quad (57)$$

which is the reciprocity relation that should be satisfied by any two eigenvectors of the matrix equation

$$\gamma\bar{C}a = Qa \quad (58)$$

which follows (48). Alternatively, because both $\bar{C}$ and Q are symmetric matrices, the general orthogonality relation (57) is a well-known property in matrix theory [16].

C. Reciprocity Relation for Two Sets of Solutions with Separate Boundary Conditions

Let us look at the boundary value problem for a set of solutions to the coupled-mode equation (48). The general solution $a(z)$ is given by

$$a(z) = Ae^{i\Gamma z}A^{-1}a(0) \quad (59)$$

where

$$\Gamma = \text{diagonal}\,(\gamma_1, \gamma_2, \cdots, \gamma_N) \quad (60)$$

for a given boundary condition $a(0)$ and the wave propagating in the $+z$ direction. Here the matrix A is defined to have the ith column given by the ith eigenvector of the matrix (58), and $\gamma_1, \cdots, \gamma_N$ are the eigenvalues of (58).

Consider a first set of solutions at $z = 0$ given the condition $a^{(1)}(z = -l)$,

$$a^{(1)}(0) = Ae^{i\Gamma l}A^{-1}a^{(1)}(-l). \quad (61)$$

Let us look at another set of solutions with the boundary condition given at $z = 0$ and the wave propagating in the $-z$ direction to $z = -l$

$$a^{(2)}(-l) = Ae^{i\Gamma l}A^{-1}a^{(2)}(0). \quad (62)$$

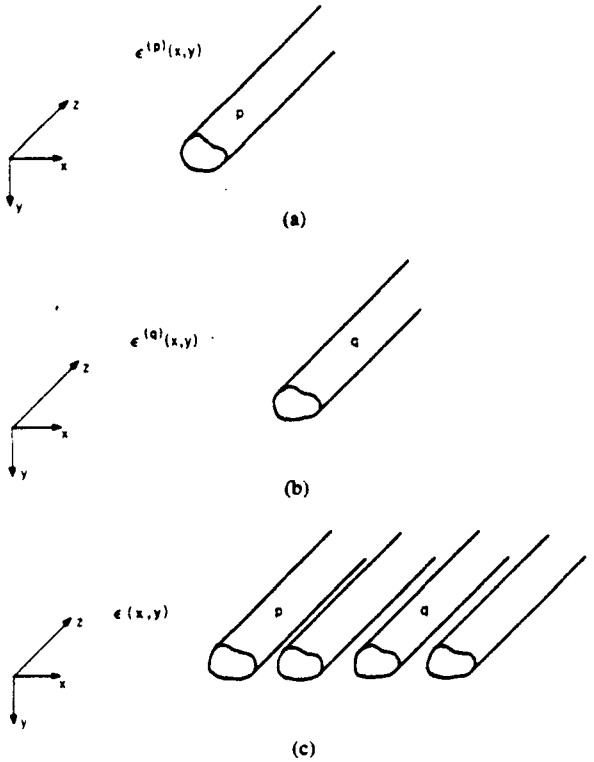

Fig. 1. (a) A single waveguide p described by $\epsilon^{(p)}(x, y)$ in whole space. (b) A single waveguide q described by $\epsilon^{(q)}(x, y)$ in whole space. (c) A multiwaveguide system described by $\epsilon(x, y)$ in whole space.

Applying the reciprocity relation (1) to a cylindrical surface enclosing the planes $z = -l$ and $z = 0$ with a radius going to infinity, one finds [12]

$$\iint_{z=-l} (\boldsymbol{E}^{\langle 1\rangle} \times \boldsymbol{H}^{\langle 2\rangle} - \boldsymbol{E}^{\langle 2\rangle} \times \boldsymbol{H}^{\langle 1\rangle}) \cdot \hat{z}\, dx\, dy = \iint_{z=0} (\boldsymbol{E}^{\langle 1\rangle} \times \boldsymbol{H}^{\langle 2\rangle} - \boldsymbol{E}^{\langle 2\rangle} \times \boldsymbol{H}^{\langle 1\rangle}) \cdot \hat{z}\, dx\, dy. \tag{63}$$

From the previous two sets of solutions, we have (Fig. 2)

$$\boldsymbol{E}_t^{\langle 1\rangle} = \sum_{p=1}^{N} a_p^{\langle 1\rangle}(z)\, \boldsymbol{E}_t^{(p)} \tag{64a}$$

$$\boldsymbol{H}_t^{\langle 1\rangle} = \sum_{p=1}^{N} a_p^{\langle 1\rangle}(z)\, \boldsymbol{H}_t^{(p)} \tag{64b}$$

and

$$\boldsymbol{E}_t^{\langle 2\rangle} = \sum_{q=1}^{N} a_q^{\langle 2\rangle}(z)\, \boldsymbol{E}_t^{(q)} \tag{65a}$$

$$\boldsymbol{H}_t^{\langle 2\rangle} = -\sum_{q=1}^{N} a_q^{\langle 2\rangle}(z)\, \boldsymbol{H}_t^{(q)} \tag{65b}$$

where the second set of fields propagates in the $-z$-direction. The vector $\boldsymbol{a}^{\langle 1\rangle}(z = 0)$ is related to $\boldsymbol{a}^{\langle 1\rangle}(z = -l)$ by (61), and $\boldsymbol{a}^{\langle 2\rangle}(z = -l)$ is related to $\boldsymbol{a}^{\langle 2\rangle}(z = 0)$ by

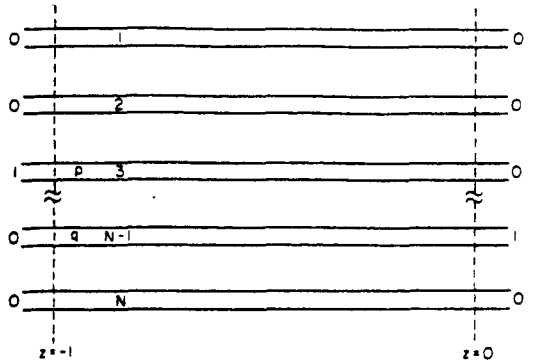

Fig. 2. A multiwaveguide system with possible excitation either at waveguide p at $z = -l$ and the wave propagating in the $+z$ direction, or at waveguide q at $z = 0$ and the wave propagating in the $-z$-direction.

(62). The reciprocity relation (62) reduces to

$$\boldsymbol{a}^{\langle 1\rangle T}(-l)\, \bar{\boldsymbol{C}}\boldsymbol{a}^{\langle 2\rangle}(-l) = \boldsymbol{a}^{\langle 1\rangle T}(0)\, \bar{\boldsymbol{C}}\boldsymbol{a}^{\langle 2\rangle}(0) \tag{66}$$

or equivalently

$$\boldsymbol{a}^{\langle 1\rangle T}(-l)\, \bar{\boldsymbol{C}}\boldsymbol{A}e^{i\Gamma l}\boldsymbol{A}^{-1}\boldsymbol{a}^{\langle 2\rangle}(0) = \boldsymbol{a}^{\langle 1\rangle T}(-l)\, (\boldsymbol{A}e^{i\Gamma l}\boldsymbol{A}^{-1})^T\, \bar{\boldsymbol{C}}\boldsymbol{a}^{\langle 2\rangle}(0). \tag{67}$$

Since the initial conditions for $\boldsymbol{a}^{\langle 1\rangle}(-l)$ and $\boldsymbol{a}^{\langle 2\rangle}$ can be

$$\boldsymbol{a}^{\langle 1\rangle}(-l) = \begin{bmatrix} 0 \\ 0 \\ 1 \\ 0 \\ 0 \\ \vdots \\ 0 \end{bmatrix} \rightarrow p\text{th position} \tag{68}$$

$$\boldsymbol{a}^{\langle 2\rangle}(0) = \begin{bmatrix} 0 \\ 0 \\ 0 \\ \vdots \\ 0 \\ 1 \\ 0 \end{bmatrix} \rightarrow q\text{th position} \tag{69}$$

where p and q can be arbitrarily set between 1 and N, we find the reciprocity condition:

$$\bar{\boldsymbol{C}}\boldsymbol{A}e^{i\Gamma l}\boldsymbol{A}^{-1} = (\bar{\boldsymbol{C}}\boldsymbol{A}e^{i\Gamma l}\boldsymbol{A}^{-1})^T \tag{70}$$

where we have used the fact that $\bar{\boldsymbol{C}}^T = \bar{\boldsymbol{C}}$. Since the matrix $\boldsymbol{A}$ has each column given by the eigenvector of (58), we have

$$\bar{\boldsymbol{C}}\boldsymbol{A}\Gamma = \boldsymbol{Q}\boldsymbol{A} \tag{71}$$

or

$$\Gamma = \boldsymbol{A}^{-1}\bar{\boldsymbol{C}}^{-1}\boldsymbol{Q}\boldsymbol{A} = \boldsymbol{A}^{-1}\boldsymbol{M}\boldsymbol{A}. \tag{72}$$

Substituting the above relation into (70), we find that the reciprocity condition (70) is the same as

$$\bar{\boldsymbol{C}}\boldsymbol{M} = (\bar{\boldsymbol{C}}\boldsymbol{M})^T \quad \text{(reciprocity condition)} \tag{73}$$

i.e., the product $\bar{C}M$ must be symmetric. We see clearly that our formulation (48) satisfies this condition because

$$\bar{C}M = Q \tag{74}$$

where Q has been proved to be symmetric in Section IV-A. To illustrate our results, we show in the next section the special cases for two coupled waveguides and three coupled waveguides.

V. Special Cases

In summary, the coupled-mode equation is put in matrix form

$$\bar{C}\frac{d}{dz}a = iQa \tag{75}$$

where both $\bar{C}$ and Q are symmetric. In another form, it is given by

$$\frac{d}{dz}a = iMa \tag{76}$$

where

$$M = \bar{C}^{-1}Q. \tag{77}$$

The reciprocity condition (74) requires $\bar{C}M$ (or Q) to be symmetric. The above formulation is very general and is applicable to both lossy as well as lossless systems.

A. Two-Coupled Waveguides

If $N = 2$, one has

$$M = \begin{bmatrix} \gamma_a & K_{ab} \\ K_{ba} & \gamma_b \end{bmatrix} \tag{78}$$

where

$$\gamma_a = \beta_1 + (K_{11} - \bar{C}_{12}K_{21})/(1 - \bar{C}_{12}^2) \tag{79a}$$

$$\gamma_b = \beta_2 + (K_{22} - \bar{C}_{12}K_{12})/(1 - \bar{C}_{12}^2) \tag{79b}$$

$$K_{ab} = (K_{12} - K_{22}\bar{C}_{12})/(1 - \bar{C}_{12}^2) \tag{79c}$$

$$K_{ba} = (K_{21} - K_{11}\bar{C}_{12})/(1 - \bar{C}_{12}^2). \tag{79d}$$

As has been pointed out in [8], the overlap integrals C_{12} and C_{21} or $\bar{C}_{12}$ are obtained from the integration over whole space in the transverse direction, and can be significantly large even if $\tilde{K}_{12}$ is small. Thus the factor $1 - \bar{C}_{12}^2$ may become very small and K_{ab} is large. The reciprocity condition that $\bar{C}M$ be symmetric gives

$$K_{ab} - K_{ba} = (\gamma_a - \gamma_b)\bar{C}_{12} \tag{80}$$

which has been shown in [12], and can also be proved by substituting (79a)–(79d) into (80). The two eigenvalues γ_1, γ_2, and eigenvectors are well known:

$$\gamma_1 = \phi + \psi \tag{81a}$$

$$\gamma_2 = \phi - \psi \tag{81b}$$

where

$$\phi = \frac{\gamma_b + \gamma_a}{2} \tag{81c}$$

$$\psi = \sqrt{\Delta^2 + K_{ab}K_{ba}} \tag{81d}$$

$$\Delta = \frac{\gamma_b - \gamma_a}{2} \tag{81e}$$

and

$$a^{(1)} = \begin{bmatrix} K_{ab} \\ \Delta + \psi \end{bmatrix} \tag{82a}$$

$$a^{(2)} = \begin{bmatrix} -\Delta - \psi \\ K_{ba} \end{bmatrix} \tag{82b}$$

where the orthogonality relation $a^{(1)T}\bar{C}a^{(2)} = 0$ is indeed satisfied and it is the same as the reciprocity condition (80).

B. Three-Coupled Waveguides

If $N = 3$, we have

$$M = B + \bar{C}^{-1}K \tag{83}$$

which can be calculated easily by inversion of $\bar{C}$, noting that $\bar{C}$ is symmetric:

$$\bar{C}_{12} = \bar{C}_{21} = (C_{12} + C_{21})/2 \tag{84a}$$

$$\bar{C}_{13} = \bar{C}_{31} = (C_{13} + C_{31})/2 \tag{84b}$$

$$\bar{C}_{11} = \bar{C}_{22} = \bar{C}_{33} = 1. \tag{84c}$$

The reciprocity condition that $\bar{C}M$ is symmetric leads to e.g., $(\bar{C}M)_{12} = (CM)_{21}$

$$m_{12} - m_{21} = \bar{C}_{12}(m_{12} - m_{22}) + \bar{C}_{21}m_{31} - \bar{C}_{13}m_{32} \tag{85}$$

which will be useful later. Let us consider a symmetric case with the two outer waveguides identical [10]:

$$K_{12} = K_{32} \neq K_{21} = K_{23} \tag{86a}$$

$$K_{13} = K_{31} \tag{86b}$$

$$K_{11} = K_{33} \neq K_{22}. \tag{86c}$$

The matrix elements of M are obtained from (83)

$$m_{11} = m_{33} = \beta_1 + [K_{11}(1 - \bar{C}_{12}^2) - K_{21}\bar{C}_{12}(1 - \bar{C}_{13}) + K_{13}(\bar{C}_{12}^2 - \bar{C}_{13})]/D \tag{87a}$$

$$m_{22} = \beta_2 + [K_{22}(1 + \bar{C}_{13}) - 2K_{12}\bar{C}_{12}](1 - \bar{C}_{13})/D \tag{87b}$$

$$m_{12} = m_{32} = (K_{12} - K_{22}\bar{C}_{12})(1 - \bar{C}_{13})/D \tag{87c}$$

$$m_{13} = m_{31} = [K_{13}(1 - \bar{C}_{12}^2) - K_{21}\bar{C}_{12}(1 - \bar{C}_{13}) + K_{11}(\bar{C}_{12}^2 - \bar{C}_{13})]/D \tag{87d}$$

$$m_{21} = m_{23} = [K_{21}(1 + \bar{C}_{13}) - (K_{11} + K_{13})\bar{C}_{12}](1 - \bar{C}_{13})/D \tag{87e}$$

$$D = (1 - \bar{C}_{13})(1 + \bar{C}_{13} - 2\bar{C}_{12}^2). \tag{87f}$$

The three eigenvalues and eigenvectors have been calculated in [10], [11], and are given here:

$$\gamma_1 = \frac{\phi + \psi}{2} \tag{88a}$$

$$\gamma_2 = m_{11} - m_{13} \tag{88b}$$

$$\gamma_3 = \frac{\phi - \psi}{2} \tag{88c}$$

where

$$\phi = m_{11} + m_{13} + m_{22} \tag{88d}$$

$$\psi = \sqrt{(m_{11} + m_{13} - m_{22})^2 + 8m_{12}m_{21}} \tag{88e}$$

and

$$a^{(1)} = \begin{bmatrix} 1 \\ (2m_{22} - \phi + \psi)/2m_{12} \\ 1 \end{bmatrix} \tag{89a}$$

$$a^{(2)} = \begin{bmatrix} 1 \\ 0 \\ -1 \end{bmatrix} \tag{89b}$$

and

$$a^{(3)} = \begin{bmatrix} 1 \\ (2m_{22} - \phi - \psi)/2m_{12} \\ 1 \end{bmatrix}. \tag{89c}$$

It is straightforward to show that these three eigenvectors satisfy the general orthogonality relation (57) by direct substitutions. Notice that the formulation in [8]–[11] does not satisfy this condition since in general $C_{12} \neq C_{21}$.

Finally, let us consider an excitation with the boundary condition at $z = 0$ given by

$$a(0) = \begin{bmatrix} 0 \\ 1 \\ 0 \end{bmatrix}. \tag{90}$$

The general solution at z is [10], [11]

$$a(z) = Ae^{i\Gamma z}A^{-1}a(0). \tag{91}$$

Here, the matrix A is given by the three eigenvectors from (89a)–(89c). (Note that our definition of A is the inverse of that in [10] and [11] with some typos corrected.)

$$A = [a^{(1)}, a^{(2)}, a^{(3)}]. \tag{92}$$

The results of $Ae^{i\Gamma z}A^{-1}$ have been calculated in [10] and [11]. The solution at position z is

$$a_1(z) = a_3(z) = i\frac{2m_{12}}{\psi}\sin\frac{\psi z}{2}e^{i\phi z/2} \tag{93a}$$

$$a_2(z) = \left[\cos\frac{\psi z}{2} + i\frac{(2m_{22} - \phi)}{\psi}\sin\frac{\psi z}{2}\right]e^{i\phi z/2}. \tag{93b}$$

The total guided power is given by

$$P(z) = \mathrm{Re}\,[a^+(z)\,Ca(z)]$$

$$= a^+(z)\,\tilde{C}a(z) = 1 + F\sin^2\frac{\psi z}{2} \tag{94}$$

where the factor F is given by

$$F = \frac{8m_{12}}{\psi^2}[m_{12}(1 + \tilde{C}_{13}) - m_{21} + \tilde{C}_{12}(m_{22} - m_{11} - m_{13})]. \tag{95}$$

For a lossless system, the power conservation requires that $P(z)$ be independent of the position z. Thus the factor F provides a check of the energy conservation. Although it has been shown before that our formulation satisfies the energy conservation exactly by using the fact that the two matrices $\tilde{C}$ and $\tilde{Q}$ are hermitian, one can also see from the reciprocity relation (85) substituted into (95) that F is indeed zero provided that we choose $E_t^{(p)}$ and $H_t^{(p)}$ to be real functions for a lossless system. Therefore, $C_{pq} = \bar{C}_{pq}$ = real. Numerical results will be given in the next section. The factor F from two previous methods [4], [10] will also be calculated.

VI. A Numerical Example and Discussions

In this section, we illustrate our theory by a numerical example [10] and compare it with those of two previous methods [4], [10]. We consider three coupled waveguides with the two outside waveguides identical and symmetric with respect to the center waveguide (Fig. 3). Using the theoretical results discussed in Section V-B, we calculate K_{pq}, C_{pq}, and β_p. The analytical relation (47) is used to check the numerical accuracies of these quantities. We show in Fig. 4(a) the three eigenvalues γ_1, γ_2, and γ_3 from (88a)–(88c), which are the propagation constants of the three supermodes, versus the separation t between the waveguides. We compare our results (dotted line) and the exact solutions (solid lines) of the multilayered structure in Fig. 4(a) and those of the method in [10] (dashed lines), the method in [4] (crosses) in Fig. 4(b). We see clearly that the results using the method in [10] and our theory agree very well with the exact calculation. There is a slight error for the third eigenvalue γ_3 near cutoff where the separation t is reduced to near 0.2 μm. In our calculation, we choose the same parameters as in [10], $n = 3.4$, $n_1 = 3.6$, $n_2 = 3.63$, $d_1 = d_2 = 0.15$ μm, and t varies. The method of [4] clearly has larger errors in γ_1 and γ_3, especially γ_3 deviates from the exact results over a wide range of t near cutoff. The result of γ_2 using three methods agree with each other very well because

$$\gamma_2 = m_{11} - m_{13} = \beta_1 + (K_{11} - K_{13})/(1 - \bar{C}_{13}) \tag{96}$$

using (87) and (88). Since $\bar{C}_{13}$ and $(K_{11} - K_{13})$ are very small, ($\bar{C}_{13} = 0.136 \sim 0.00436$ and $(K_{11} - K_{13}) = -0.0237 \sim -0.0004$ $(1/\mu\mathrm{m})$ at $t = 0.2$ μm ~ 0.6 μm),

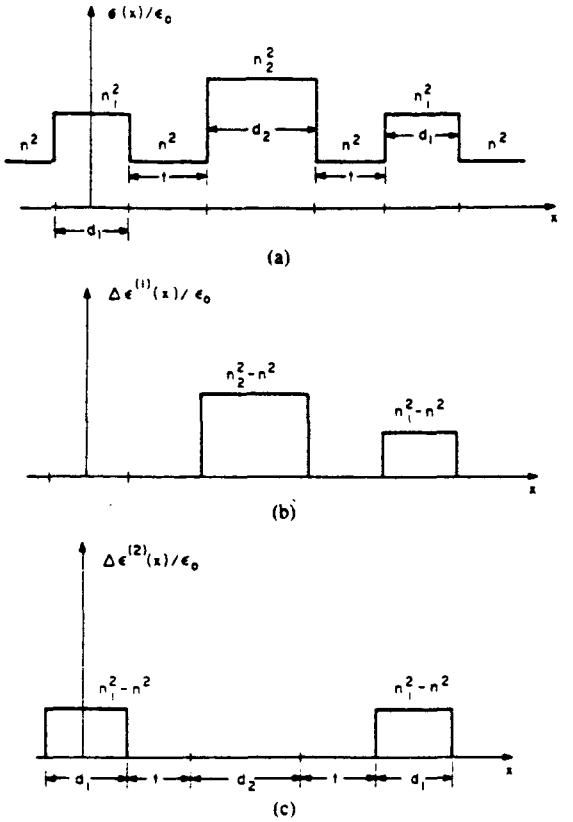

Fig. 3. Three coupled waveguides under investigation. (a) $\epsilon(x)/\epsilon_0$ for the three-waveguide system. (b) $\Delta\epsilon^{(1)}(x)/\epsilon_0$. (c) $\Delta\epsilon^{(2)}(x)/\epsilon_0$.

if we have $\bar{C}_{13} = 0$ (theory of [4]) the difference is negligible. Since $C_{13} = C_{31} = \bar{C}_{13}$, the theory of [10] gives the same results for γ_2 as the results of this paper.

In Fig. 5, we show the power conservation violation factor F for the initial excitation at the center waveguide, $a(0)$ = column (0, 1, 0). We see clearly that our results indeed satisfy the power conservation very well and F is always zero. The factor F calculated from [10] is always very small (less than 0.08 percent), but F calculated from [4] can be as much as 42 percent.

Numerically speaking, our results are as good as or slightly better than those obtained from [10]. The new features are that our formulation is derived using a simpler approach, and it satisfies both the reciprocity theorem and the power conservation law analytically, while [8]–[11] can only show numerically that their method satisfies the power conservation and the reciprocity theorem approximately. (One should note that power conservation and reciprocity are only satisfied self-consistently and not exactly since the modal expansions (11) of the fields are approximate.) Our formulation also leads to the general orthogonality relations (38) and (57) with the overlap integrals properly taken into account, that cannot be obtained from the formulation in [8]–[11]. By setting the matrix $\bar{C}$ or $\tilde{C}$ to be the identity matrix, the coupled-mode equations and the orthogonality relations all reduce to the results of a conventional analysis [4]. Our numerical results also show that ignoring the overlap integrals does

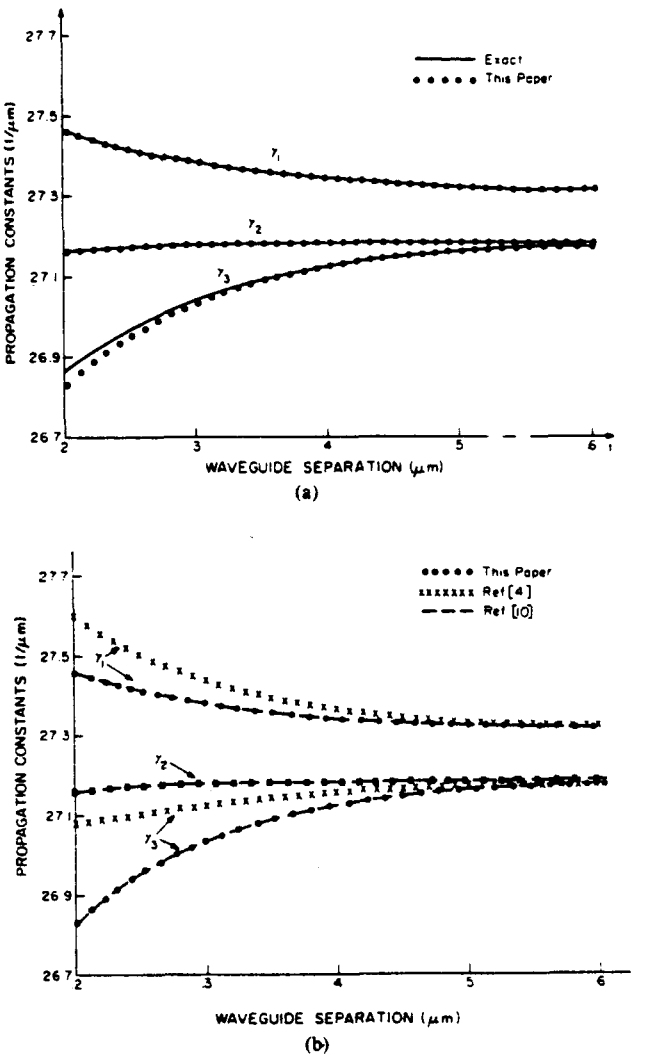

Fig. 4. (a) A comparison of the propagation constants of the three supermodes between the exact results (solid lines) and the results of this paper (dotted lines) for the three coupled waveguides in Fig. 3. (b) A comparison with other two methods: results using [10] (dashed lines), results using [4] (crosses). The results of this paper are given by dotted lines.

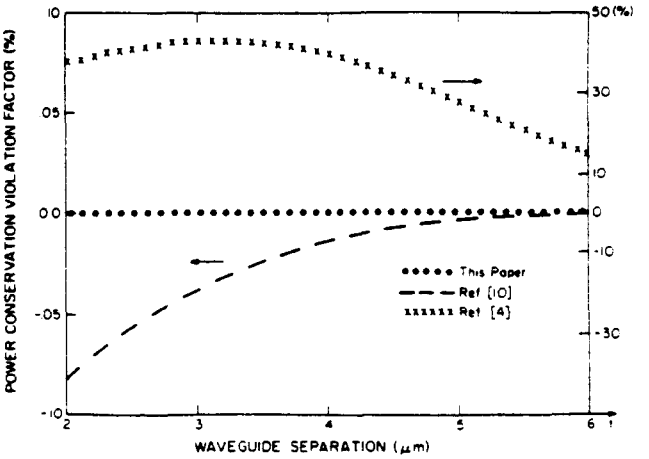

Fig. 5. The power conservation violation factor F for an excitation at the center waveguide of Fig. 3. The results of F using [10] (dashed line), and results of this paper (dotted line) are shown using the left scale, and the results of [4] (crosses) follow the right scale.

lead to erroneous results violating the power conservation significantly as has also been pointed out in [8] and [12].

VII. Conclusions

Two sets of coupled-mode equations for a multiwaveguide system have been derived using a generalized reciprocity relation, one set for a lossless, and the other for a lossy or lossless system. New general orthogonality relations between the eigenvectors of the supermodes have been derived. We have derived the conditions on the matrix elements for the reciprocity theorem and the power conservation laws and have shown that our formulations do indeed satisfy those conditions analytically.

References

[1] E. Kapon, J. Katz, and A. Yariv, "Supermode analysis of phase-locked arrays of semiconductor lasers," *Opt. Lett.*, vol. 9, pp. 125–127, 1984.

[2] L. A. Molter-Orr and H. A. Haus, "$N \times N$ coupled waveguide switch," *Opt. Lett.*, vol. 9, pp. 466–467, 1984.

[3] A. Yariv, "Coupled-mode theory for guided-wave optics," *IEEE J. Quantum Electron.*, vol. QE-9, pp. 919–933, 1973.

[4] H. F. Taylor and A. Yariv, "Guided wave optics," *Proc. IEEE*, vol. 62, pp. 1044–1060, 1974.

[5] Y. Suematsu and K. Kishino, "Coupling coefficient in strongly coupled dielectric waveguides," *Radio Sci.*, vol. 12, pp. 587–592, 1977.

[6] E. Marom, O. G. Ramer, and S. Ruschin, "Relation between normal-mode and coupled-mode analyses of parallel waveguides," *IEEE J. Quantum Electron.*, vol. QE-20, pp. 1311–1319, 1984.

[7] B. Broberg, B.S. Lindgren, M. Öberg, and H. Jiang, "A novel integrated optics wavelength filter in InGaAsP-InP," *J. Lightwave Technol.*, vol. LT-4, pp. 196–203, 1986.

[8] A. Hardy and W. Streifer, "Coupled-mode theory of parallel waveguides," *J. Lightwave Technol.*, vol. LT-3, pp. 1135–1146, 1985.

[9] A. Hardy and W. Streifer, "Analysis of phased array diode lasers," *Opt. Lett.*, vol. 10, pp. 335–337, 1985.

[10] A. Hardy and W. Streifer, "Coupled-modes of multiwaveguide systems and phased arrays," *J. Lightwave Technol.*, vol. LT-4, pp. 90–99, 1986.

[11] A. Hardy and W. Streifer, "Coupled-mode solutions of multiwaveguide systems," *IEEE J. Quantum Electron.*, vol. QE-22, pp. 528–534, 1986.

[12] S. L. Chuang, "A Coupled-mode formulation by reciprocity and a variational principle," *J. Lightwave Technol.*, this issue, p. 5.

[13] H. Kogelnik, "Theory of dielectric waveguides," in *Integrated Optics*, T. Tamir, Ed., 2nd ed. New York: Springer-Verlag, 1979, ch. 2.

[14] R. F. Harrington, *Time-Harmonic Electric Fields*. New York: McGraw-Hill, 1961.

[15] R. E. Collin, *Foundations for Microwave Engineering*. New York: McGraw-Hill, 1966.

[16] F. B. Hildebrand, *Methods of Applied Mathematics*, 2nd ed. Englewood Cliffs, NJ: Prentice-Hall, 1965, ch. 1.

[17] H. A. Haus, W. P. Huang, S. Kawakami, and N. A. Whitaker, "Coupled-mode theory of optical waveguides," to be published.

*

Shun-Lien Chuang (S'78-M'82) was born in Taiwan in 1954. He received the B.S. degree in electrical engineering from National Taiwan University in 1976, and the M.S., E.E., and Ph.D. degrees in electrical engineering from the Massachusetts Institute of Technology in 1980, 1981, and 1983, respectively.

While in graduate school, he held Research and Teaching Assistantships, and also served as a Recitation Instructor. He conducted research at Schlumberger-Doll Research in Ridgefield, CT, during the summers of 1981 and 1982 and also in 1983 as a Member of the Professional Staff. He is now an Assistant Professor in the Department of Electrical and Computer Engineering at the University of Illinios at Urbana-Champaign. He is conducting research in electromagnetics, integrated optics, and semiconductor devices including superlattice photodetectors and microwave transistors. He teaches courses on Electromagnetics and Solid-State Electronic Devices. He has been cited several times in the list for Excellence in Teaching. He recently developed a new graduate course on Integrated Optics and Optoelectronics.

Dr. Chuang is a member of the Optical Society of America, Sigma Xi, and the American Physical Society.

ORIGINAL PAGE IS
OF POOR QUALITY

Appendix G

S. L. Chuang, "Application of the strongly coupled-mode theory to integrated optical devices," IEEE J. Quantum Electronics, to appear in May, 1987.

APPLICATION OF THE STRONGLY COUPLED-MODE THEORY TO INTEGRATED OPTICAL DEVICES

S. L. Chuang
University of Illinois at Urbana-Champaign
Department of Electrical and Computer Engineering
Urbana, Illinois 61801

ABSTRACT

A theory for strongly coupled waveguides is discussed and applied to two- and three-waveguide couplers and optical wavelength filters. This theory makes use of an exact analytical relation governing the coupling coefficients and the overlap integrals. It removes almost all of the constraints imposed by a simpler and approximate coupled-mode theory by Marcatili. It also satisfies the energy conservation and the reciprocity theorem self-consistently. We show very good numerical results with the overlap integral as large as 49 percent. The applications to electrooptical modulators, power dividers, power transfer devices, and optical filters are all presented with numerical results.

1. INTRODUCTION

The applications of the coupled-mode theory in integrated optical devices, such as waveguide couplers [1] - [3], laser arrays [4], [5], and optical filters [6] - [8], have been well known. However, theoretical improvements for strongly coupled waveguides have only been attempted very recently [9] - [14]. A simple and approximate version of coupled-mode equations for parallel dielectric waveguides has also been presented by Marcatili [15] to account for the asymmetric properties of waveguides using a newly found relation between the coupling coefficients and the overlap integral of two coupled waveguides. A few conditions are assumed in that paper:

(1) A scalar formulation of the fields is considered.

(2) The refractive index perturbation is very small such that second-order terms can be ignored.

$$\begin{aligned} n^2 &= n_0^2[1 + \Delta_a(x,y) + \Delta_b(x,y)]^2 \\ &\approx n_0^2[1 + 2\Delta_a(x,y) + 2\Delta_b(x,y)] \end{aligned} \tag{1}$$

Thus the new relation between the two coupling coefficients in [15] is only approximate.

(3) The overlap integral c is assumed to be small (weakly coupling) and is not included in the coupled-mode equations because the coupled-mode equations in [15] are almost the same as those for the conventional theory [2] without including the overlap integrals in the four coupling parameters, γ_a, γ_b, K_{ab} and K_{ba}.

In this paper, we apply the theory developed in [9] - [14] and show that all the above conditions are not required. It is shown that an exact analytical

relation governing the coupling coefficients, the overlap integrals and the propagation constants derived in [13] using a generalized reciprocity theorem can be combined with the formulation of Marcatili and will give very good numerical results even for strongly coupled waveguides. It has been pointed out in [9] that the four parameters γ_a, γ_b, K_{ab} and K_{ba} should include the overlap integrals to obtain correct propagation constants of the supermodes. Since only β_a, β_b of individual waveguides and K_{ab}, K_{ba} of the conventional coupling coefficients are used in the coupled-mode equations in [15], that theory will not yield accurate numerical results and may violate energy conservation significantly [9], [13] unless the overlap integral $c \ll 1$ which is assumed in [15].

In Section 2, we briefly review the strongly coupled-mode equations derived in [9] - [11], [13] and [14], their orthogonality relation, and an exact relation between the coupling coefficients K_{ab} and K_{ba}. We also show that this exact relation can also be derived from power conservation or reciprocity relation for a lossless medium. In Section 3, we consider the two coupled waveguides combining the strong coupling of mode equations and the formulation of [15] and illustrate the electrooptic effect. We then study the three waveguide couplers as power transfer devices and power dividers. Previous studies in [16] and [17] assume all three guides have the same refractive indices, and a direct numerical approach for the multilayered structure is taken. In Section 4, the cross-talk problems for both two and three coupled waveguides are investigated. Numerical results are presented and compared with those in [18] and [19]. In Section 5, the application of the coupled-mode theory to the optical wavelength filters is studied and the theoretical results are compared with the experimental results in [8]. Finally, we give conclusions in Section 6.

2. THEORY OF STRONGLY COUPLED WAVEGUIDES

Three very similar formulations of strongly coupled waveguides have been presented in [9], [12], [13]. The formulation by Haus et al. [12] is limited to the lossless system and has a small difference in the z-component of the electric field for the trial functions in the variational approach. The formulation of Hardy-Streifer [9] does not satisfy energy conservation and the reciprocity theorem and still contains a small error, while the theory of [13] (which was derived in a much simpler way) satisfies these laws analytically. Independently, a reformulation of [9] has been made [20] recently and is identical to that of [13] after the modifications. The coupled-mode equation in [13], [14] and its properties are summarized below.

2.1 Strongly Coupled-mode Equation

The coupled-mode equation in vector form is given [13], [14], [20] by

$$\bar{\mathbf{C}} \frac{d}{dz} \mathbf{a}(z) = \mathbf{Q}\mathbf{a}(z) \tag{2}$$

or

$$\frac{d}{dz} \mathbf{a}(z) = \mathbf{M}\mathbf{a}(z) \tag{3}$$

where

$$\mathbf{Q} = \mathbf{C}\mathbf{B} + \mathbf{K} \tag{4}$$

$$\mathbf{M} = \bar{\mathbf{C}}^{-1}\mathbf{Q} = \mathbf{B} + \bar{\mathbf{C}}^{-1}\mathbf{K} \tag{5}$$

where the vector $\mathbf{a}(z)$ has each element $a_p(z)$ given by the electric field amplitude for the transverse component of the mode in waveguide p, and the matrix elements $\bar{C}_{pq}$ and K_{pq} are defined in Appendix A. The matrix $\mathbf{B}$ is a diagonal

matrix with the diagonal elements given by β_1, β_2, ..., β_N of each individual waveguide in the absence of all other waveguides. It should be noted that (1) the two matrices $\bar{C}$ and Q are symmetric [13], [14], [20] and that is very important to prove the orthogonality property of the supermodes, and (2) the matrix M is not necessarily symmetric in general.

2.2 Orthogonality of the Supermodes

The supermodes of the multiwaveguide system satisfy the orthogonality relation [14] for symmetric matrices $\bar{C}$ and Q in Eq. (2)

$$\mathbf{a}^{(i)T}\,\bar{C}\mathbf{a}^{(j)} = 0 \quad \text{for } \gamma_i \neq \gamma_j \tag{6}$$

where $\mathbf{a}^{(i)}$ ($\mathbf{a}^{(j)}$) is the eigenvector of the supermode with the propagation constant γ_i (γ_j), and the superscript T denotes the transpose of the matrix or vector.

2.3 Reciprocity Condition

To satisfy the reciprocity relation, one finds that [14]

$$\bar{C}M = (\bar{C}M)^T \quad , \tag{7}$$

i.e., the matrix Q must be symmetric which is true as derived in [14]. For two coupled waveguides,

$$M = \begin{bmatrix} \gamma_a & K_{ab} \\ K_{ba} & \gamma_b \end{bmatrix} \quad . \tag{8}$$

Equations (7) and (8) give

$$K_{ab} - K_{ba} = (\gamma_a - \gamma_b)\bar{c} \tag{9}$$

where $\bar{c} = \bar{C}_{12} = \dfrac{C_{12} + C_{21}}{2}$ (see Appendix A). The above formulation is true in

general for both lossy and lossless systems. If the system is lossless, one may also have a slightly different formulation as presented in [12], [14] using field quantities involving complex conjugates.

2.4 Power Conservation

If the multiwaveguide system is lossless, one can choose the transverse field components $\mathbf{E}_t$ and $\mathbf{H}_t$ to be real functions and find that $\mathbf{E}_z$ and $\mathbf{H}_z$ are purely imaginary and C_{pq} and K_{pq} are real [14]. The total power guided by the multiwaveguide system is

$$\begin{aligned} P(z) &= \frac{1}{2}\,\mathrm{Re}\iint \mathbf{E}_t \times \mathbf{H}_t^{*}\cdot\hat{z}\,dxdy \\ &= \mathbf{a}^{+}(z)\overline{\mathbf{C}}\mathbf{a}(z) \end{aligned} \tag{10}$$

where the superscript + denotes the conjugate and transpose of the vector a(z), and one has chosen $\mathbf{E}_t^{(q)}$ and $\mathbf{H}_t^{(p)}$ to be real. Thus using the fact that $\overline{\mathbf{C}}$ and Q are real matrices, one finds that the condition $\frac{dP(z)}{dz} = 0$ also leads to $Q = Q^T$ or $\overline{\mathbf{C}}\mathbf{M} = (\overline{\mathbf{C}}\mathbf{M})^T$, which is the same as the reciprocity condition in (7). Actually, condition (7) is very general since it is applicable to both lossy and lossless cases. A similar formulation (for a lossless medium) leads to the fact that Q is Hermitian provided one uses complex conjugate quantities with $\overline{\overline{C}}_{pq}$ and $\overline{\overline{C}}_{pq}$ matrices as defined in [14]. The Hermitian matrix becomes obviously symmetric when it is real. Another derivation of the lossless condition for two coupled waveguides is shown in Appendix B, which also leads to Eq. (9) when γ_a, γ_b, K_{ab}, K_{ba} are real.

3. TWO AND THREE COUPLED WAVEGUIDES AND IMPROVEMENT OF MARCATILI'S THEORY

In this section, we present a combination of the vector formulation for strongly coupled waveguides and Marcatili's theory which assumes two weakly coupled waveguides. We also discuss the applications to three coupled waveguides used as either power transfer devices transferring power from one outer guide to another or as power dividers. The electrooptic effects when these devices are used as modulators are discussed.

3.1 Two Coupled Waveguides

3.1.1 Improvement of Marcatili's formulation

We start with the coupled-mode equations

$$\frac{da}{dz} = i\gamma_a a + iK_{ab} b \tag{11a}$$

$$\frac{db}{dz} = i\gamma_b b + iK_{ba} b \tag{11b}$$

where

$$\gamma_a = \beta_1 + (K_{11} - \bar{C}_{12}K_{21})/(1 - \bar{C}_{12}^2) \tag{12a}$$

$$\gamma_b = \beta_2 + (K_{22} - \bar{C}_{12}K_{12})/(1 - \bar{C}_{12}^2) \tag{12b}$$

$$K_{ab} = (K_{12} - K_{22}\bar{C}_{12})/(1 - \bar{C}_{12}^2) \tag{12c}$$

$$K_{ba} = (K_{21} - K_{11}\bar{C}_{12})/(1 - \bar{C}_{12}^2) \tag{12d}$$

where the subscript 1 refers to waveguide a or 1, and 2 refers to waveguide b or 2, whichever is convenient.

One notes that in the theory of Marcatili [15], (1) $\bar{C}_{12}$ is assumed to be zero in the above four parameters, (2) K_{11} and K_{22} are ignored, and (3) K_{12} and K_{21} are defined only for scalar fields (pure TE case). Thus that formulation is almost the same as that for the conventional theory [2] and will lead to significant errors if $\bar{C}_{12}$ becomes larger than, say, 10 percent (C_{11} and C_{22} are normalized to be 1) [9], [13]. One notes that an exact relation holds between the conventional coupling coefficients [13],

$$K_{12} - K_{21} = (\beta_1 - \beta_2) \frac{C_{12} + C_{21}}{2} \quad , \tag{13}$$

while a similar relation found in [15] is only approximate since the derivations there have assumed the refractive index variation $\Delta_a(x,y)$ and $\Delta_b(x,y) \ll 1$ (which is a good practical approximation). Using this relation, one can show that the following relation is true using (12), (13) and $\bar{c} = \bar{C}_{12} = \bar{C}_{21}$,

$$K_{ab} - K_{ba} = (\gamma_a - \gamma_b)\bar{c} \quad , \tag{14}$$

which is precisely the reciprocity condition, and it is the same as the power conservation condition for a lossless case (Appendix B). We define the asynchronism factor [15] in terms of the more correct parameters γ_a, γ_b, K_{ab} and K_{ba} in (12a)-(12d).

$$\delta = \frac{\gamma_b - \gamma_a}{2\sqrt{K_{ab}K_{ba}}} \quad . \tag{15}$$

Given the initial excitation at $z = 0$ of a two-coupled waveguide, $a(0) = 1$, $b(0) = 0$, we obtain [9], [13]

$$a(\ell) = [\cos \psi\ell - i \frac{\Delta}{\psi} \sin \psi\ell]e^{i\phi\ell} \tag{16a}$$

$$b(\ell) = \frac{iK_{ba}}{\psi} \sin \psi\ell \; e^{i\phi\ell} \tag{16b}$$

where

$$\phi = \frac{\gamma_b + \gamma_a}{2} \tag{17a}$$

$$\psi = \sqrt{\Delta^2 + K_{ab}K_{ba}} \tag{17b}$$

$$\Delta = \frac{\gamma_b - \gamma_a}{2} \quad . \tag{17c}$$

It is easy to show also

$$\delta = \frac{1}{2\bar{c}} \left[\sqrt{\frac{K_{ba}}{K_{ab}}} - \sqrt{\frac{K_{ab}}{K_{ba}}} \right] \tag{18}$$

or

$$\sqrt{\frac{K_{ba}}{K_{ab}}} = \bar{c}\delta + \sqrt{1 + \bar{c}\delta} = e^{\sinh^{-1}\bar{c}\delta} \quad . \tag{19}$$

The solutions (16a) and (16b) can be written as

$$a(\ell) = \left\{ \cos \left[\sqrt{K_{ab}K_{ba}}\ell(1+\delta^2)^{1/2} \right] - i \frac{\delta}{(1+\delta^2)^{1/2}} \sin \left[\sqrt{K_{ab}K_{ba}}\ell(1+\delta^2)^{1/2} \right] \right\} e^{i\phi\ell} \tag{20a}$$

$$b(\ell) = i \frac{e^{\sinh^{-1}\bar{c}\delta}}{\sqrt{1+\delta^2}} \sin [\sqrt{K_{ab}K_{ba}}\ell \; (1+\delta^2)^{1/2}] \; e^{i\phi\ell} \quad . \tag{20b}$$

The output power P_a in waveguide a when waveguide b terminates at $z = \ell$ is obtained using

$$E_t(x,y,z = \ell) \approx a(\ell)E_t^{(a)}(x,y) + b(\ell)E_t^{(b)}(x,y) \tag{21a}$$

$$= \sum_{n=1}^{\infty} u_n^{(a)} E_t^{(a)n}(x,y) \tag{21b}$$

$$H_t(x,y,z = \ell) \approx a(\ell)H_t^{(a)}(x,y) + b(\ell)H_t^{(b)}(x,y) \tag{22a}$$

$$= \sum_{n=1}^{\infty} v_n^{(a)} H_t^{(a)n}(x,y) \tag{22b}$$

where the expansion in (21a) or (22a) is in terms of individual waveguide modes and in (21b) or (22b) is in terms of all the guided and radiation modes of waveguide a alone since they form a complete set [9]. Multiplying (21) by $H_t^{(a)}$ and integrating over the cross section, one obtains

$$u_1^{(a)} = a(\ell) + C_{12}b(\ell) \quad . \tag{23}$$

Similarly, one finds

$$v_1^{(a)} = a(\ell) + C_{21}b(\ell) \quad . \tag{24}$$

These boundary conditions at $z = 0$ and $z = \ell$ follow very closely those in [15]. The guided power due to the first mode β_1 in waveguide a is, thus,

$$P_a = \frac{1}{2} \mathrm{Re}\left[u_1^{(a)} v_1^{(a)*} \frac{1}{2} \iint E_t^{(a)1} \times H_t^{(a)1} \cdot \hat{z} dxdy\right]$$

$$= 1 - \left(\frac{1 - C_{12}C_{21}}{1 + \delta^2}\right) e^{2\sinh^{-1}c\delta} \sin^2 \left[\sqrt{K_{ab}K_{ba}}\,\ell(1 + \delta^2)^{1/2}\right] \tag{25}$$

using Eqs. (20), (23) and (24). A similar procedure for the output power in waveguide b when waveguide a is terminated at $z = \ell$ leads to

$$P_b = \mathrm{Re}[(C_{21}a + b)(C_{12}^{*}a^{*} + b^{*})]$$

$$= C_{12}C_{21} + \frac{1 - C_{12}C_{21}}{1 + \delta^2} \sin^2 \left(\sqrt{K_{ab}K_{ba}}\,\ell(1 + \delta^2)^{1/2}\right) \quad . \tag{26}$$

These results are very similar to those in [15] except the parameters are defined in terms of the more accurate parameters γ_a, γ_b, K_{ab} and K_{ba}.

3.1.2 Numerical results for two strongly coupled waveguides

In Figs. 1(a) - (d), we show numerical results for two coupled Ti-diffused $LiNbO_3$ channel waveguides modeled as two coupled slab waveguides (which is possible using the effective index method [11]) with the refractive index in waveguide a, $n_a = 2.2 + \frac{\Delta n}{2}$, the effective refractive index in waveguide b, $n_b = 2.2 - \frac{\Delta n}{2}$, where the refractive index difference

$$\Delta n = n_a - n_b \tag{27}$$

is proportional to the externally applied voltage V across the two waveguides. The refractive index outside the two waveguides is assumed to be constant, $n_0 = 2.19$. The waveguide dimensions are $d_a = d_b = 2$ μm; the edge-to-edge separation $t = 1.9$ μm. The wavelength λ is 1.06 μm. In Fig. 1(a), the asynchronism δ is plotted versus the refractive index difference. We see clearly that $|\delta|$ is linearly proportional to $|\Delta n|$. The overlap integrals C_{12} (dashed line) and C_{21} (dotted line) with their arithmetic average $\bar{c}$ (solid line) are shown in Fig. 1(b), where they vary between 0.168 at $\Delta n = 0$ to around 0.178 which do not satisfy the condition in [15] for weak coupling ($c \lesssim 0.1$).

The numerical results for the propagation constants are calculated with more than 7 digits of accuracy, and the energy conservation law [14] is also checked to be valid with errors always less than 10^{-7}. (In [14], two energy conservation violation factors have been defined and are used to check the numerical accuracy of the results.) Figure 1(b) differs slightly from the qualitative drawing of [15] with a range of variation in the overlap integrals around (0.178 - 0.168)/0.168 ≈ 6.0 percent. The coupling coefficients K_{ab}, K_{ba}, and $\sqrt{K_{ab}K_{ba}}$ are shown in Fig. 1(c), which agree well with the qualitative results of [15]. The output powers P_a (solid curve) and P_b (dashed curve) are shown in Fig. 1(c). They do agree very well with the qualitative drawing of [15]. One notes that the minimum of P_a does not occur right at $\Delta n = 0$ (where $P_b = 1.0$) due to the cross-talk problems which are discussed in Section 4. The power P_a actually goes to almost zero ($P_a = 0.00051 = 33$ dB) at $\Delta n \equiv -0.0002$, where P_b reduces to 0.9723. The asymmetry of P_a and the symmetric properties of P_b versus Δn or the applied voltage agree very well with what has been presented in [15]. However, our numerical approach provides very good numerical results even for the strongly coupled case with $\bar{c} > 0.1$, while the theory of [15], although taking into account the asymmetry properties of coupled waveguides, is limited to weak coupling cases.

3.2 Three Coupled Waveguides

Let us consider a symmetric case for which the two outer waveguides are identical. Solutions for this case have been obtained in [10], [11], and [14] and will not be derived here.

3.2.1 Power transfer devices

When used as power transfer devices, the three coupled waveguides are assumed to have an initial excitation at $z = 0$

$$a(0) = \begin{bmatrix} 1 \\ 0 \\ 0 \end{bmatrix} \tag{28}$$

and the input power P_{IN} is easily found to be 1.

The solutions at position z are found to be [10], [11]

$$a_1(z) = \frac{1}{2}\left\{\left(\cos\frac{\psi z}{2} - i\,\frac{2m_{22} - \phi}{\psi}\sin\frac{\psi z}{2}\right) e^{i\frac{\phi}{2}z} + e^{i\gamma_2 z}\right\} \tag{29a}$$

$$a_2(z) = i\,\frac{2m_{21}}{\psi}\sin\left(\frac{\psi z}{2}\right) e^{i\frac{\phi}{2}z} \tag{29b}$$

and

$$a_3(z) = \frac{1}{2}\left\{\left[\cos\frac{\psi z}{2} - i\,\frac{2m_{22} - \phi}{\psi}\sin\frac{\psi z}{2}\right] e^{i\frac{\phi}{2}z} - e^{i\gamma_2 z}\right\} \tag{29c}$$

where

$$\psi = \sqrt{(m_{11} + m_{13} - m_{22})^2 + 8m_{12}m_{21}} \tag{30a}$$

$$\phi = m_{11} + m_{13} + m_{22} \tag{30b}$$

and the three propagation constants of the supermodes are

$$\gamma_1 = \frac{\phi + \psi}{2} \tag{31a}$$

$$\gamma_2 = m_{11} - m_{13} \tag{31b}$$

$$\gamma_3 = \frac{\phi - \psi}{2} \tag{31c}$$

where the matrix elements m_{ij} have been derived in [10], [11], and [14].

The output power in waveguide 1 at $z = \ell$, where waveguides 2 and 3 terminate, is

$$P_{out,1} = Re\{[a_1(\ell) + C_{12}a_2(\ell) + C_{13}a_3(\ell)][a_1(\ell) + C_{21}a_2(\ell) + C_{31}a_3(\ell)]^*\} \tag{32}$$

following a similar procedure as in Eqs. (21) - (26). The output power at waveguide 3 when waveguides 1 and 2 terminate at $z = \ell$ is

$$P_{out,3} = Re\{[C_{31}a_1(\ell) + C_{32}a_2(\ell) + a_3(\ell)][C_{13}a_1(\ell) + C_{23}a_2(\ell) + a_3(\ell)]^*\} \quad . \tag{33}$$

When applying (32) and (33) to a power transfer device, one may need to assume $|C_{13}|$ and $|C_{31}|$ are small since waveguides 1 and 3 are not terminated.

3.2.2 Power dividers

When used as power dividers, the three coupled waveguides have an initial excitation at $z = 0$,

$$\mathbf{a}(0) = \begin{bmatrix} 0 \\ 1 \\ 0 \end{bmatrix} \tag{34}$$

and the input power P_{IN} can be found to be 1. The solutions at position z are [10], [14]

$$a_1(z) = a_3(z) = i\frac{2m_{12}}{\psi} \sin\frac{\psi z}{2} e^{i\frac{\phi}{2}z} \tag{35a}$$

$$a_2(z) = \left[\cos\frac{\psi z}{2} + i\frac{2m_{22} - \phi}{\psi} \sin\frac{\psi z}{2}\right] e^{i\frac{\phi}{2}z} \quad . \tag{35b}$$

One finds the output powers in waveguide 1 and 3 to be equal using (35) in (32) or (33) since the two outer guides are identical.

3.2.3 Numerical results for power transfer devices and power dividers

The three coupled waveguides considered here are assumed to be symmetric with respect to the center guide. We assume the dimensions of the three waveguides to be $d_1 = d_2 = d_3 = 2$ μm. The edge-to-edge separation of two nearby waveguides $t = 1.9$ μm. The wavelength λ is 1.06 μm. The refractive indices are assumed to be

$$n_1 = n_3 = 2.2 + \frac{\Delta n}{2} \tag{36a}$$

$$n_2 = 2.2 - \frac{\Delta n}{2} \tag{36b}$$

where the refractive index difference between either one of the outer guides and the center guide $\Delta n = n_1 - n_2$ is proportional to the applied voltage V. We first plot the unnormalized asynchronism $2\gamma_2 - \gamma_1 - \gamma_3$ versus the refractive index difference Δn. One sees clearly at $\Delta n = 0$ the fact that all three guides are identical does not imply the synchronism condition

$$2\gamma_2 - \gamma_1 - \gamma_3 = 0 \tag{37}$$

is met. At $\Delta n = 0$, we find

$$\gamma_1 = 13.0172261$$

$$\gamma_2 = 13.0138696$$

$$\gamma_3 = 13.0094738$$

and

$$2\gamma_2 - \gamma_1 - \gamma_3 = 0.0010393.$$

Choosing the coupling length ℓ to be fixed at $L_{C0} = 2\pi/\psi_0$ where

$$\psi_0 = (\gamma_1 - \gamma_3) \text{ at } \Delta n = 0 \tag{38}$$

we find the output powers $P_{out,1}$ (solid curve) and $P_{out,3}$ (dashed curve) as shown in Fig. 2(b) when the waveguides are used as power transfer devices. Peak power transfer from guide 1 to guide 3 actually does not occur at $\Delta n = 0$ as can be seen from Fig. 2(b). This is due to the cross-talk problem when the synchronism condition is not met. It occurs actually at $2\gamma_2 - \gamma_1 - \gamma_3 = 0$, i.e., when $\Delta n \cong -0.00023$. The cross talks are calculated in Section 4. When used as power dividers, the three coupled waveguides are assumed to have a coupling length $\ell = \pi/\psi_0 = L_{C0}/2$. The output powers in guides 1 and 3 versus the refractive index difference Δn are shown in Figure 2(c). Maximum output power does occur at $\Delta n = 0$ for the power dividers.

In Figs. 3(a) and 3(b), we show the output powers $P_{out,1}$ and $P_{out,3}$ versus the coupling distance ℓ normalized to $L_C = 2\pi/(\gamma_1 - \gamma_3)$ for $\Delta n = 0$ ($L_C = L_{C0}$ in this case). Since the synchronism condition is not met, $P_{out,1}$ does not go to zero due to the cross-talk problems. Both $P_{out,1}$ and $P_{out,3}$ do not show periodic behaviors for the power transfer devices that have been discussed in [10], [11], although only the magnitudes of $|a_1(\ell)|$, $|a_2(\ell)|$ or $|a_3(\ell)|$ instead of powers are presented there. This nonperiodic behavior is due to the asynchronism ($2\gamma_2 - \gamma_1 - \gamma_3 \neq 0$) of the three supermodes. When this condition is met (it occurs at $\Delta n = -0.00023$), $P_{out,1}$ and $P_{out,3}$ do show periodic behaviors as shown in Fig. 4(a), where $L_C = 2\pi/(\gamma_1 - \gamma_3)$ is evaluated at that $\Delta n \neq 0$. However, the output powers for the power dividers always show periodic functions because of the symmetry of the excitation and the waveguide structure (only two of the three supermodes, γ_1 and γ_3, are excited). It is easy to see

from Eq. (35) that the output powers will be periodic functions of the distance ℓ for both Figs. 3(b) ($2\gamma_2 - \gamma_1 - \gamma_3 \neq 0$) and 4(b) ($2\gamma_2 - \gamma_1 - \gamma_3 = 0$).

4. CROSS-TALK PROBLEMS

Cross-talk problems have been investigated recently for two coupled waveguides [18] and three coupled waveguides [19] using either the conventional coupled-mode theory or direct numerical approach for the propagation constants. We apply the strongly coupled mode equations here to investigate the cross-talk problems.

4.1 Cross Talks in Two Coupled Waveguides

In the design of two coupled waveguides, one usually chooses the coupling length ℓ such that

$$\psi\ell = n\pi/2 \quad , \quad n = \text{odd integer} \tag{39}$$

and $b(\ell)$ is maximum, $a(\ell) = 0$ provided that $\Delta = 0$, i.e., two waveguides are identical. One finds immediately that the output power in waveguide b is maximum. However, the output power in waveguide a is not zero because there is still an overlap of fields between modes in waveguides a and b. This cross-talk power is easily obtained by setting $\delta = 0$ in Eq. (25) as a conservative estimation [18]

$$\text{Extinction ratio} = P_a(\delta = 0) = C_{12}C_{21} = \overline{C}_{12}^{\,2} \tag{40}$$

since $C_{12} = C_{21}$ when two waveguides are identical. The formula (40) only provides a conservative estimation since it assumes waveguide a continues. In reality, guides a and b may start to separate at $z = \ell$ gradually. Thus, (40) is only an approximation [18].

This result showing that the cross talk is proportional to the square of the overlap integral agrees with that obtained in [18]. However, our numerical

calculations show that for two-coupled GaAs waveguides with the dimensions $d_a = d_b = 2$ μm, the edge-to-edge separation $t = 1.9$ μm, the refractive indices $n_a = n_b = 3.44$, and the outside refractive index $n_0 = 3.436$, the cross talk is -10 dB, which is close to -12.6 dB of [18] but not identical. We believe our number here is more accurate since we have calculated the propagation constants β_1 and β_2 up to 7 digits (after the decimal point) of accuracy; the power conservation and the exact analytical relations are all checked so that the errors are always less than 10^{-7}. The studies of cross talks in [18], [19] assume identical waveguides and the refractive indices are fixed ($\Delta n = 0$). One finds using Fig. 1(d) that the cross talk P_a can actually be given by Eq. (25). At $\Delta n \simeq -0.0002$, the extinction ratio goes to zero! Thus a very good extinction ratio can be obtained with a slight asymmetry introduced in the two waveguides with $\Delta n \neq 0$.

4.2 Cross Talks in Three Coupled Waveguides

Three coupled waveguides have been introduced to decrease the cross talks when used as power transfer devices from one outer waveguide to another. However, the synchronism condition

$$2\gamma_2 - \gamma_1 - \gamma_3 = 0$$

needs to be satisfied; otherwise, the cross talks may be proportional to the overlap integrals C_{12} and C_{23} of the two nearby modes instead of the two outer guided modes C_{13}. When used as power transfer devices, one chooses

$$\ell = 2\pi/(\gamma_1 - \gamma_3) = 2\pi/\psi \tag{41}$$

or an integral multiple of ℓ such that $a_2(\ell) = 0$. We find the extinction ratio to be (using $\sin \psi\ell = 0$)

$$\text{Extinction ratio} = P_{out,1}$$

$$= \sin^2\left[\frac{2\gamma_2 - \gamma_1 - \gamma_3}{4}\ell\right] + C_{13}^2 \cos^2\left[\frac{2\gamma_2 - \gamma_1 - \gamma_3}{4}\ell\right]$$

$$= \sin^2\left[\frac{2\gamma_2 - \gamma_1 - \gamma_3}{2(\gamma_1 - \gamma_3)}\pi\right] + C_{13}^2 \cos^2\left[\frac{2\gamma_2 - \gamma_1 - \gamma_3}{2(\gamma_1 - \gamma_3)}\pi\right] \tag{42}$$

and similarly, the output power

$$P_{out,3} = \cos^2\left[\frac{2\gamma_2 - \gamma_1 - \gamma_3}{2(\gamma_1 - \gamma_3)}\pi\right] + C_{13}^2 \sin^2\left[\frac{2\gamma_2 - \gamma_1 - \gamma_3}{2(\gamma_1 - \gamma_3)}\pi\right] \tag{43}$$

This analytical result for cross talks is useful since it explains clearly

(1) If the synchronism condition is met,

$$2\gamma_2 - \gamma_1 - \gamma_3 = 0$$

$$\text{Extinction ratio} = C_{13}^2$$

which is expected.

(2) If the synchronism condition is not met, the first term will contribute, and it will be proportional to the square of its argument if the synchronism condition is only approximately met. For this case, we show directly numerical results instead of using the approximate analysis in [19].

In Figs. 5(a) - (d), we illustrate the numerical results for a three-coupled waveguide used as a power transfer device. The waveguide widths are $d_1 = d_2 = d_3 = 2$ μm, the refractive indices are $n_1 = n_2 = n_3 = 3.44$, and the outside refractive index $n_0 = 3.436$ [19]. The wavelength λ is 1.06 μm. The waveguides' edge-to-edge separations t are varied between 0.9 μm (near cutoff) to 4.4 μm. In Fig. 5(a), the propagation constants of the three supermodes using

the strongly coupled-mode theory are plotted and compared with those calculated exactly from solving the multilayered (slab) structure numerically. One finds very good agreement. A small discrepancy occurs for γ_3 when that mode is close to cutoff near t = 0.9 μm. The overlap integrals C_{12} (solid curve) and C_{13} (dashed curve) are plotted in Fig. 5(b) where C_{12} is as large as 0.49, i.e., coupling is indeed very strong. (C_{13} ≈ 0.125 at t = 0.9 μm is also large). The coupling length $L_c = 2\pi/(\gamma_1 - \gamma_3)$ is plotted in Fig. 5(c) versus the waveguide separation t. One finds the extinction ratio $P_{out,1}$ due to cross talks as shown in Fig. 5(d) decays as the waveguide separation t is increased. This has been discussed in [19] for a fixed separation t = 1.9 μm using a different approach. Our result, at that separation, gives $P_{out,1}$ = 0.1082 = -9.66 dB which is actually higher than -12 dB given in [19] where the overlap integral between the two outer guides C_{13} (= 0.0435) has been ignored. The results here should be more accurate since the exact propagation constants γ_1, γ_2, and γ_3 at t = 1.9 μm are calculated accurately up to 7 digits after the decimal point and are also confirmed by the strongly coupled-mode theory. Taking the ratio of the extinction ratio $P_{out,1}$ to the square of the overlap integral, C_{12}^2, one finds $P_{out,1}/C_{12}^2$ ≈ 0.78 at t = 0.9 μm; 1.08 at t = 1.9 μm; 1.42 at t = 2.9 μm, and 1.75 at t = 3.9 μm. Thus one may only say that the extinction ratio is roughly proportional to the square of the overlap integral C_{12}. The proportional constant estimated in [19] is ≈ $\pi^2/2$ = 4.9 for weak coupling and 4.9/3 ≈ 1.63 for strong coupling. The latter seems to agree better with our results since the coupling is pretty strong here. Thus the factor $\pi^2/2$ is not appropriate for the example presented in [19]. The strongly coupled-mode theory should be applied when numerical accuracy is essential.

5. OPTICAL WAVELENGTH FILTERS

Optical wavelength filters using waveguide couplers have been reported for $Ti:LiNbO_3$ and InGaAsP - InP materials. The $In_{1-x}Ga_xAs_yP_{1-y}$ - InP material system is especially interesting because of its applications at 1.3 μm or 1.55 μm wavelength and its potential for optoelectronic integrated circuits. The experiment reported in [8] has two coupled waveguides: one has a narrower guide width $d_a = 0.42$ μm, but a larger refractive index n_a (obtained following [21]) with $y_a = 0.127$; the other has the guide width $d_b = 0.91$ μm and $y_b = 0.078$ (n_b is also obtained following [21]). The Ga mole fraction x_a (or x_b) depends on the As mole fraction y_a (or y_b) for lattice matching [21]. The input power is assumed to be 1 in waveguide b. The results of a direct numerical approach have been shown in [8] and compared with the experimental data. We have applied the strongly coupled-mode theory using Eqs. (25) and (26) (exchanging a and b since the input is in guide b instead of in a) and compared our theoretical results with the experimental results in Fig. 6. The agreement is very similar to that in [8]. The parameters reported in [8] used for the theoretical calculations are within the measurement accuracy. No detailed explanations are given for the small discrepancy between the results for the theory and the experiment. We think the possible reasons may be (1) there is still some difference between the theoretical model in [21] and the experimental values for the refractive index, and (2) the losses in the waveguides are not taken into account. However, the comparison shown in Fig. 6 does show very good results.

6. CONCLUSIONS

A strongly coupled-mode theory [9] - [11], [13], [14] has been presented and combined with the theory of Marcatili [15] for the two coupled waveguide case. The applications to two- and three-waveguide couplers, including power transfer devices and power dividers, have been investigated. This coupled-mode theory is applicable to very general cases for parallel dielectric waveguides with strong coupling and modes of general polarizations. It also accounts for the asymmetry of the waveguides and satisfies the energy conservation law and the reciprocity theorem self-consistently [13], [14]. The cross-talk problems in two and three coupled waveguides and their applications as optical wavelength filters have also been investigated and compared with the experimental data [8].

ACKNOWLEDGMENT

This work was supported in part by NASA Grant NAG1-500.

APPENDIX A

THE MATRIX ELEMENTS C_{pq}, $\overline{C}_{pq}$, K_{pq}, $\overline{K}_{pq}$ AND THE FIELD EXPRESSIONS

(a) Matrix elements for the overlap integrals.

$$C_{pq} = \frac{1}{2} \iint_{-\infty}^{\infty} E_t^{(q)} \times H_t^{(p)} \cdot \hat{z} \, dxdy \tag{A1}$$

$$\begin{aligned} \overline{C}_{pq} &= \frac{1}{2} (C_{pq} + C_{qp}) \\ &= \overline{C}_{qp} \quad . \end{aligned} \tag{A2}$$

(b) Matrix elements for the coupling coefficients.

"Conventional" coupling coefficients:

$$\overline{K}_{pq} = \frac{\omega}{4} \iint \Delta\varepsilon^{(q)} \left[E_t^{(p)} \cdot E_t^{(q)} - E_z^{(p)} E_z^{(q)} \right] dxdy \tag{A3}$$

$$\Delta\varepsilon^{(q)} = \varepsilon(x,y) - \varepsilon^{(q)}(x,y) \tag{A4}$$

where $\varepsilon(x,y)$ is the permittivity function of the multiwaveguide system and $\varepsilon^{(q)}(x,y)$ is the permittivity function of a single waveguide q.

New K_{pq} used in Eq. (4) of this paper [13], [14]:

$$K_{pq} = \frac{\omega}{4} \iint \Delta\varepsilon^{(q)} \left[E_t^{(p)} \cdot E_t^{(q)} - \frac{\varepsilon^{(p)}}{\varepsilon} E_z^{(p)} E_z^{(q)} \right] dxdy \quad . \tag{A5}$$

(c) The field expressions for the supermode.

The transverse components are

$$E_t = \sum_p a_p(z) E_t^{(p)}(x,y) \tag{A6}$$

$$H_t = \sum_p a_p(z) H_t^{(p)}(x,y) \quad . \tag{A7}$$

The longitudinal components are

$$E_z = \sum_p a_p(z) \frac{\varepsilon^{(p)}}{\varepsilon} E_z^{(p)}(x,y) \tag{A8}$$

$$H_z = \sum_p a_p(z) H_z^{(p)}(x,y) \quad . \tag{A9}$$

APPENDIX B

A FORMAL TREATMENT OF TWO COUPLED WAVEGUIDES FOR A LOSSLESS SYSTEM

The coupled-mode equations are assumed to be of the form in general:

$$\frac{d}{dz} a(z) = i\gamma_a a(z) + iK_{ab} b(z) \tag{B1}$$

$$\frac{d}{dz} b(z) = i\gamma_b b(z) + iK_{ba} a(z) \tag{B2}$$

where we have assumed for the transverse fields

$$E_t = a(z)E_t^{(a)} + b(z)E_t^{(b)} \tag{B3}$$

$$H_t = a(z)H_t^{(a)} + b(z)H_t^{(b)} \quad , \tag{B4}$$

and the transverse components $E_t^{(a)}$, $E_t^{(b)}$, $H_t^{(a)}$ and $H_t^{(b)}$ are all real. Thus, one finds that γ_a, γ_b, K_{ab} and K_{ba} are all real. Power conservation leads to

$$\begin{aligned} 0 = \frac{d}{dz} P(z) &= \frac{d}{dz} \frac{1}{2} \mathrm{Re} \iint E_t \times H_t^* \cdot \hat{z} dx dy \\ &= \frac{d}{dz} \mathrm{Re} \left[aa^* + ab^* \bar{\bar{C}}_{21} + ba^* \bar{\bar{C}}_{12}^* + bb^* \right] \\ &= \frac{d}{dz} \left[aa^* + (ab^* + ba^*)\bar{c} + bb^* \right] \\ &= ab^* i(\gamma_a \bar{c} - \gamma_b \bar{c} + K_{ba} - K_{ab}) \\ &\quad + ba^* i(\gamma_b \bar{c} - \gamma_a \bar{c} + K_{ab} - K_{ba}) \end{aligned} \tag{B5}$$

where we have used Eqs. (B1), (B2), the fact that $\bar{\bar{C}}_{12}$, $\bar{\bar{C}}_{21}$ are real, and

$$\begin{aligned} \bar{c} &= \frac{\bar{\bar{C}}_{12} + \bar{\bar{C}}_{21}^*}{2} \\ &= \bar{C}_{12} \quad . \end{aligned} \tag{B6}$$

Since both a and b are arbitrary, we conclude that the coefficients in front of ab^* and ba^* are zero and obtain:

$$K_{ab} - K_{ba} = (\gamma_a - \gamma_b)\overline{c} \quad , \tag{B7}$$

which is the general lossless condition that the four parameters in the coupled-mode equations (B1) and (B2) must satisfy.

REFERENCES

[1] H. Kogelnik, "Theory of dielectric waveguides," in Integrated Optics, T. Tamir, Ed., Second Edition, ch. 2. New York: Springer-Verlag, 1979.

[2] A. Yariv, "Coupled-mode theory for guided-wave optics," IEEE J. Quantum Electron., vol. QE-9, pp. 919-933, 1973.

[3] H. F. Taylor and A. Yariv, "Guided wave optics," Proc. IEEE, vol. 62, pp. 1044-1060, 1974.

[4] E. Kapon, J. Katz and A. Yariv, "Supermode analysis of phase-locked arrays of semiconductor lasers," Opt. Lett., vol. 9, pp. 125-127, 1984.

[5] A. Hardy and W. Streifer, "Analysis of phased array diode lasers," Opt. Lett., vol. 10, pp. 335-337, 1985.

[6] R. C. Alferness and R. V. Schmidt, "Tunable optical waveguide directional coupler filter," Appl. Phys. Lett., vol. 33, pp. 161-163, July 1978.

[7] R. C. Alferness and J. J. Veselka, "Tunable Ti:$LiNbO_3$ waveguide filter for long-wavelength (λ = 1.3-1.6 μm) multiplexing/demultiplexing," in Tech. Dig. Conf. Lasers and Electrooptics (Anaheim, CA), 1984, pp. 230-231.

[8] B. Broberg, B. S. Lindgren, M. Öberg and H. Jiang, "A novel integrated optics wavelength filter in InGaAsP-InP," IEEE J. Lightwave Technol., vol. LT-A, pp. 196-203, 1986.

[9] A. Hardy and W. Streifer, "Coupled mode theory of parallel waveguides," IEEE J. Lightwave Technol., vol. LT-3, pp. 1135-1146, 1985.

[10] A. Hardy and W. Streifer, "Coupled modes of multiwaveguide systems and phase arrays," IEEE J. Lightwave Technol., vol. LT-4, pp. 90-99, 1986.

[11] A. Hardy and W. Streifer, "Coupled mode solutions of multiwaveguide guide systems," IEEE J. Quantum Electron., vol. QE-22, pp. 528-534, 1986.

[12] H. A. Haus, W. P. Huang, S. Kawakami and N. A. Whitaker, "Coupled-mode theory of optical waveguides," to be published.

[13] S. L. Chuang, "A coupled-mode formulation by reciprocity and a variational principle," IEEE J. Lightwave Technol., accepted for publication.

[14] S. L. Chuang, "A coupled-mode theory for multiwaveguide systems satisfying the reciprocity theorem and power conservation," IEEE J. Lightwave Technol., to be published.

[15] E. Marcatili, "Improved coupled-mode equations for dielectric guides," IEEE J. Quantum Electron., vol. QE-22, pp. 988-993, 1986.

[16] J. P. Donnelly, N. L. DeMeo, Jr., and G. A. Ferrante, "Three-guide optical couplers in GaAs," IEEE J. Lightwave Technol., vol. LT-1, pp. 417-424, 1983.

[17] J. P. Donnelly, "Limitations on power-transfer efficiency in three-guide optical couplers," IEEE J. Quantum Electron., vol. QE-22, pp. 610-616, 1986.

[18] K. L. Chen and S. Wang, "Cross-talk problems in optical directional couplers," Appl. Phys. Lett., 44, pp. 166-168, 1984.

[19] K. L. Chen and S. Wang, "The crosstalk in three-waveguide optical directional couplers," IEEE J. Quantum Electron., vol. QE-22, pp. 1039-1041, 1986.

[20] W. Streifer, M. Osinski, and A. Hardy, "Reformation of the coupled mode theory of multiwaveguide systems," IEEE J. Lightwave Technol., to be published.

[21] B. Broberg and S. Lindgren, "Refractive index of $In_{1-x}Ga_xAs_yP_{1-y}$ layers and InP in the transparent wavelength region," J. Appl. Phys., vol. 55, pp. 3376-3381, 1984.

FIGURE CAPTIONS

Figure 1. (a) The asynchronism δ is plotted versus the refractive index difference of two coupled waveguides, $\Delta n = n_a - n_b$, which is proportional to the applied voltage V.

(b) The overlap integrals C_{12} (dashed line), C_{21} (dotted line) and $\overline{C} = (C_{12} + C_{21})/2$ (solid line) are shown.

(c) The coupling coefficients K_{ab}, K_{ba} and $\sqrt{K_{ab}K_{ab}}$ are plotted versus Δn.

(d) The output powers in guide a, P_a (solid curve), and in guide b, P_b (dashed curve), are plotted versus Δn. The parameters are $d_a = d_b = 2$ μm, waveguide edge-to-edge separation $t = 1.9$ μm, wavelength $\lambda = 1.06$ μm. $n_a = 2.2 + \Delta n/2$, $n_b = 2.2 - \Delta n/2$. The outside refractive index $n_0 = 2.19$. The coupler length $\ell = 0.5811$ mm.

Figure 2. (a) The asynchronism $2\gamma_2 - \gamma_1 - \gamma_3$ of three coupled waveguides are plotted versus the refractive index difference $\Delta n = n_1 - n_2$ which is proportional to the applied voltage. The parameters are all similar to those in Fig. 1. $d_1 = d_2 = d_3 = 2$ μm. $t = 1.9$ μm, $\lambda = 1.06$ μm, $n_1 = n_3 = 2.2 + \Delta n/2$, $n_2 = 2.2 - \Delta n/2$. $L_{C0} = 0.8105$ mm.

(b) The output powers $P_{OUT,1}$ (solid curve) and $P_{OUT,3}$ (dashed curve) are shown for the power transfer devices with input power $P_{IN} = 1$ in waveguide 1.

(c) The output powers $P_{OUT,1} = P_{OUT,3}$ are plotted versus Δn when the three waveguide couplers in (a) are used as a power divider.

Figure 3. (a) The output powers $P_{OUT,1}$ (solid curve) and $P_{OUT,3}$ (dashed curve) are plotted versus the coupling distance ℓ normalized to L_C for a power transfer device. The same parameters from Fig. 2 are used except that Δn is fixed to be zero and ℓ is varying.

(b) The output powers $P_{OUT,1} = P_{OUT,3}$ are plotted versus the normalized distance ℓ/L_C when the three coupled waveguides in Fig. 2(c) are used as power dividers. ($\Delta n = 0$, ℓ is varying here.)

Figure 4. (a) The output powers $P_{OUT,1}$ (solid curve) and $P_{OUT,3}$ (dashed curve) are plotted versus the normalized coupling distance ℓ/L_C for the case $\Delta n = -0.00023$ where $2\gamma_2 - \gamma_1 - \gamma_3 = 0$.

(b) Similar conditions hold as 4(a) except that the device is used as a power divider.

Figure 5. (a) The propagation constants of the three supermodes using the strongly coupled-mode theory (dotted lines) are compared with the exact numerical calculations (solid lines). The waveguide edge-to-edge separation t is varied. The parameters are $d_1 = d_2 = d_3 = 2\ \mu m$, $n_1 = n_2 = n_3 = 3.44$, $n_0 = 3.436$. $\lambda = 1.06\ \mu m$.

(b) The overlap integrals $C_{12}(=C_{21})$ and $C_{13}(=C_{31})$ are plotted versus the wavelength edge-to-edge separation t.

(c) The coupling distance $L_C = 2\pi/(\gamma_1 - \gamma_3)$ is illustrated.

(d) The output power $P_{OUT,3}$ (dashed line) in the guide 3 and the extinction ratio $P_{OUT,1}$ (solid line) due to cross talk are shown.

Figure 6. (a) The output powers of two coupled $In_xGa_{1-x}As_yP_{1-y}$ - InP waveguides used as an optical wavelength filter. The input power is assumed to be 1 in waveguide b. The theoretical results for output powers at waveguide a, P_a (solid curve), at waveguide b, P_b (dashed curve), are compared with the experimental data (circles) for P_a.

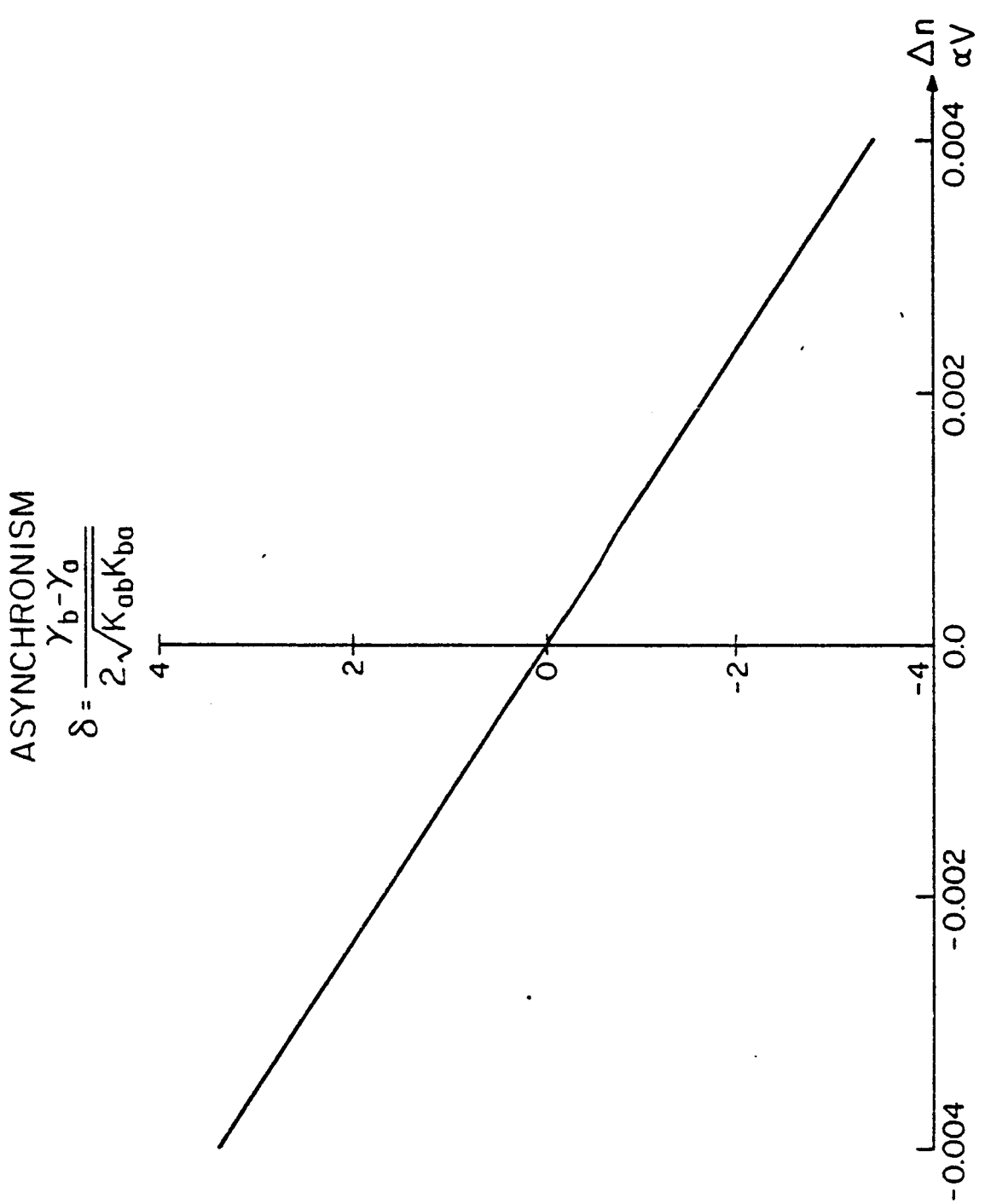
ASYNCHRONISM
$\delta = \frac{\gamma_b - \gamma_a}{2\sqrt{K_{ab}K_{ba}}}$
4
2
0
-2
-4
-0.004
-0.002
0.0
0.002
0.004
Δn
αV
REFRACTIVE INDEX DIFFERENCE

Fig. 1(a)

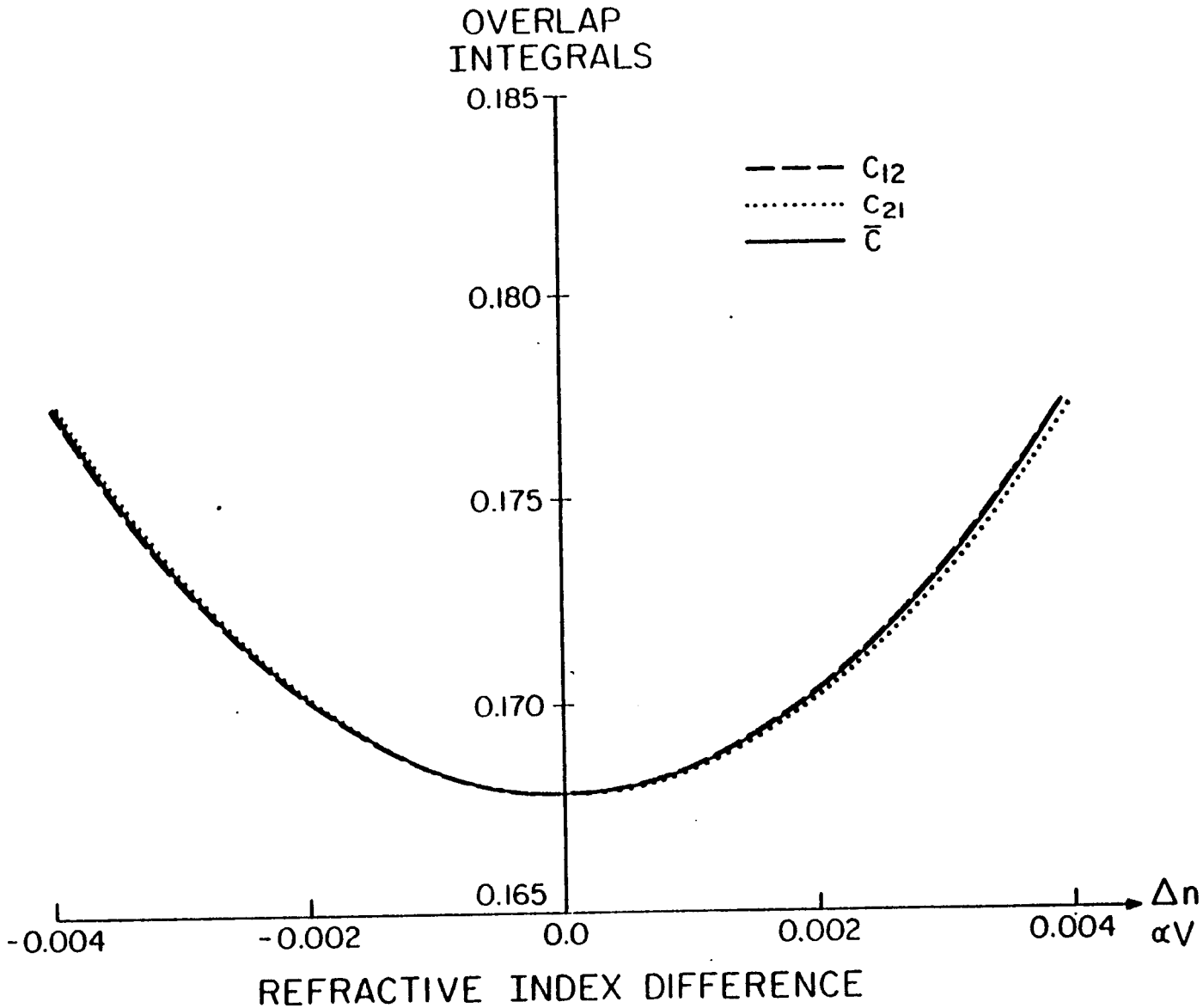
OVERLAP
INTEGRALS
0.185
0.180
0.175
0.170
0.165
C_{12}
C_{21}
$\bar{C}$
-0.004
-0.002
0.0
0.002
0.004
Δn
αV
REFRACTIVE INDEX DIFFERENCE

Fig. 1(b)

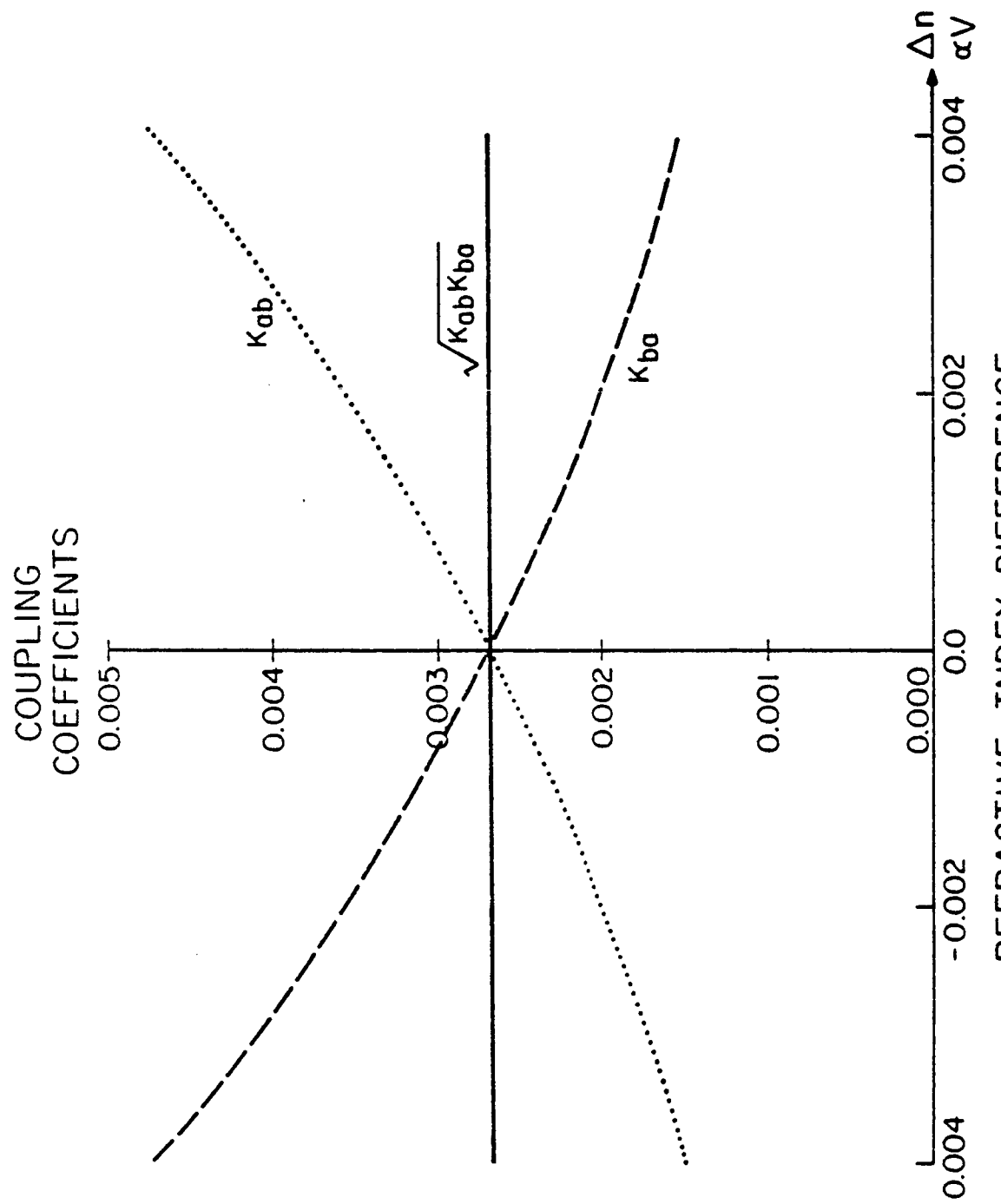
COUPLING
COEFFICIENTS
0.005
0.004
0.003
0.002
0.001
K_{ab}
$\sqrt{K_{ab}K_{ba}}$
K_{ba}
0.000
0.0
0.002
0.004
-0.004
-0.002
REFRACTIVE INDEX DIFFERENCE
Δn
αV

Fig. 1(c)

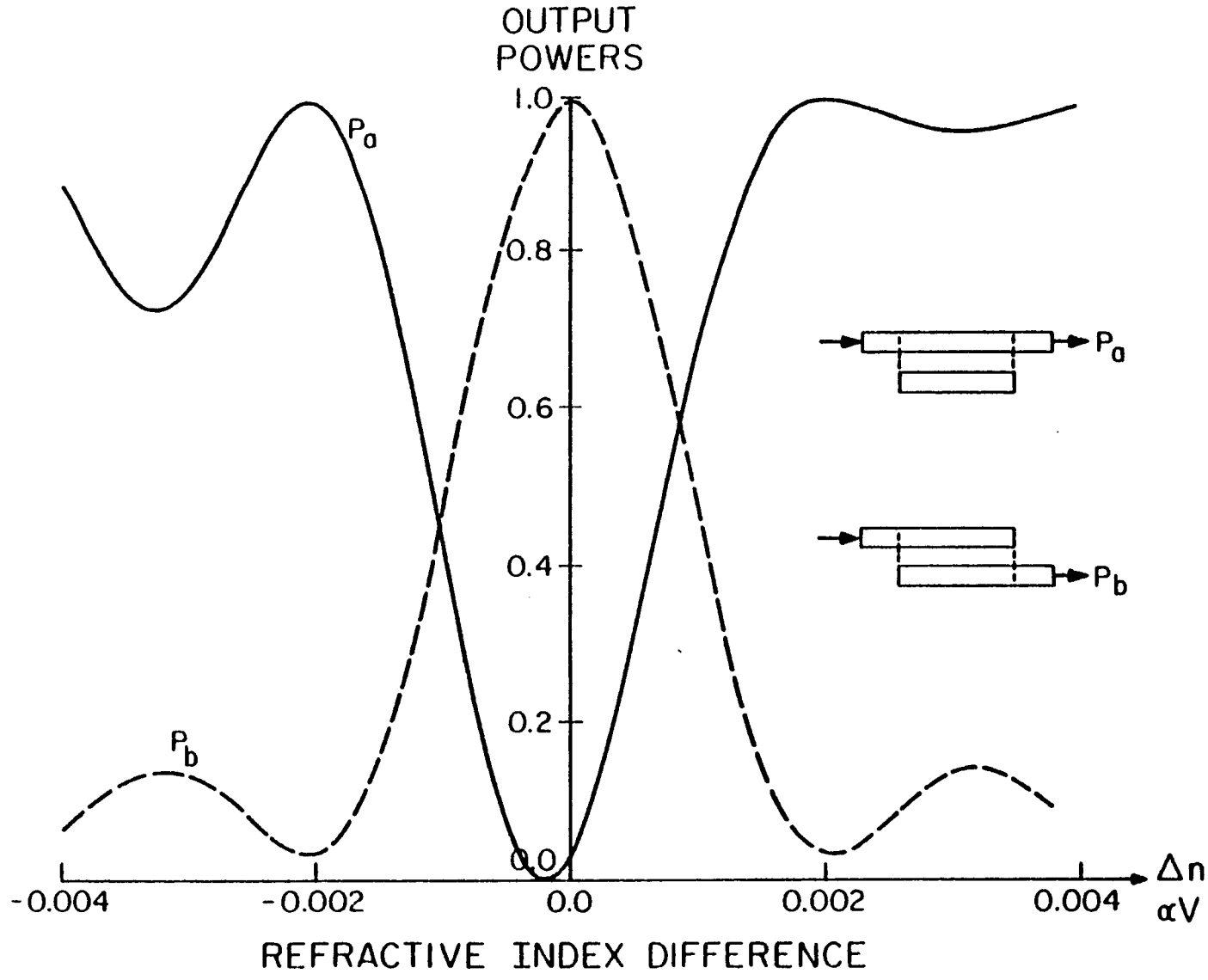
OUTPUT
POWERS
1.0
0.8
0.6
0.4
0.2
0.0
P_a
P_b
P_a
P_b
-0.004
-0.002
0.0
0.002
0.004
Δn
αV
REFRACTIVE INDEX DIFFERENCE

Fig. 1(d)

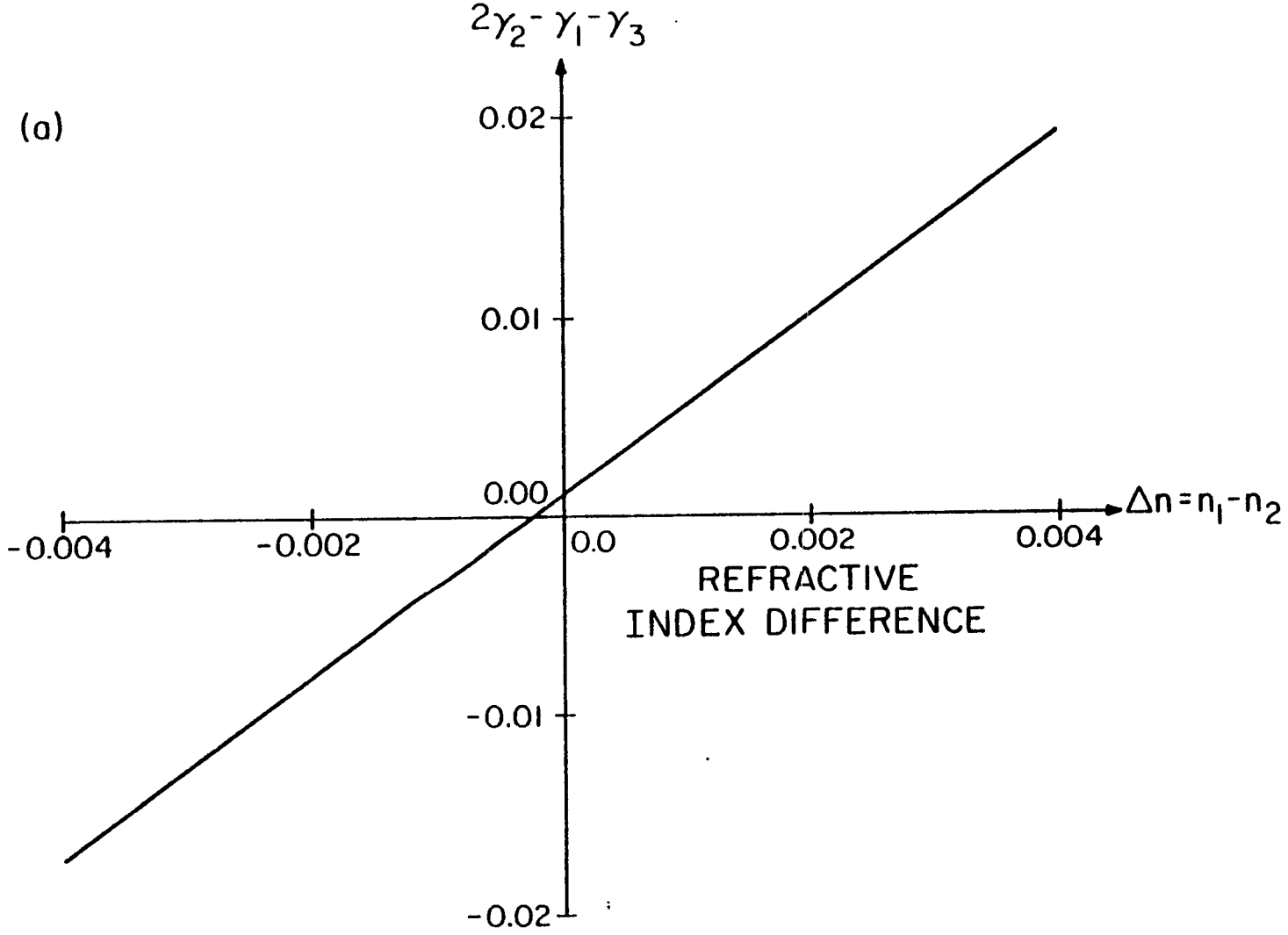
(a)
$2\gamma_2 - \gamma_1 - \gamma_3$
0.02
0.01
0.00
-0.01
-0.02
-0.004
-0.002
0.0
0.002
0.004
$\Delta n = n_1 - n_2$
REFRACTIVE
INDEX DIFFERENCE

Fig. 2(a)

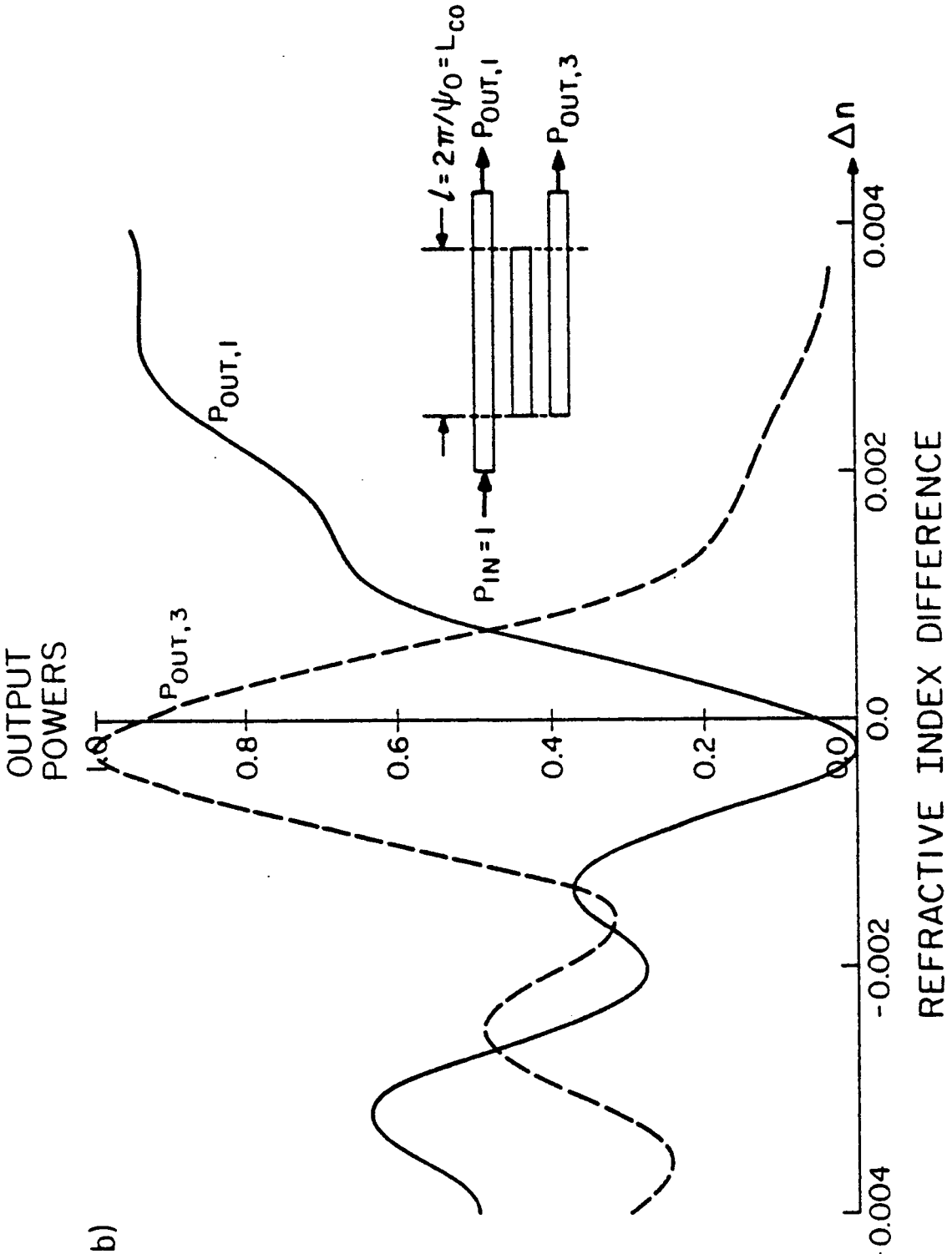
(b)
OUTPUT POWERS
1.0
0.8
0.6
0.4
0.2
0.0
$P_{OUT,1}$
$P_{OUT,3}$
$P_{IN}=1$
$l=2\pi/\psi_0=L_{CO}$
$P_{OUT,1}$
$P_{OUT,3}$
-0.004
-0.002
0.0
0.002
0.004
Δn
REFRACTIVE INDEX DIFFERENCE

Fig. 2(b)

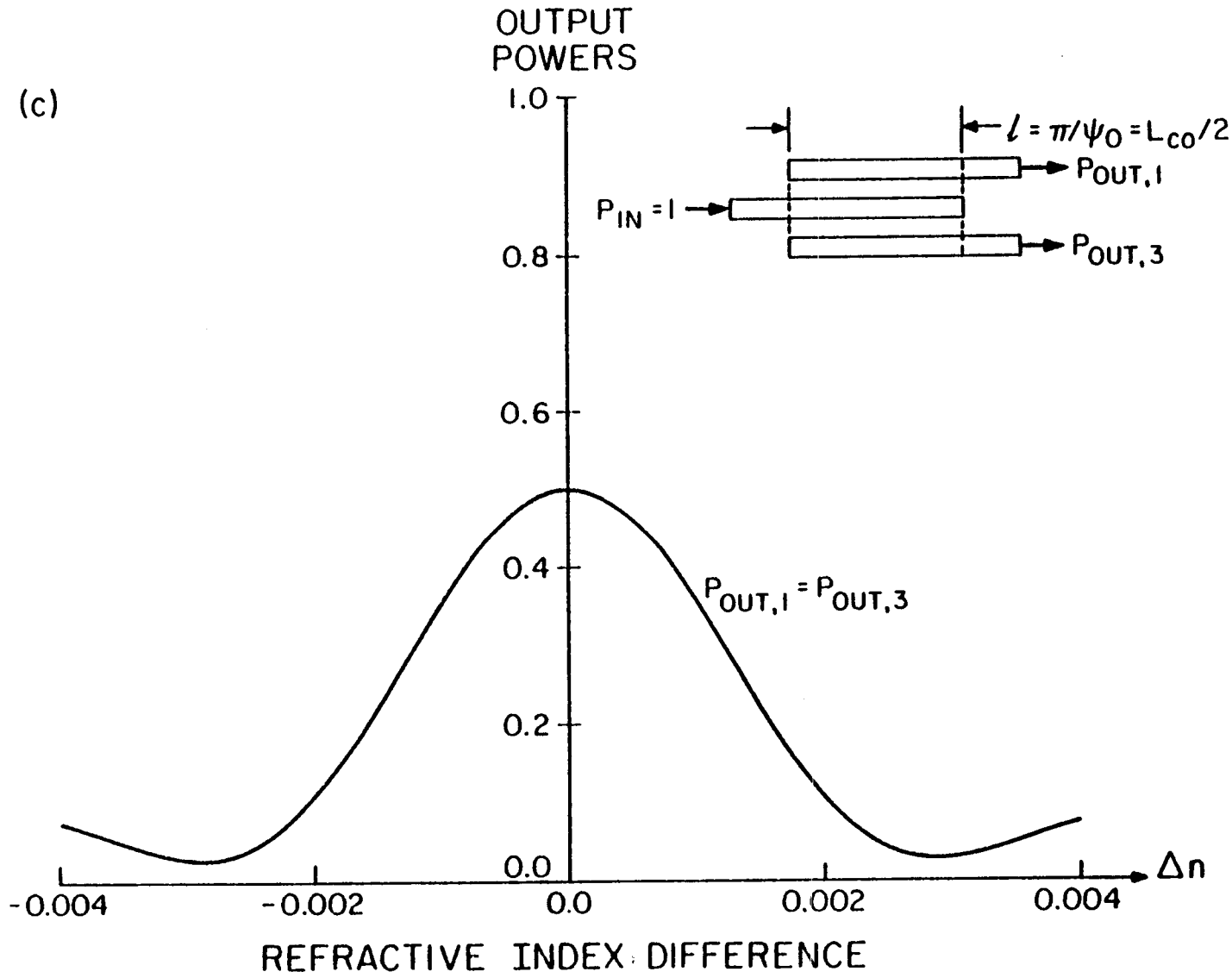
(c)
OUTPUT
POWERS
1.0
0.8
0.6
0.4
0.2
0.0
$\ell = \pi/\psi_0 = L_{co}/2$
$P_{IN} = 1$
$P_{OUT,1}$
$P_{OUT,3}$
$P_{OUT,1} = P_{OUT,3}$
-0.004
-0.002
0.0
0.002
0.004
Δn
REFRACTIVE INDEX DIFFERENCE

Fig. 2(c)

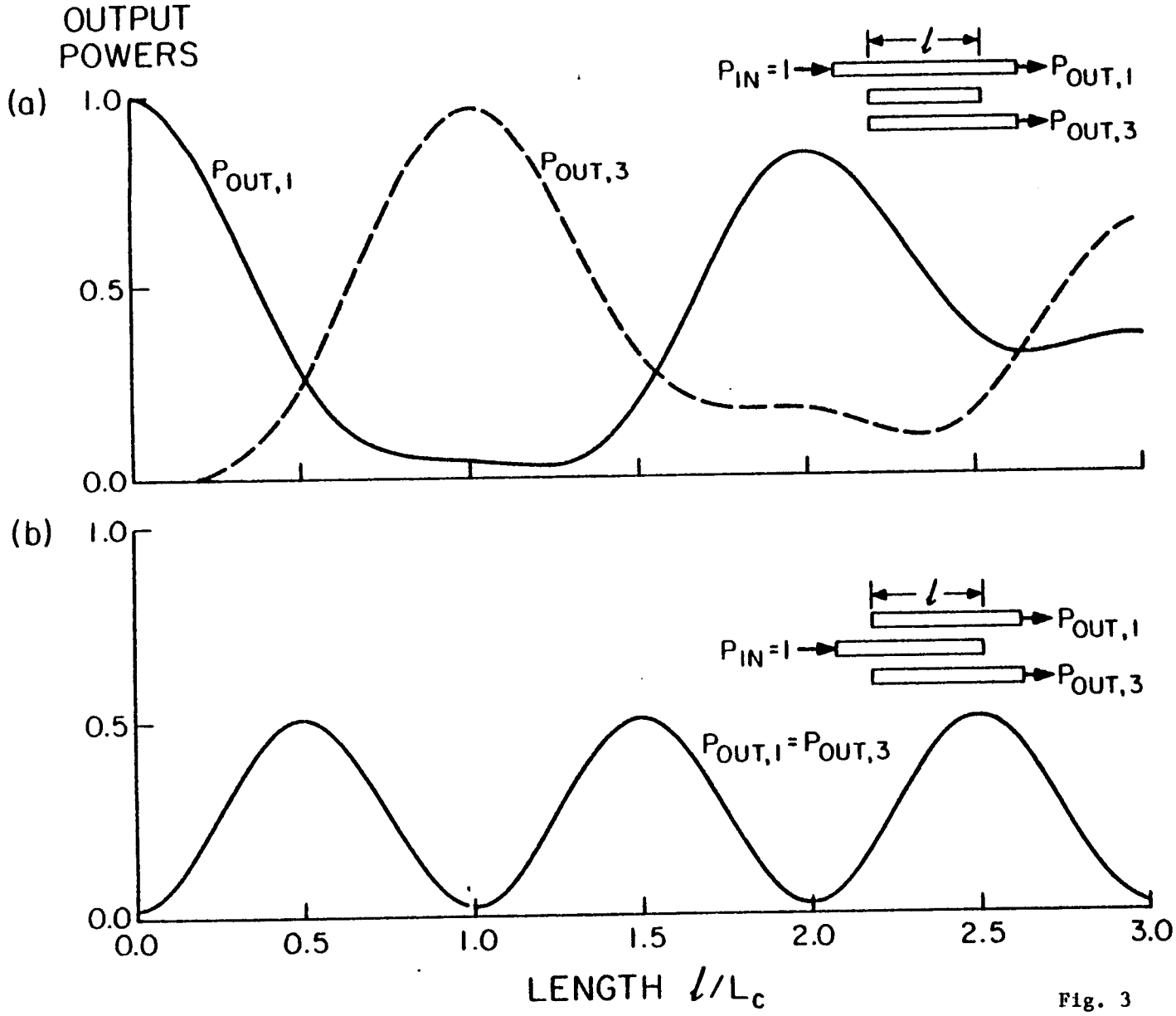
OUTPUT
POWERS
(a)
1.0
0.5
0.0
$P_{OUT,1}$
$P_{OUT,3}$
$P_{IN}=1$
$P_{OUT,1}$
$P_{OUT,3}$
ℓ
(b)
1.0
0.5
0.0
$P_{IN}=1$
$P_{OUT,1}$
$P_{OUT,3}$
$P_{OUT,1}=P_{OUT,3}$
0.0
0.5
1.0
1.5
2.0
2.5
3.0
LENGTH ℓ/L_c

Fig. 3

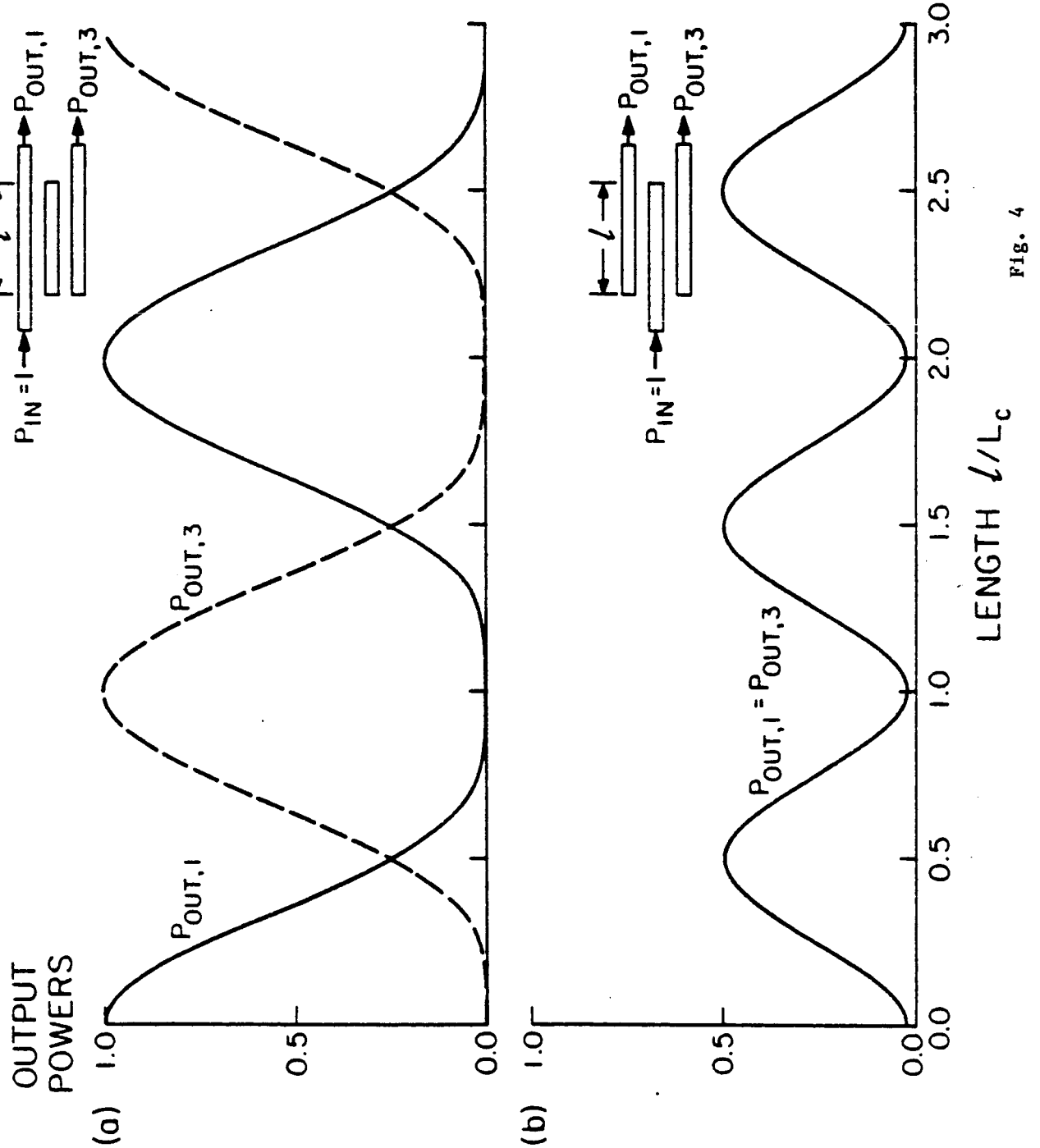
OUTPUT POWERS
(a)
(b)
1.0
0.5
0.0
$P_{OUT,1}$
$P_{OUT,3}$
$P_{IN}=1$
ℓ
$P_{OUT,1} = P_{OUT,3}$
0.0
0.5
1.0
1.5
2.0
2.5
3.0
LENGTH ℓ/L_c

Fig. 4

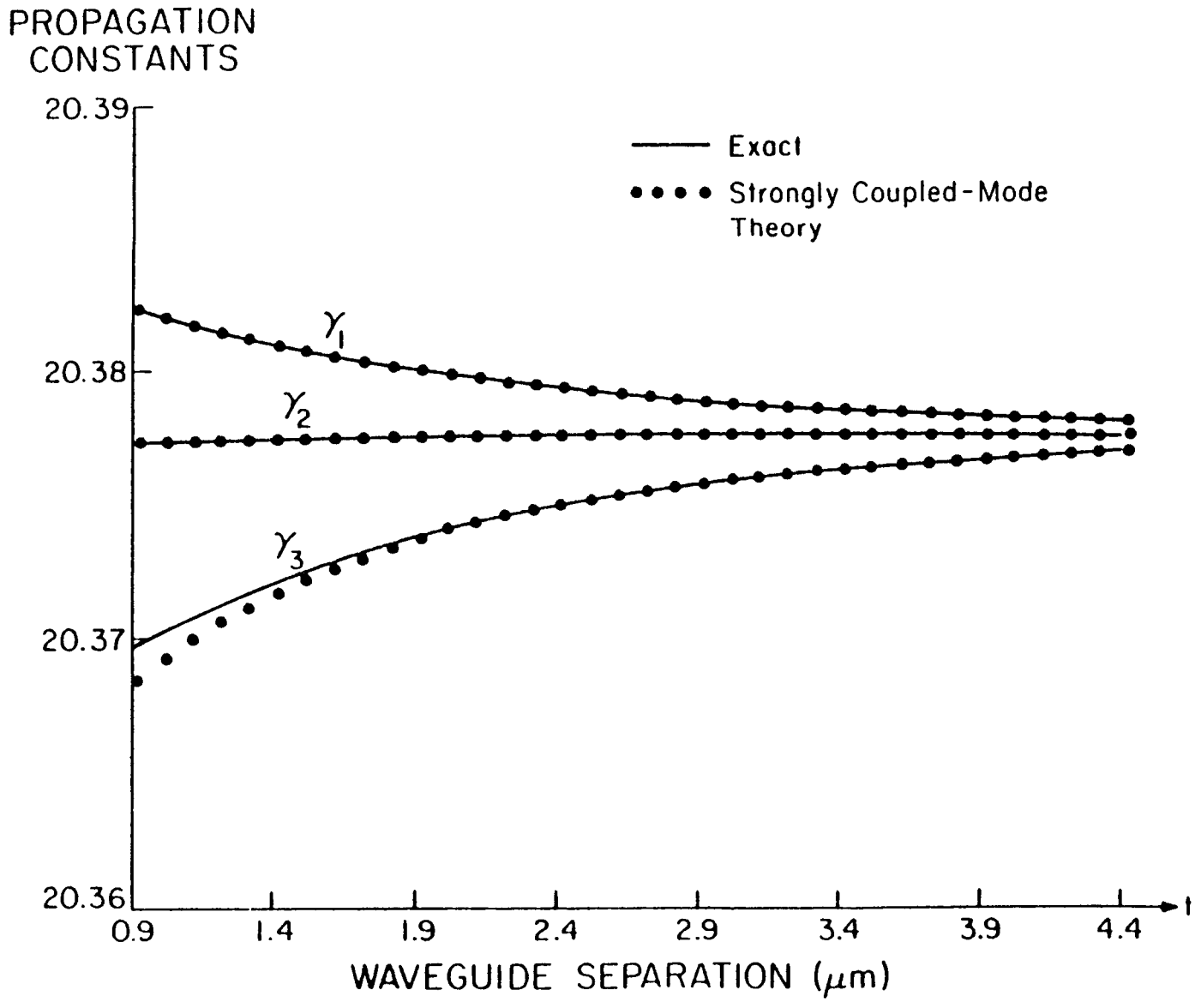
PROPAGATION CONSTANTS
20.39
20.38
20.37
20.36
Exact
Strongly Coupled-Mode Theory
γ_1
γ_2
γ_3
0.9
1.4
1.9
2.4
2.9
3.4
3.9
4.4
WAVEGUIDE SEPARATION (μm)

Fig. 5(a)

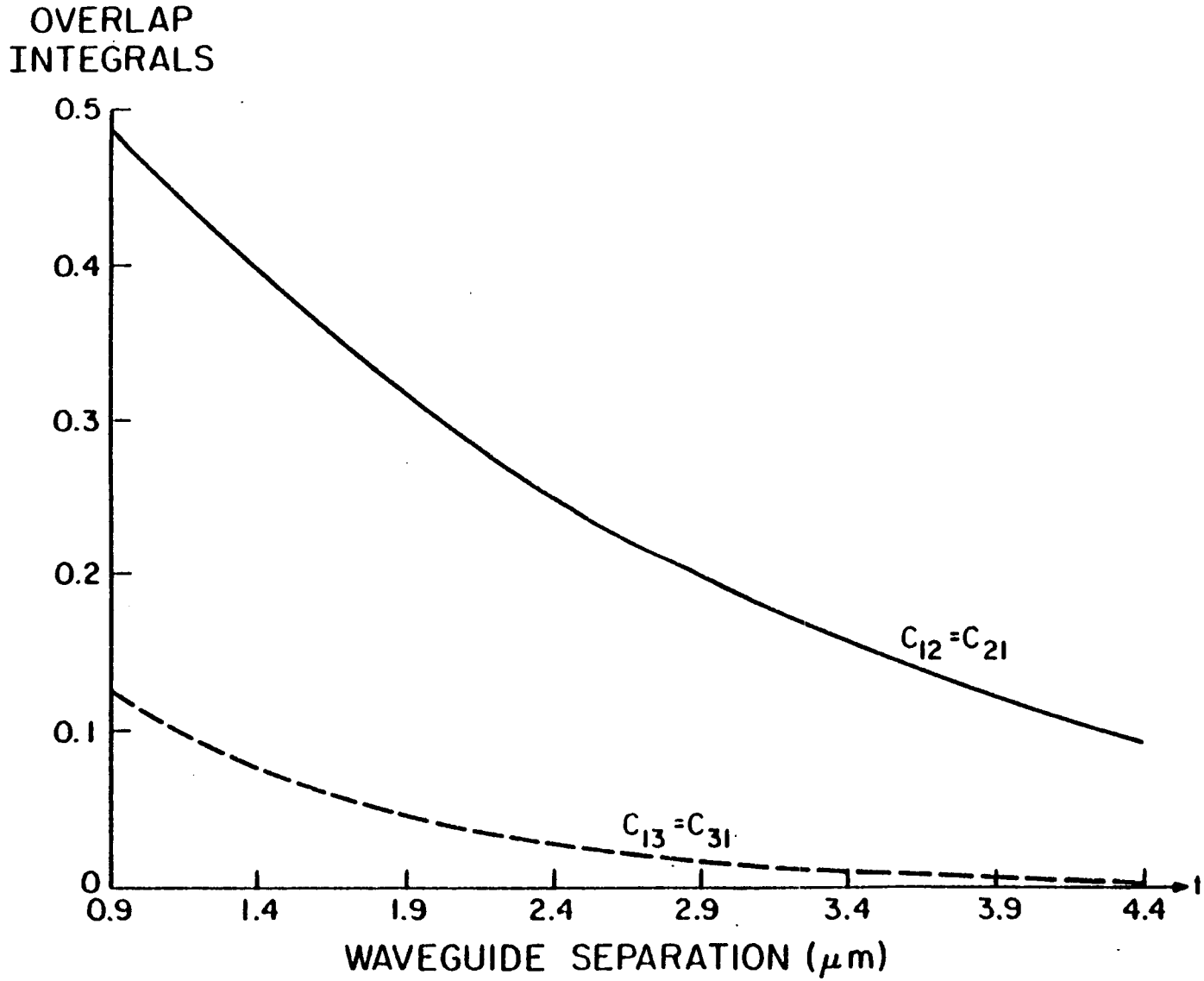
OVERLAP
INTEGRALS
0.5
0.4
0.3
0.2
0.1
0
$C_{12}=C_{21}$
$C_{13}=C_{31}$
0.9
1.4
1.9
2.4
2.9
3.4
3.9
4.4
WAVEGUIDE SEPARATION (μm)

Fig. 5(b)

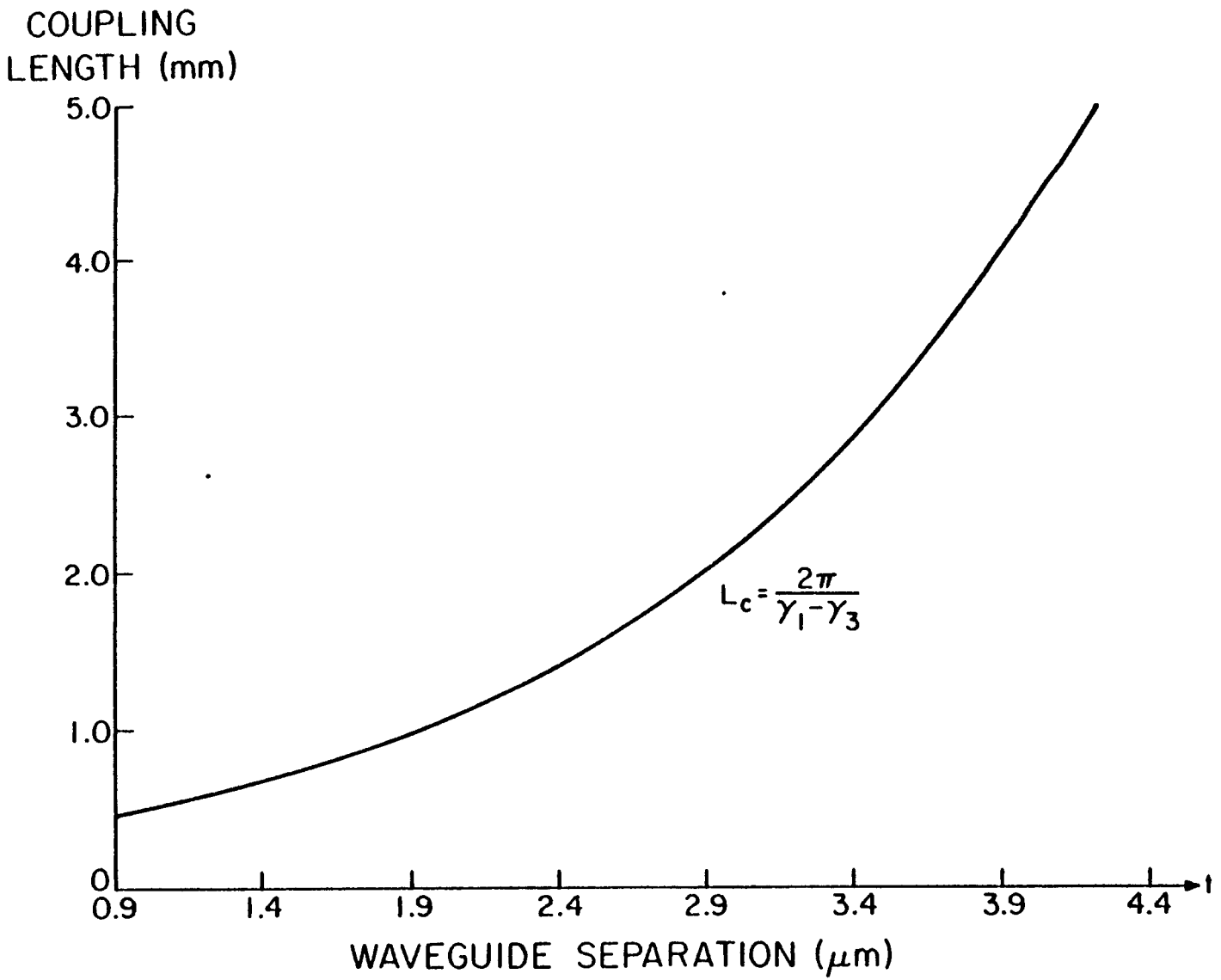
COUPLING
LENGTH (mm)
5.0
4.0
3.0
2.0
1.0
0
0.9
1.4
1.9
2.4
2.9
3.4
3.9
4.4
$L_c = \frac{2\pi}{\gamma_1 - \gamma_3}$
WAVEGUIDE SEPARATION (μm)

Fig. 5(c)

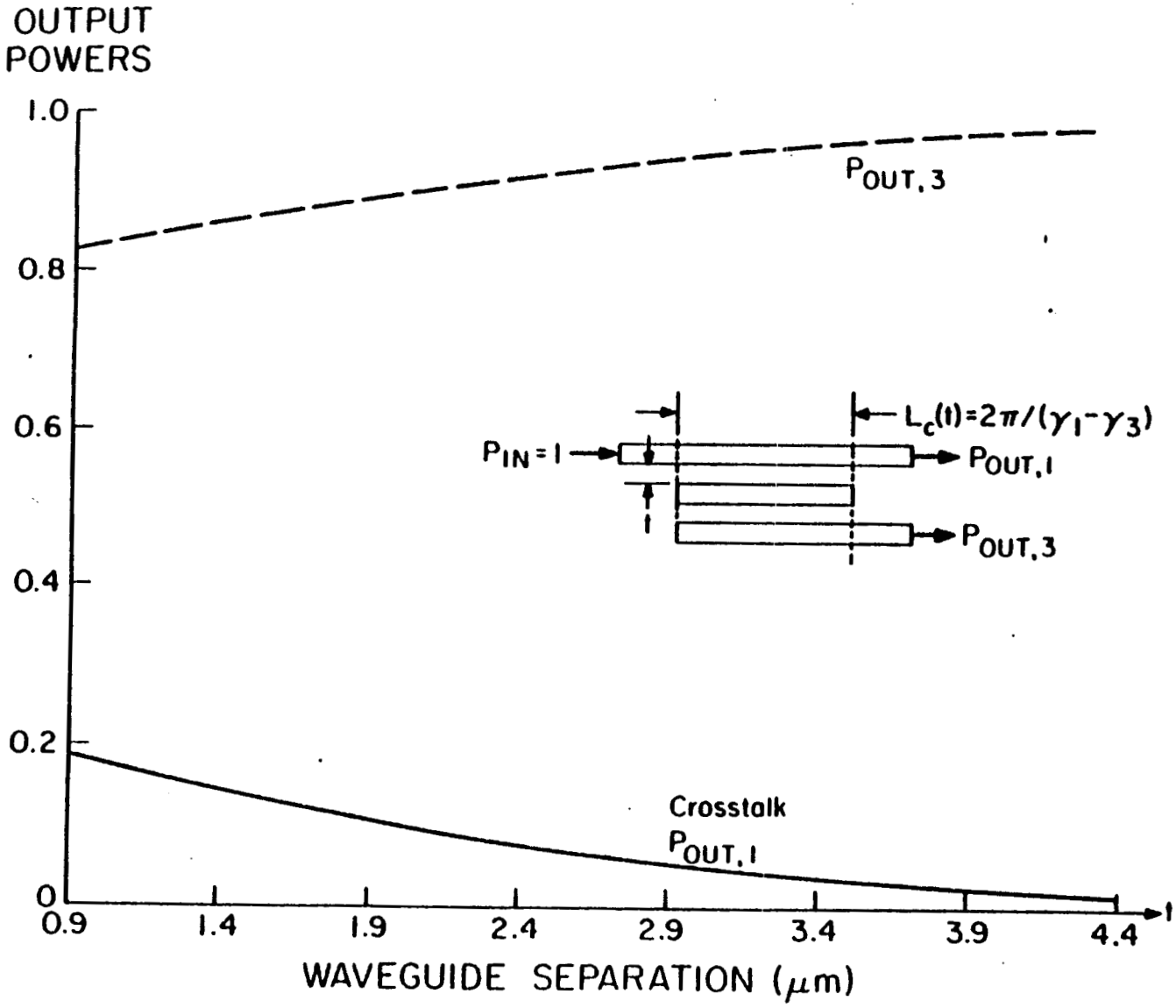
OUTPUT
POWERS
1.0
0.8
0.6
0.4
0.2
0
$P_{OUT,3}$
$L_c(l)=2\pi/(\gamma_1-\gamma_3)$
$P_{IN}=1$
$P_{OUT,1}$
$P_{OUT,3}$
l
Crosstalk
$P_{OUT,1}$
0.9
1.4
1.9
2.4
2.9
3.4
3.9
4.4
l
WAVEGUIDE SEPARATION (μm)

Fig. 5(d)

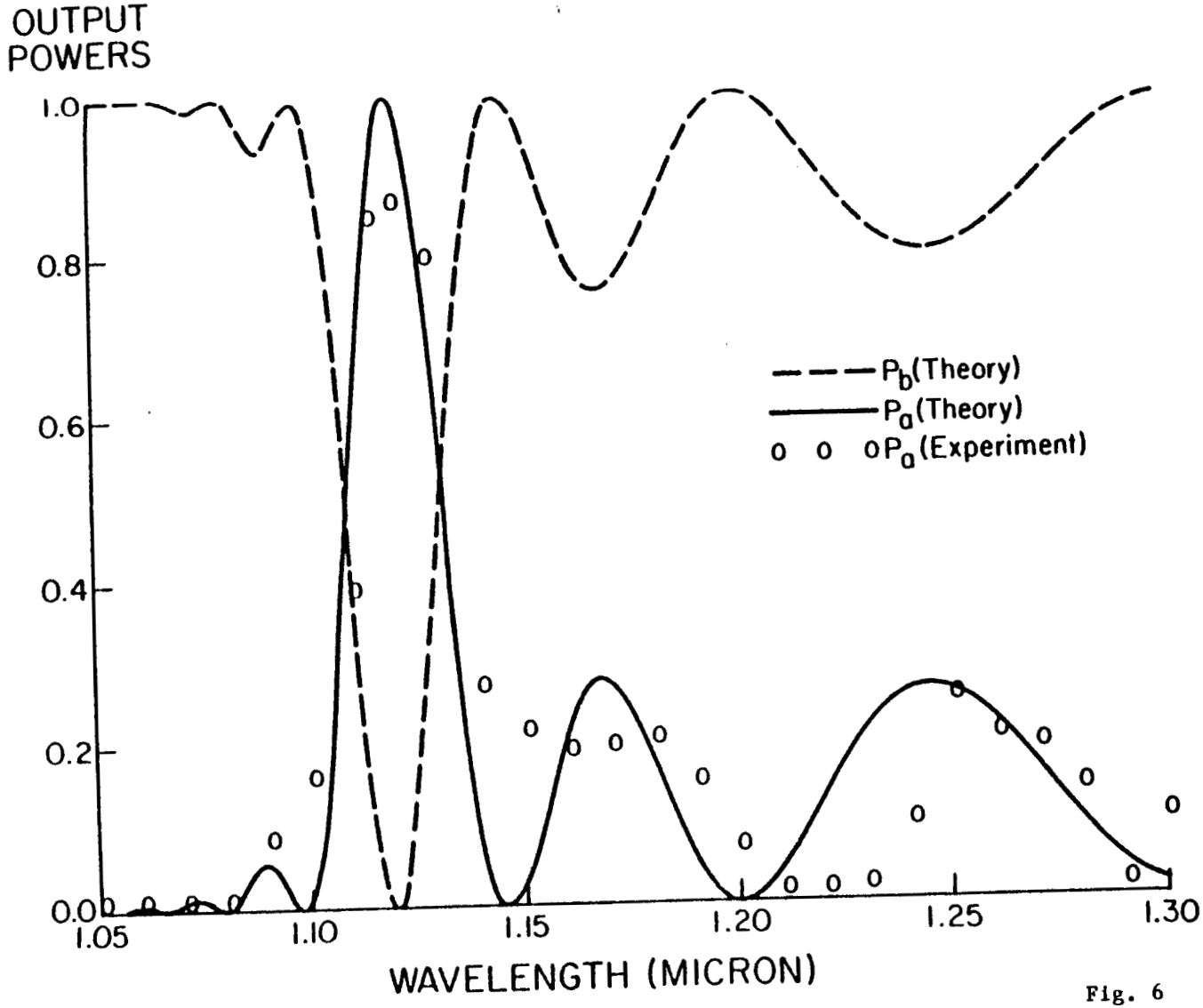
OUTPUT
POWERS
1.0
0.8
0.6
0.4
0.2
0.0
1.05
1.10
1.15
1.20
1.25
1.30
WAVELENGTH (MICRON)
P_b(Theory)
P_a(Theory)
o o o P_a(Experiment)

Fig. 6

Appendix H

L. Tsang and S. L. Chuang, "Strongly coupled-mode theory for reciprocal anisotropic multiwaveguide system," IEEE J. Lightwave Technology, submitted for publication.

STRONGLY COUPLED-MODE THEORY FOR RECIPROCAL ANISOTROPIC MULTIWAVEGUIDE SYSTEM

L. Tsang

Department of Electrical Engineering
University of Washington
Seattle, WA 98195

S. L. Chuang

Department of Electrical and Computer Engineering
University of Illinois at Urbana-Champaign
Urbana, IL 61801

ABSTRACT A strongly coupled-mode theory for reciprocal anisotropic multiwaveguide system is derived. The general reciprocal anisotropic medium is described by a symmetric permittivity tensor that can have non-zero off-diagonal elements. The derivation is based on the generalized reciprocity relation. The coupled mode equations are applicable to both lossy (gain) and lossless systems. For the special case of lossless systems, it is shown that the matrices in the coupled mode equation are Hermitian so that energy conservation is obeyed exactly. For the special case of a single anisotropic waveguide, our results also reduce to the previously derived solutions by Marcuse. The strongly coupled-mode theory in an anisotropic multiwaveguide system is also illustrated with numerical examples.

The work at University of Washington was supported by National Science Foundation, Grant No. ECS-8500886.

The work at University of Illinois is partially supported by NASA Grant NAG1-500 and the Joint Services Electronics Program.

1. Introduction

The application of the coupled mode theory to integrated optical devices such as waveguide couplers [1]-[3], laser arrays [4]-[5] and optical filters [6]-[8] has been well known. Although it has long been recognized that the previous coupled mode theory is only applicable to weakly coupled systems [3]-[4], significant improvements for strongly coupled waveguides have only been developed recently in a series of papers [9]-[17]. The major improvement is the inclusion of the overlap integral C_{pq} between modes of different waveguides that have been neglected in the conventional theory.

Many of the integrated optical devices are made of materials that are anisotropic [18]-[22]. In anisotropic coupled waveguides, numerical solutions are usually difficult to calculate. In this paper we generalize the strongly coupled mode theory to an anisotropic medium in multiwaveguide systems. The strongly coupled mode equations are derived for a general reciprocal anisotropic medium. The general reciprocal anisotropic medium is described by a symmetric permittivity tensor that can have nonzero off-diagonal elements. The derivation is based on the generalized reciprocity relation [14]-[15]. In Section 2, the generalized reciprocity relation is extended to an anisotropic reciprocal medium. In Section 3, we briefly discuss the mode solutions and mode orthogonality relations for a general reciprocal anisotropic medium. In Section 4, the coupled mode equations for a general reciprocal anisotropic medium are derived for multiwaveguide systems. Expressions for the overlap integrals and the coupling coefficients are given. The derived coupled-mode equations are applicable to both lossy (gain) and lossless systems. In matrix notation, the coupled mode equations are of the form

$$\bar{\bar{C}} \frac{da}{dz} = i \bar{\bar{Q}} a$$

where $\bar{\bar{C}}$ is the overlap integral matrix. The elements of the vector **a** represent the amplitudes of the modes $a_p(z)$ in the waveguides, which can be modes of different polarizations in the same waveguides and/or different waveguides. Two special cases are examined next. In Section 5, the special case of a lossless system is studied. It is shown that in this case both $\bar{\bar{C}}$ and $\bar{\bar{Q}}$ are Hermitian matrices. Hence energy conservation is obeyed self-consistently. In Section 6, the special case of coupling of modes in a single waveguide is examined. In this case, the matrix $\bar{\bar{C}}$ is diagonal. It is then shown that in this case the coupling coefficients are identical to those previously derived by Marcuse [19]. In Section 7, the coupled mode theory is illustrated with a numerical example using Ti-diffused $LiNbO_3$ waveguides. The application of voltages introduces nonzero off-diagonal elements in the permittivity tensor. Thus there is coupling between the TE and TM modes in addition to coupling between modes of different waveguides.

2. Generalized Reciprocity Relation for Anisotropic Medium

Let $\mathbf{E}^{\langle 1\rangle}$, $\mathbf{H}^{\langle 1\rangle}$ be the solution to Maxwell's equations and the boundary conditions in a medium $\overline{\overline{\varepsilon}}^{\langle 1\rangle}(x,y)$ for the whole space and $\mathbf{E}^{\langle 2\rangle}$, and $\mathbf{H}^{\langle 2\rangle}$ be the solutions to Maxwell's equations and the boundary conditions in another medium $\overline{\overline{\varepsilon}}^{\langle 2\rangle}(x,y)$. Both media are reciprocal so that the permittivity tensors satisfy the relations

$$\overline{\overline{\varepsilon}}^{\langle 1\rangle T}(x,y) = \overline{\overline{\varepsilon}}^{\langle 1\rangle}(x,y) \tag{1}$$

$$\overline{\overline{\varepsilon}}^{\langle 2\rangle T}(x,y) = \overline{\overline{\varepsilon}}^{\langle 2\rangle}(x,y) \tag{2}$$

where superscript T denotes transpose.

It is straightforward to show that

$$\nabla \cdot (\mathbf{E}^{\langle 1\rangle} \times \mathbf{H}^{\langle 2\rangle} - \mathbf{E}^{\langle 2\rangle} \times \mathbf{H}^{\langle 1\rangle}) = i\omega\, \mathbf{E}^{\langle 1\rangle} \cdot (\overline{\overline{\varepsilon}}^{\langle 2\rangle} - \overline{\overline{\varepsilon}}^{\langle 1\rangle}) \cdot \mathbf{E}^{\langle 2\rangle} \tag{3}$$

with the same procedure used for deriving the Lorentz reciprocity relation. The time convention $\exp(-i\omega t)$ is used in this paper. When applied to a cylindrical geometry, the generalized reciprocity equation (3) becomes [14]

$$\frac{\partial}{\partial z} \iint dxdy\, \hat{z} \cdot (\mathbf{E}^{\langle 1\rangle} \times \mathbf{H}^{\langle 2\rangle} - \mathbf{E}^{\langle 2\rangle} \times \mathbf{H}^{\langle 1\rangle})$$

$$= i\omega \iint dxdy\, \mathbf{E}^{\langle 1\rangle} \cdot \left(\overline{\overline{\varepsilon}}^{\langle 2\rangle}(x,y) - \overline{\overline{\varepsilon}}^{\langle 1\rangle}(x,y)\right) \cdot \mathbf{E}^{\langle 2\rangle} \tag{4}$$

3. Mode Solutions in Reciprocal Anisotropic Medium and Mode Orthogonality

In this section, we review the mode solutions and orthogonal relations in an anisotropic medium. In a reciprocal anisotropic medium,

$$\bar{\bar{\varepsilon}} = \begin{pmatrix} \varepsilon_{xx} & \varepsilon_{xy} & \varepsilon_{xz} \\ \varepsilon_{xy} & \varepsilon_{yy} & \varepsilon_{yz} \\ \varepsilon_{xz} & \varepsilon_{yz} & \varepsilon_{zz} \end{pmatrix} \tag{5}$$

The following decomposition is convenient for analyzing waveguide modes

$$\bar{\bar{\varepsilon}} = \bar{\bar{\varepsilon}}_t + \bar{\bar{\varepsilon}}_{tz} + \bar{\bar{\varepsilon}}_{zt} + \bar{\bar{\varepsilon}}_{zz} \tag{6}$$

where subscript t denotes transverse components.

$$\bar{\bar{\varepsilon}}_t = \varepsilon_{xx}\,\hat{x}\hat{x} + \varepsilon_{xy}\,(\hat{x}\hat{y} + \hat{y}\hat{x}) + \varepsilon_{yy}\,\hat{y}\hat{y} \tag{7}$$

$$\bar{\bar{\varepsilon}}_{tz} = \varepsilon_{xz}\,\hat{x}\hat{z} + \varepsilon_{yz}\,\hat{y}\hat{z} \tag{8}$$

$$\bar{\bar{\varepsilon}}_{zt} = \bar{\bar{\varepsilon}}_{tz}^{\,T} \tag{9}$$

$$\bar{\bar{\varepsilon}}_{zz} = \hat{z}\hat{z}\,\varepsilon_{zz} \tag{10}$$

Both $\bar{\bar{\varepsilon}}_t$ and $\bar{\bar{\varepsilon}}_{zz}$ are symmetric while the transpose of $\bar{\bar{\varepsilon}}_{tz}$ is $\bar{\bar{\varepsilon}}_{zt}$ and vice versa. The longitudinal field components can be expressed in terms of the transverse field components as follows

$$H_z = \frac{1}{i\omega\mu}\,\nabla_t \times E_t$$

$$E_z = \frac{i}{\omega\,\varepsilon_{zz}}\left\{\nabla_t \times H_t + i\omega\,\bar{\bar{\varepsilon}}_{zt} \cdot E_t\right\} \tag{11}$$

If $\bar{\bar{\varepsilon}}(x,y)$ is translational invariant in the $\hat{z}$ direction, then mode solutions exist. For modes propagating in the +z direction, the modal solutions of the electromagnetic fields are

$$\mathbf{E}^{(q)}(x,y)\, e^{i\beta_q z}$$
$$\mathbf{H}^{(q)}(x,y)\, e^{i\beta_q z}$$

where q is the mode index. There also exists a mode with the same propagation constant β_q and propagating in the $-\hat{z}$ direction. These are denoted by

$$\mathbf{E}^{(-q)}(x,y)\, e^{-i\beta_q z}$$
$$\mathbf{H}^{(-q)}(x,y)\, e^{-i\beta_q z}\ .$$

For lossless systems, the two sets of mode functions $(\mathbf{E}^{(q)}, \mathbf{H}^{(q)})$ and $(\mathbf{E}^{(-q)}, \mathbf{H}^{(-q)})$ have a simple relation (Section 5, equations (31)-(34)). However, for a general lossy (gain) reciprocal anisotropic medium, there is no simple relation relating the two sets of solutions [19], [23]. (If $\overline{\overline{\varepsilon}}_{tz} = 0$ and $\overline{\overline{\varepsilon}}_{zt} = 0$, a simple relation such as that in [15] for z-inversion symmetry also exists.)

Using the generalized reciprocity relation (4), mode orthogonality relations can be derived readily. Let $\overline{\overline{\varepsilon}}^{<2>} = \overline{\overline{\varepsilon}}^{<1>} = \overline{\overline{\varepsilon}}$, $(\mathbf{E}^{<1>}, \mathbf{H}^{<1>}) = (\mathbf{E}^{(q)}, \mathbf{H}^{(q)}) \exp(i\beta_q z)$, and $(\mathbf{E}^{<2>}, \mathbf{H}^{<2>}) = (\mathbf{E}^{(p)}, \mathbf{H}^{(p)}) \exp(i\beta_p z)$. It then follows that

$$\iint dxdy\ \hat{z} \cdot (\mathbf{E}_t^{(q)} \times \mathbf{H}_t^{(p)} - \mathbf{E}_t^{(p)} \times \mathbf{H}_t^{(q)}) = 0 \qquad (12)$$

for $\beta_p \neq -\beta_q$. Similarly, the following orthogonality relation

$$\iint dxdy\ \hat{z} \cdot (\mathbf{E}_t^{(q)} \times \mathbf{H}_t^{(-p)} - \mathbf{E}_t^{(-p)} \times \mathbf{H}_t^{(q)}) = 0 \qquad (13)$$

also holds for $\beta_q \neq \beta_p$.

4. Coupled Mode Equations

Consider a multiwaveguide system (Figure 1) with permittivity $\overline{\overline{\varepsilon}}(x,y)$. Also let $\overline{\overline{\varepsilon}}^{(p)}(x,y)$ be the permittivity for a single waveguide p. We use the generalized reciprocity relation in the following manner. Let

$$\overline{\overline{\varepsilon}}^{\langle 2\rangle}(x,y) = \overline{\overline{\varepsilon}}^{(p)}(x,y) \tag{14}$$

$$\mathbf{E}^{\langle 2\rangle} = (\mathbf{E}_t^{(-p)} + \mathbf{E}_z^{(-p)})\, e^{-i\beta_p z} \tag{15}$$

$$\mathbf{H}^{\langle 2\rangle} = (\mathbf{H}_t^{(-p)} + \mathbf{H}_z^{(-p)})\, e^{-i\beta_p z} \tag{16}$$

be the permittivity and mode solution for a single waveguide p. For $\langle 1\rangle$ we let

$$\overline{\overline{\varepsilon}}^{\langle 1\rangle}(x,y) = \overline{\overline{\varepsilon}}(x,y) \tag{17}$$

of the multiwaveguide system (Figure 1). The transverse field components of the multiwaveguide system are then approximated by linear superpositions of the individual waveguide modes of single waveguides.

$$\mathbf{E}_t^{\langle 1\rangle} \approx \sum_{q=1}^{N} a_q(z)\, \mathbf{E}_t^{(q)}(x,y) \tag{18}$$

$$\mathbf{H}_t^{\langle 1\rangle} \approx \sum_{q=1}^{N} a_q(z)\, \mathbf{H}_t^{(q)}(x,y) \tag{19}$$

where N is the number of modes that enter into the approximation. Note that each single waveguide q can contribute more than one mode (e.g., TE_0 and TM_0 modes).

It then follows from Maxwell's equations that the longitudinal components are then given by the expansion (Appendix A)

$$\mathbf{E}_z^{\langle 1\rangle} \equiv \sum_{q=1}^{N} \frac{a_q(z)}{\varepsilon_{zz}} \left\{ \varepsilon_{zz}^{(q)}\, \mathbf{E}_z^{(q)} + (\overline{\overline{\varepsilon}}_{zt}^{(q)} - \overline{\overline{\varepsilon}}_{zt}) \cdot \mathbf{E}_t^{(q)} \right\} \tag{20}$$

$$H_z^{<1>} = \sum_{q=1}^{N} a_q(z)\ H_z^{(q)} \tag{21}$$

Substitute (14) - (21) into both sides of the generalized reciprocity relation (4). The left-hand side of (4) gives

$$-\sum_{q=1}^{N} \frac{d}{dz}\left(a_q(z)\ e^{-i\beta_p z}\right) 4\ C_{pq} \tag{22}$$

where

$$C_{pq} = \frac{1}{4} \iint_{-\infty}^{\infty} dxdy\ \hat{z} \cdot \left[-\mathbf{E}_t^{(q)}(x,y) \times \mathbf{H}_t^{(-p)}(x,y) + \mathbf{E}_t^{(-p)}(x,y) \times \mathbf{H}_t^{(q)}(x,y)\right] \tag{23}$$

is the overlap integral which generally is not zero. The formulation with the neglect of the C_{pq} terms with $p \neq q$ has been referred to as the conventional coupled mode theory. The right-hand side of equation (4) gives

$$-i \sum_{q=1}^{N} 4\ K_{qp}\ a_q(z)\ e^{-i\beta p z} \tag{24}$$

where

$$\begin{aligned} K_{qp} = -\frac{\omega}{4} \iint dxdy \Big\{ & \mathbf{E}_t^{(-p)} \cdot (\bar{\bar{\varepsilon}}_t^{(p)} - \bar{\bar{\varepsilon}}_t) \cdot \mathbf{E}_t^{(q)} \\ & + \mathbf{E}_t^{(-p)} \cdot (\bar{\bar{\varepsilon}}_{tz}^{(p)} - \bar{\bar{\varepsilon}}_{tz}) \frac{\varepsilon_{zz}^{(q)}}{\varepsilon_{zz}} \cdot \mathbf{E}_z^{(q)} \\ & + \mathbf{E}_t^{(-p)} \cdot \frac{(\bar{\bar{\varepsilon}}_{tz}^{(p)} - \bar{\bar{\varepsilon}}_{tz})}{\varepsilon_{zz}} \cdot (\bar{\bar{\varepsilon}}_{zt}^{(q)} - \bar{\bar{\varepsilon}}_{zt}) \cdot \mathbf{E}_t^{(q)} \\ & + \mathbf{E}_z^{(-p)} \cdot (\bar{\bar{\varepsilon}}_{zt}^{(p)} - \bar{\bar{\varepsilon}}_{zt}) \cdot \mathbf{E}_t^{(q)} \\ & + \mathbf{E}_z^{(-p)} \cdot \frac{(\varepsilon_{zz}^{(p)} - \varepsilon_{zz})}{\varepsilon_{zz}} (\bar{\bar{\varepsilon}}_{zt}^{(q)} - \bar{\bar{\varepsilon}}_{zt}) \cdot \mathbf{E}_t^{(q)} \\ & + E_z^{(-p)} \frac{(\varepsilon_{zz}^{(p)} - \varepsilon_{zz})}{\varepsilon_{zz}}\ \varepsilon_{zz}^{(q)}\ E_z^{(q)} \Big\} \end{aligned} \tag{25}$$

Equating (22) and (24) gives the coupled mode equation

$$\sum_{q=1}^{N} C_{pq} \frac{da_q(z)}{dz} = i \sum_{q=1}^{N} Q_{pq} a_q(z) \quad . \tag{26}$$

where

$$Q_{pq} = K_{qp} + \beta_p C_{pq} \tag{27}$$

The coupled mode equation (26) can be conveniently cast in matrix form,

$$\bar{\bar{C}} \frac{d\mathbf{a}(z)}{dz} = i \bar{\bar{Q}} \mathbf{a}(z) \ , \tag{28}$$

where the matrices $\bar{\bar{C}}$ and $\bar{\bar{Q}}$ are of dimension N × N and the column vector $\mathbf{a}$ is of dimension N × 1.

5. Coupled Mode Equations for Lossless Multiwaveguide Systems

The lossless (gain) medium is a special case of the general lossy system when the loss approaches zero. In this section, we shall derive the coupled mode equations for lossless systems. It will be shown that in this special case the $\bar{\bar{C}}$ and $\bar{\bar{Q}}$ matrices of the last section are both Hermitian so that energy conservation is obeyed exactly.

For a lossless reciprocal anisotropic medium for both $\bar{\bar{\varepsilon}}$ and $\bar{\bar{\varepsilon}}^{(q)}$, we have

$$\bar{\bar{\varepsilon}}^{T*} = \bar{\bar{\varepsilon}} \tag{29}$$

$$\bar{\bar{\varepsilon}}^{(q)T*} = \bar{\bar{\varepsilon}}^{(q)} \tag{30}$$

Let

$$(\mathbf{E}_t^{(q)} + \mathbf{E}_z^{(q)})\, e^{i\beta_q z}$$

$$(\mathbf{H}_t^{(q)} + \mathbf{H}_z^{(q)})\, e^{i\beta_q z}$$

be the field solutions of a waveguide in a single waveguide q with real β_q. Then by taking complex conjugates of the Maxwell equations, it follows that

$$(\mathbf{E}_t^{(q)*} + \mathbf{E}_z^{(q)*})\, e^{-i\beta_q z}$$

$$(-\mathbf{H}_t^{(q)*} - \mathbf{H}_z^{(q)*})\, e^{-i\beta_q z}$$

is also a set of modal solutions and is propagating in the $-\hat{z}$ direction with a propagation constant β_q. In this case, the modal fields propagating in the $-\hat{z}$ direction are simply related to those of the $+\hat{z}$ direction as follows

$$\mathbf{E}_t^{(-q)} = \mathbf{E}_t^{(q)*} \tag{31}$$

$$\mathbf{H}_t^{(-q)} = -\mathbf{H}_t^{(q)*} \tag{32}$$

$$\mathbf{E}_z^{(-q)} = \mathbf{E}_z^{(q)*} \tag{33}$$

$$\mathbf{H}_z^{(-q)} = -\mathbf{H}_z^{(q)*} \tag{34}$$

Using (31) - (32) in (23), it follows that

$$C_{pq} = \frac{1}{4} \iint dxdy\ \hat{z} \cdot [\mathbf{E}_t^{(q)} \times \mathbf{H}_t^{(p)*} + \mathbf{E}_t^{(p)*} \times \mathbf{H}_t^{(q)}] \tag{35}$$

Hence

$$C_{pq} = C_{qp}^* \tag{36}$$

and $\overline{\overline{C}}$ is Hermitian.

To show that $\overline{\overline{Q}}$ is Hermitian, we make the following choices for the generalized reciprocity relation (4). Let

$$\overline{\overline{\varepsilon}}^{<1>} = \overline{\overline{\varepsilon}}^{(q)} \tag{37}$$

$$\mathbf{E}^{<1>} = (\mathbf{E}_t^{(q)} + \mathbf{E}_z^{(q)})\ e^{i\beta_q z} \tag{38}$$

$$\mathbf{H}^{<1>} = (\mathbf{H}_t^{(q)} + \mathbf{H}_z^{(q)})\ e^{i\beta_q z} \tag{39}$$

and

$$\overline{\overline{\varepsilon}}^{<2>} = \overline{\overline{\varepsilon}}^{(p)} \tag{40}$$

$$\mathbf{E}^{<2>} = (\mathbf{E}_t^{(p)*} + \mathbf{E}_z^{(p)*})\ e^{-i\beta_p z} \tag{41}$$

$$\mathbf{H}^{<2>} = (-\mathbf{H}_t^{(p)*} - \mathbf{H}_z^{(p)*})\ e^{-i\beta_p z} \tag{42}$$

Then, from (4) it follows that

$$(\beta_q - \beta_p)\, C_{pq} = -\frac{\omega}{4} \iint dxdy\, \mathbf{E}^{(p)*} \cdot (\bar{\bar{\varepsilon}}^{(p)} - \bar{\bar{\varepsilon}}^{(q)}) \cdot \mathbf{E}^{(q)}$$

$$= -\frac{\omega}{4} \iint dxdy \{\mathbf{E}_t^{(p)*} \cdot (\bar{\bar{\varepsilon}}_t^{(p)} - \bar{\bar{\varepsilon}}_t^{(q)}) \cdot \mathbf{E}_t^{(q)}$$

$$+ \mathbf{E}_t^{(p)*} \cdot (\bar{\bar{\varepsilon}}_{tz}^{(p)} - \bar{\bar{\varepsilon}}_{tz}^{(q)}) \cdot \mathbf{E}_z^{(q)}$$

$$+ \mathbf{E}_z^{(p)*} \cdot (\bar{\bar{\varepsilon}}_{zt}^{(p)} - \bar{\bar{\varepsilon}}_{zt}^{(q)}) \cdot \mathbf{E}_t^{(q)}$$

$$+ E_z^{(p)*} \; (\varepsilon_{zz}^{(p)} - \varepsilon_{zz}^{(q)}) \; E_z^{(q)}\} \tag{43}$$

Using (31) - (34) in (25), the quantity $K_{qp} - K_{pq}^*$ can be calculated. After a moderate amount of algebraic manipulations, it can be shown that $K_{qp} - K_{pq}^*$ is equal to the right-hand side of (43). Hence,

$$(\beta_q - \beta_p)\, C_{pq} = K_{qp} - K_{pq}^* \tag{44}$$

It then follows from (27), (36) and (44) that

$$Q_{pq} - Q_{qp}^* = K_{qp} + \beta_p C_{pq} - K_{pq}^* - \beta_q C_{qp}^*$$

$$= 0 \tag{45}$$

Hence, $\bar{\bar{Q}}$ is Hermitian. It is straightforward to show that these relations (44) and (45) reduce identically to those of the isotropic waveguide case in [15].

Energy conservation can be demonstrated as follows. The power P(z) in the multiwaveguide system is

$$P(z) = \frac{1}{2} \operatorname{Re} \iint dxdy\, \hat{z} \cdot \mathbf{E}_t \times \mathbf{H}_t^* \tag{46}$$

Using (18) and (19) in (46) gives

$$P(z) = \sum_{p,q=1}^{N} a_p^* a_q C_{pq} \tag{47}$$

Using (28) and the fact that both $\overline{\overline{C}}$ and $\overline{\overline{Q}}$ are Hermitian, it follows that $dP/dz = 0$ and the power $P(z)$ is independent of z. Energy conservation is obeyed.

6. Coupled Mode Equations for Single Waveguide System

In a single waveguide system, we have $\bar{\bar{\varepsilon}}^{(p)} = \bar{\bar{\varepsilon}}^{(q)}$ and $\bar{\bar{\varepsilon}}$ is the perturbed permittivity that causes coupling among the modes in the single waveguide. The coupled mode equations for a single waveguide with a general reciprocal anisotropic medium were derived previously by Marcuse [19]. In this section, we shall show that for this special case, our results are identical to those in [19].

Let

$$\bar{\bar{\varepsilon}}^{(p)} = \bar{\bar{\varepsilon}}^{(q)} = \bar{\bar{\varepsilon}}', \tag{48}$$

denote the unperturbed permittivity of the single waveguide. Then $\mathbf{E}^{(p)}$ and $\mathbf{E}^{(q)}$ are the mode solutions of $\bar{\bar{\varepsilon}}'$ with propagation constants β_p and β_q. Hence they obey the mode orthogonality relation of (13). Using the mode orthogonal relation, it is easy to see that $\bar{\bar{C}}$ as given by (23) is a diagonal matrix. Hence

$$C_{pq} = C_p \, \delta_{pq} \tag{49}$$

where δ_{pq} is the Kronecker delta. The coupled mode equations become

$$C_p \left(\frac{da_p}{dz} - i \beta_p a_p(z)\right) = i \sum_q K_{qp} a_q(z) \tag{50}$$

for $p = 1, \ldots, N$. Using (48) in (25), it follows that some of the terms are cancelled and the expression for K_{qp} becomes

$$K_{qp} = -\frac{\omega}{4}\iint dxdy \Big\{ \mathbf{E}_t^{(-p)} \cdot (\bar{\bar{\varepsilon}}_t' - \bar{\bar{\varepsilon}}_t) \cdot \mathbf{E}_t^{(q)}$$

$$+ \mathbf{E}_t^{(-p)} \cdot \frac{(\bar{\varepsilon}_{tz}' - \bar{\varepsilon}_{tz})}{\varepsilon_{zz}} \cdot (\bar{\bar{\varepsilon}}_{zt}' - \bar{\bar{\varepsilon}}_{zt}) \cdot \mathbf{E}_t^{(q)}$$

$$+ \mathbf{E}_t^{(-p)} \cdot \frac{\varepsilon_{zz}'}{\varepsilon_{zz}} (\bar{\bar{\varepsilon}}_{tz}' - \bar{\bar{\varepsilon}}_{tz}) \cdot \mathbf{E}_z^{(q)}$$

$$+ \mathbf{E}_z^{(-p)} \cdot \frac{\varepsilon_{zz}'}{\varepsilon_{zz}} (\bar{\bar{\varepsilon}}_{zt}' - \bar{\bar{\varepsilon}}_{zt}) \cdot \mathbf{E}_t^{(q)}$$

$$+ \mathbf{E}_z^{(-p)} \frac{\varepsilon_{zz}'}{\varepsilon_{zz}} (\varepsilon_{zz}' - \varepsilon_{zz}) \mathbf{E}_z^{(q)} \Big\} \qquad (51)$$

It can be shown (Appendix B) that (51) is identical to equation (46) of Marcuse [19].

7. Numerical Example

In this section we illustrate the coupled mode theory developed in the previous sections with a numerical example using Ti-diffused $LiNbO_3$ waveguides. Consider two coupled slab waveguides, a and b, of thicknesses, d_a and d_b, and edge to edge separation, t. Voltages V_a and V_b are applied respectively to the two slabs. The uniaxial axis is assumed to be in the y direction for both guiding and substrate regions (Figure 2). In the following analysis we shall include four modes coupling (N=4). The four modes are TE_0, TM_0 of guide a and TE_0 and TM_0 of guide b, which are denoted as TE_0^a, TM_0^a, TE_0^b and TM_0^b with the corresponding amplitudes $a_1(z)$, $a_2(z)$, $a_3(z)$ and $a_4(z)$ in the same order. Then we make the following substitutions. Let $\bar{\bar{\varepsilon}}_a$ represent the permittivity profile of a single waveguide a and $\bar{\bar{\varepsilon}}_b$ represent the permittivity profile of single waveguide b with zero voltages.

$$\bar{\bar{\varepsilon}}_a = \begin{cases} \varepsilon_o \begin{bmatrix} n_{oa}^2 & 0 & 0 \\ 0 & n_{ea}^2 & 0 \\ 0 & 0 & n_{oa}^2 \end{bmatrix} & \text{for } |x| < \dfrac{d_a}{2} \\ \bar{\bar{\varepsilon}}_c & \text{for } |x| > \dfrac{d_a}{2} \end{cases} \tag{52}$$

for guide a, where

$$\bar{\bar{\varepsilon}}_c = \varepsilon_o \begin{bmatrix} n_o^2 & 0 & 0 \\ 0 & n_e^2 & 0 \\ 0 & 0 & n_o^2 \end{bmatrix} \tag{53}$$

For guide b

$$\bar{\bar{\varepsilon}}_b = \begin{cases} \varepsilon_o \begin{bmatrix} n_{ob}^2 & 0 & 0 \\ 0 & n_{eb}^2 & 0 \\ 0 & 0 & n_{ob}^2 \end{bmatrix} & \text{for } |x - x_b| < \frac{d_b}{2} \\ \bar{\bar{\varepsilon}}_c & \text{for } |x - x_b| > \frac{d_b}{2} \end{cases}$$

$$\text{with } x_b = t + \frac{d_a}{2} + \frac{d_b}{2} \qquad (54)$$

Then, let $\bar{\bar{\varepsilon}}^{(1)} = \bar{\bar{\varepsilon}}_a$ and $(E^{(1)}, H^{(1)}) = (E, H)$ of the TE_0 mode of $\bar{\bar{\varepsilon}}_a$. Also let $\bar{\bar{\varepsilon}}^{(2)} = \bar{\bar{\varepsilon}}_a$ and $(E^{(2)}, H^{(2)}) = (E, H)$ of the TM_0 mode of $\bar{\bar{\varepsilon}}_a$. Note that both $\bar{\bar{\varepsilon}}^{(1)}$ and $\bar{\bar{\varepsilon}}^{(2)}$ are equal to $\bar{\bar{\varepsilon}}_a$. Similarly, $\bar{\bar{\varepsilon}}^{(3)} = \bar{\bar{\varepsilon}}^{(4)} = \bar{\bar{\varepsilon}}_b$ and let $(E^{(3)}, H^{(3)}) = (E, H)$ of the TE_0 mode of $\bar{\bar{\varepsilon}}_b$ and $(E^{(4)}, H^{(4)}) = (E, H)$ of the TM_0 mode of $\bar{\bar{\varepsilon}}_b$.

The permittivity $\bar{\bar{\varepsilon}}$ is then taken to be the permittivity profile of the multiwaveguide system with voltages V_a and V_b. Based on the characteristics of $LiNbO_3$, the permittivity $\bar{\bar{\varepsilon}}(x,y)$ can be approximated [22] by the following expressions (55) and (56).

Let

$$\bar{\bar{\varepsilon}}'_{\gamma} = \varepsilon_o \begin{bmatrix} n_{o\gamma}^2 - n_{o\gamma}^4 \, r_{22}^{\gamma} \frac{V_\gamma}{d_\gamma} & - r_{51}^{\gamma} \, n_{o\gamma}^2 \, n_{e\gamma}^2 \frac{V_\gamma}{d_\gamma} & 0 \\ -r_{51}^{\gamma} \, n_{o\gamma}^2 \, n_{e\gamma}^2 \frac{V_\gamma}{d_\gamma} & n_{e\gamma}^2 & 0 \\ 0 & 0 & n_{o\gamma}^2 + n_{o\gamma}^4 \, r_{22}^{\gamma} \frac{V_\gamma}{d_\gamma} \end{bmatrix} \tag{55}$$

with $\gamma = a, b$. Then

$$\bar{\bar{\varepsilon}} = \begin{cases} \bar{\bar{\varepsilon}}'_a & \text{for } |x| < \frac{d_a}{2} \\ \bar{\bar{\varepsilon}}'_b & \text{for } |x - x_b| < \frac{d_b}{2} \\ \bar{\bar{\varepsilon}}_c & \text{otherwise} \end{cases} \tag{56}$$

In the numerical results to be illustrated, we have assumed the input wave to be the TM_0 mode of guide a. Hence the coupled mode equations are solved and the initial conditions are set by letting $a_q(z=0)=1$, for q=2 and 0 for q=1,3,4. The mode functions are normalized such that $C_{qq} = 1$, $q = 1,2,3,4$. In the calculations, we have tested the power conservation with equation (47). Power conservation is checked numerically to within 10^{-10} percent. The reason for using high accuracy is because the cross-polarization powers can be very small (of the order 10^{-4} or less). Thus this high accuracy based on double precision is only for self-consistent check. The transfer efficiency of the two modulators of Figure 3 are considered. Note that the two directional couplers have identical input guides but different output guides. The coupling section is of length ℓ. By matching the field solution to the output guides, it then readily follows that [13], [17]

$$P_a^{TE_0} = \mathrm{Re}\left(\sum_{j,k=1}^{4} C'_{1j}\, C'^{*}_{k1}\, a_j(\ell)\, a_k^{*}(\ell)\right) \tag{57}$$

$$P_a^{TM_0} = \mathrm{Re}\left(\sum_{j,k=1}^{4} C'_{2j}\, C'^{*}_{k2}\, a_j(\ell)\, a_k^{*}(\ell)\right) \tag{58}$$

for the output power of directional coupler 1. Similarly, the output powers of directional coupler 2 are

$$P_b^{TE_0} = \mathrm{Re}\left(\sum_{j,k=1}^{4} C'_{3j}\, C'^{*}_{k3}\, a_j(\ell)\, a_k^{*}(\ell)\right) \tag{59}$$

$$P_b^{TM_0} = \mathrm{Re}\left(\sum_{j,k=1}^{4} C'_{4j}\, C'^{*}_{k4}\, a_j(\ell)\, a_k^{*}(\ell)\right) \tag{60}$$

where

$$C'_{pq} = \frac{1}{2}\iint dxdy\ \hat{z} \cdot \left(\mathbf{E}_t^{(q)} \times \mathbf{H}_t^{(p)*}\right) \tag{61}$$

In the numerical results of Figures 4 to 6 we have used the following parameters: $d_a = d_b = 1.6\ \mu m$, $t = 1.6\ \mu m$, $\lambda = 0.633\ \mu m$, $n_o = 2.281$, $n_e = 2.195$, $n_{oa} = n_{ob} = 2.286$, $n_{ea} = n_{eb} = 2.2$, $r_{22}^{a} = r_{22}^{b} = 3.4 \times 10^{-12}$ m/V, and $r_{51}^{a} = r_{51}^{b} = 28.0 \times 10^{-12}$ m/V. In Figure 4, $P_a^{TM_0}$ and $P_b^{TM_0}$ are plotted as functions of the coupling length ℓ for $V_a = V_b = 0$. There are no off-diagonal elements for $\bar{\bar{\varepsilon}}(x,y)$ in this case and $P_a^{TE_0} = P_b^{TE_0} = 0$, so that there is no coupling to the TE modes. We note that when the output power in waveguide b is maximum at around $\ell = 700\ \mu m$, the output power in waveguide a is not zero. This cross-talk is due to the overlap of fields between modes in waveguide a and waveguide b [17]. The computed overlap integral C_{24} in this case is equal to 0.1753076 which is outside the region of validity of the conventional coupled-mode theory. The computed coupling coefficient $K_{24} = K_{42} = 0.2284878 \times 10^{-2}$.

In Figures 5 and 6 the output powers are plotted as functions of the modulating voltage V with $V_a = V$ and $V_b = -V$ and $\ell = 700$ μm. For the parameters chosen and a voltage range of -20 volts $< V <$ 20 volts, there is appreciable transfer of power between the two guides. The results of Figure 6 indicate that the transfer of power to the TE modes is of the order of -40 dB to -30 dB with $P_b^{TE_0}$ larger than $P_a^{TE_0}$ because of the larger overlap of the fields between the TM_0 mode of guide a and the TE_0 mode of guide b.

8. Conclusions

The strongly coupled-mode theory for a reciprocal anisotropic medium in multiwaveguide systems has been derived in this paper. Both lossy (gain) and lossless cases are considered. In general, the TE and the TM modes of separate waveguides are coupled due to the anisotropy of the medium. For the lossless case, the energy conservation is shown to be satisfied in this coupled mode formulation. For the case of a single anisotropic waveguide, we show that our results reduce identically to those of Marcuse [19]. The numerical results for two coupled anisotropic waveguides with both TE_0 and TM_0 mode couplings have been illustrated.

Appendix A: Derivation of the Longitudinal Field Components

To derive the expansion of the longitudinal field components as given by (20) and (21), we note that

$$E_z^{<1>} = \frac{i}{\omega \epsilon_{zz}} \{\nabla_t \times H_t^{<1>} + i\omega \overline{\overline{\epsilon}}_{zt} \cdot E_t^{<1>}\} \tag{A1}$$

Substitute the expansions (18) and (19) in (A1) and note that for the qth mode of waveguide q

$$\nabla_t \times H_t^{(q)} = - i\omega \overline{\overline{\epsilon}}_{zt}^{(q)} \cdot E_t^{(q)} - i\omega \epsilon_{zz}^{(q)} E_z^{(q)} \tag{A2}$$

One then obtains (20). To derive (21), note that

$$H_z^{<1>} = \frac{1}{i\omega\mu} \nabla_t \times E_t^{<1>} \tag{A3}$$

$$\nabla_t \times E_t^{(q)} = i\omega\mu H_z^{(q)} \tag{A4}$$

Substituting (18) in (A3) and using (A4) gives (21).

Appendix B: Comparison of K_{qp} in (51) with the Result of Marcuse [19]

In comparing (51) with equation (46) of Marcuse [19], it is to be noted that the permittivity tensor elements are defined differently.

$$\bar{\bar{\varepsilon}} = \bar{\bar{\varepsilon}}_t^{(m)} + \bar{\bar{\varepsilon}}_z^{(m)} \tag{B1}$$

where superscript (m) denotes Marcuse. Also

$$\bar{\bar{\varepsilon}}_t^{(m)} = \bar{\bar{\varepsilon}}_t + \bar{\bar{\varepsilon}}_{tz} \tag{B2}$$

$$\bar{\bar{\varepsilon}}_z^{(m)} = \bar{\bar{\varepsilon}}_{zt} + \bar{\bar{\varepsilon}}_{zz} \tag{B3}$$

With the above substitution in equation (46) of [19], it can be shown, after a moderate amount of algebra, that the coupling coefficient K_{qp} is identical to expression (51).

References

[1] H. Kogelnik, "Theory of dielectric waveguides," in Integrated Optics, T. Tamir, Ed., Second Edition, Ch. 2. New York: Springer-Verlag, 1979.

[2] A. Yariv, "Coupled-mode theory for guided wave optics," IEEE J. Quantum Electron., vol. QE-9, pp. 919-933, 1973.

[3] H. F. Taylor and A. Yariv, "Guided wave optics," Proc. IEEE, vol. 62, pp. 1044-1060, 1974.

[4] E. Kapon, J. Katz and A. Yariv, "Supermode analysis of phase locked arrays of semiconductor lasers," Opt. Lett., vol. 9, pp. 125-127, 1984.

[5] A. Hardy and W. Streifer, "Analysis of phase array diode lasers," Opt. Lett., vol. 10, pp. 335-337, 1985.

[6] R. C. Alferness and R. V. Schmidt, "Tunable optical waveguide directional coupler filter," Appl. Phys. Lett., vol. 33, pp. 161-163, July 1978.

[7] R. C. Alferness and J. J. Veselka, "Tunable Ti: $LiNbO_3$ waveguide filter for long-wavelength (λ = 1.3 - 1.6 μm) multiplexing/demultiplexing," in Tech. Dig. Conf. Lasers and Electro-optics, (Anaheim, CA), pp. 230-231, 1984.

[8] B. Broberg, B. S. Lindgren, M. Öberg and H. Jiang, "A novel integrated optics wavelength filter in In Ga As P - In P," IEEE J. Lightwave Technol., vol. LT-4, pp. 196-203, 1986.

[9] A. Hardy and W. Streifer, "Coupled mode theory of parallel waveguides," IEEE J. Lightwave Technol., vol. LT-3, pp. 1135-1146, 1985.

[10] A. Hardy and W. Streifer, "Coupled modes of multiwaveguide systems and phase arrays," IEEE J. Lightwave Technol., vol. LT-4, pp. 90-99, 1986.

[11] A. Hardy and W. Streifer, "Coupled mode solutions of multiwaveguide systems," IEEE J. Quantum Electron., vol. QE-22, pp. 528-534, 1986.

[12] H. A. Haus, W. P. Huang, S. Kawakami and N. A. Whitaker, "Coupled-mode theory of optical waveguides," IEEE J. Lightwave Technol., vol. LT-4, 1986.

[13] E. Marcatili, "Improved coupled-mode equations for dielectric guides," IEEE J. Quantum Electron., vol. QE-22, pp. 988-993, 1986.

[14] S. L. Chuang, "A coupled-mode formulation by reciprocity and a variational principle," IEEE J. Lightwave Technol., vol. LT-5, pp. 5-15, 1987.

[15] S. L. Chuang, "A coupled-mode theory for multiwaveguide systems satisfying the reciprocity theorem and power conservation," IEEE J. Lightwave Technol., vol. LT-5, pp. 174-183, 1987.

[16] W. Streifer, M. Osiński and A. Hardy, "Reformulation of the coupled mode theory of multiwaveguide systems," IEEE J. Lightwave Technol., vol. LT-4, 1986.

[17] S. L. Chuang, "Application of the strongly coupled-mode theory to integrated optical devices," submitted to IEEE J. Quantum Electron.

[18] E. G. Spencer, P. V. Lenzo and A. A. Ballman, "Dielectric materials for electro-optic, elasto-optic and ultrasonic device applications," Proc. IEEE, vol. 55, pp. 2074-2108, 1967.

[19] D. Marcuse, "Coupled-mode theory for anisotropic optical waveguides," Bell Sys. Tech. J., vol. 54, pp. 985-995, 1975.

[20] R. A. Steinberg and T. G. Giallorenzi, "Modal fields of anisotropic channel waveguides," J. Opt. Soc. Am., vol. 67, pp. 523-532, 1977.

[21] O. G. Ramer, "Integrated optic electro-optic modulator electrode analysis," IEEE J. Quantum Electron., vol. QE-18, pp. 386-392, 1982.

[22] A. Yariv and P. Yeh, Optical Waves in Crystals New York: Wiley International, 1984.

[23] L. B. Felsen and N. Marcuritz, Radiation and Scattering of Waves Englewood Cliffs, New Jersey: Prentice-Hall, 1973.

Figure Captions

Figure 1 (a) A single waveguide p described by $\overline{\overline{\varepsilon}}^{(p)}(x,y)$ for the entire space

(b) A single waveguide q described by $\overline{\overline{\varepsilon}}^{(q)}(x,y)$ for the entire space

(c) A multiwaveguide system described by $\overline{\overline{\varepsilon}}(x,y)$ in the entire space.

Figure 2 Geometric configuration of two coupled anisotropic waveguides for the numerical example in Section 7.

Figure 3 Directional couplers with identical input guides a but different output guides a (directional coupler 1) or b (directional coupler 2).

Figure 4 The output powers in the TM_0 mode of guide a, $P_a^{TM_0}$, and in the TM_0 mode of guide b, $P_b^{TM_0}$, as functions of the coupling length ℓ without applied voltage, $V = 0$.

Figure 5 The output powers in the TM_0 mode of guide a, $P_a^{TM_0}$, and in the TM_0 mode of guide b, $P_b^{TM_0}$, as functions of the applied voltage $V_a = -V_b = V$.

Figure 6 The output powers in the TE_0 mode of guide a, $P_a^{TE_0}$, and in TE_0 mode of guide b, $P_b^{TE_0}$, as functions of the applied voltage $V_a = -V_b = V$.

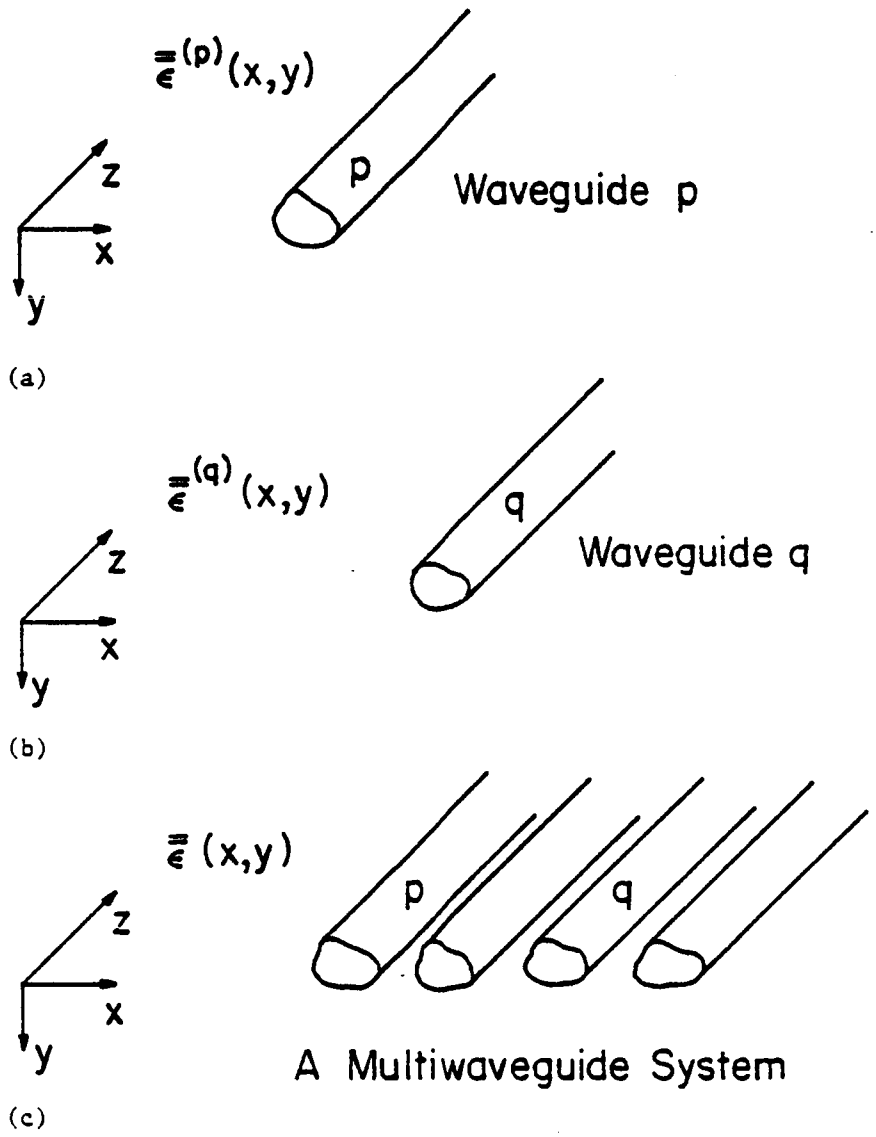
$\overline{\overline{\epsilon}}^{(p)}(x,y)$
z
x
y
p
Waveguide p
(a)
$\overline{\overline{\epsilon}}^{(q)}(x,y)$
z
x
y
q
Waveguide q
(b)
$\overline{\overline{\epsilon}}(x,y)$
z
x
y
p
q
A Multiwaveguide System
(c)

Figure 1

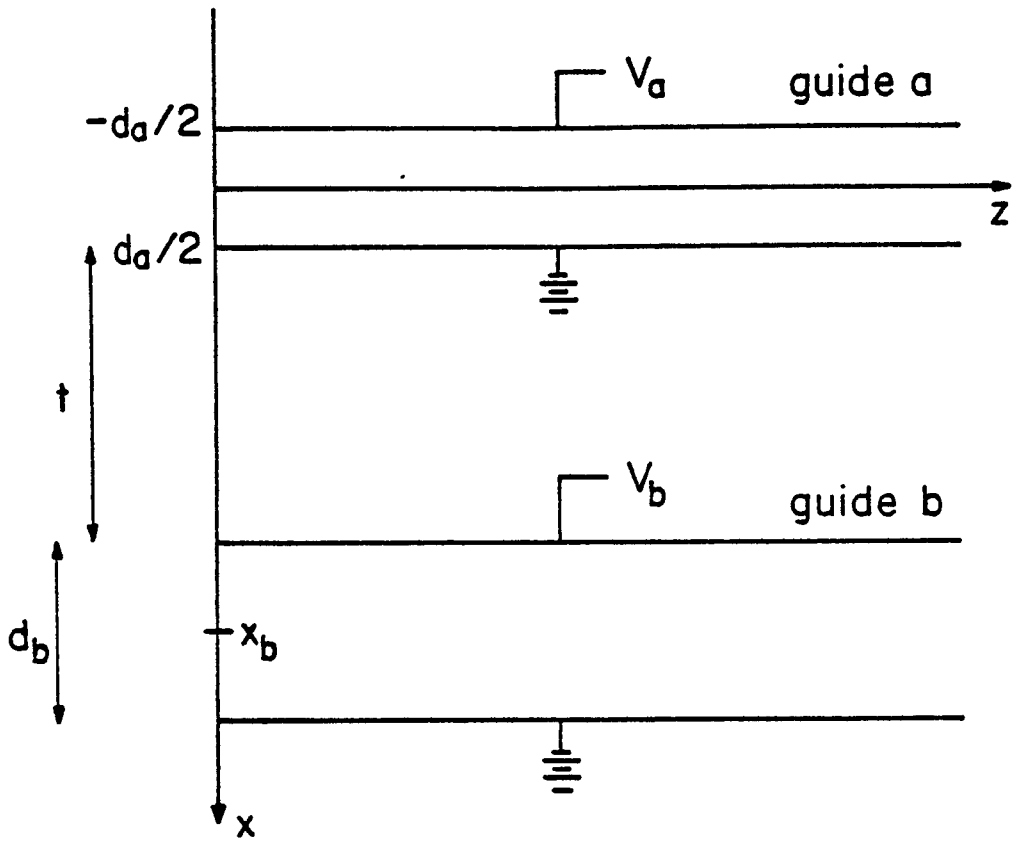

Figure 2

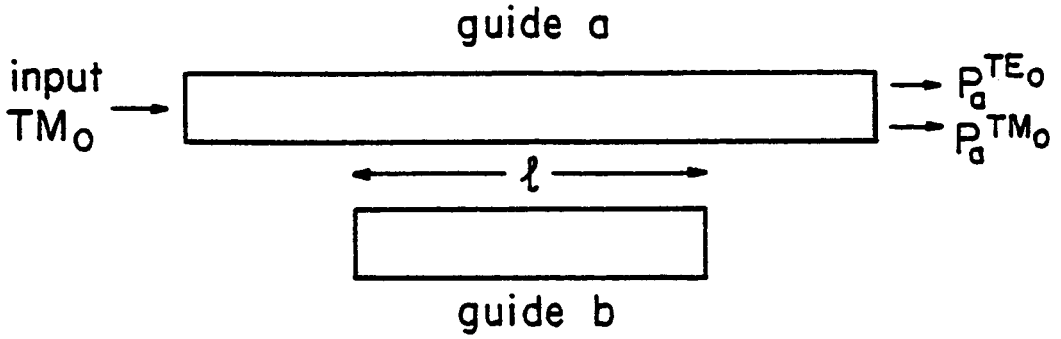

Directional Coupler 1

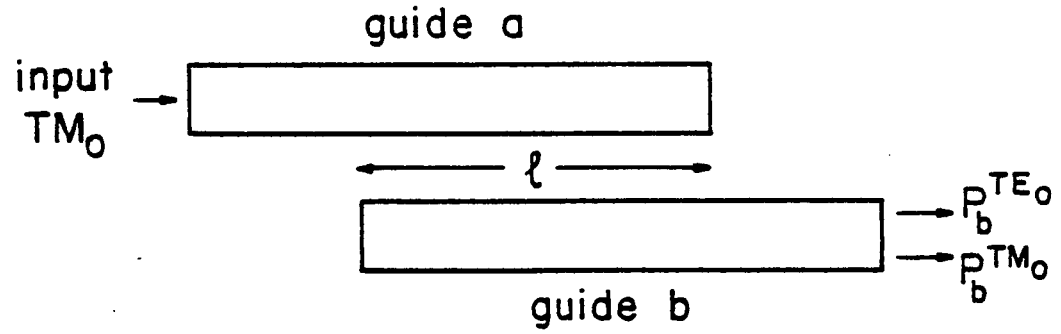

Directional Coupler 2

Figure 3

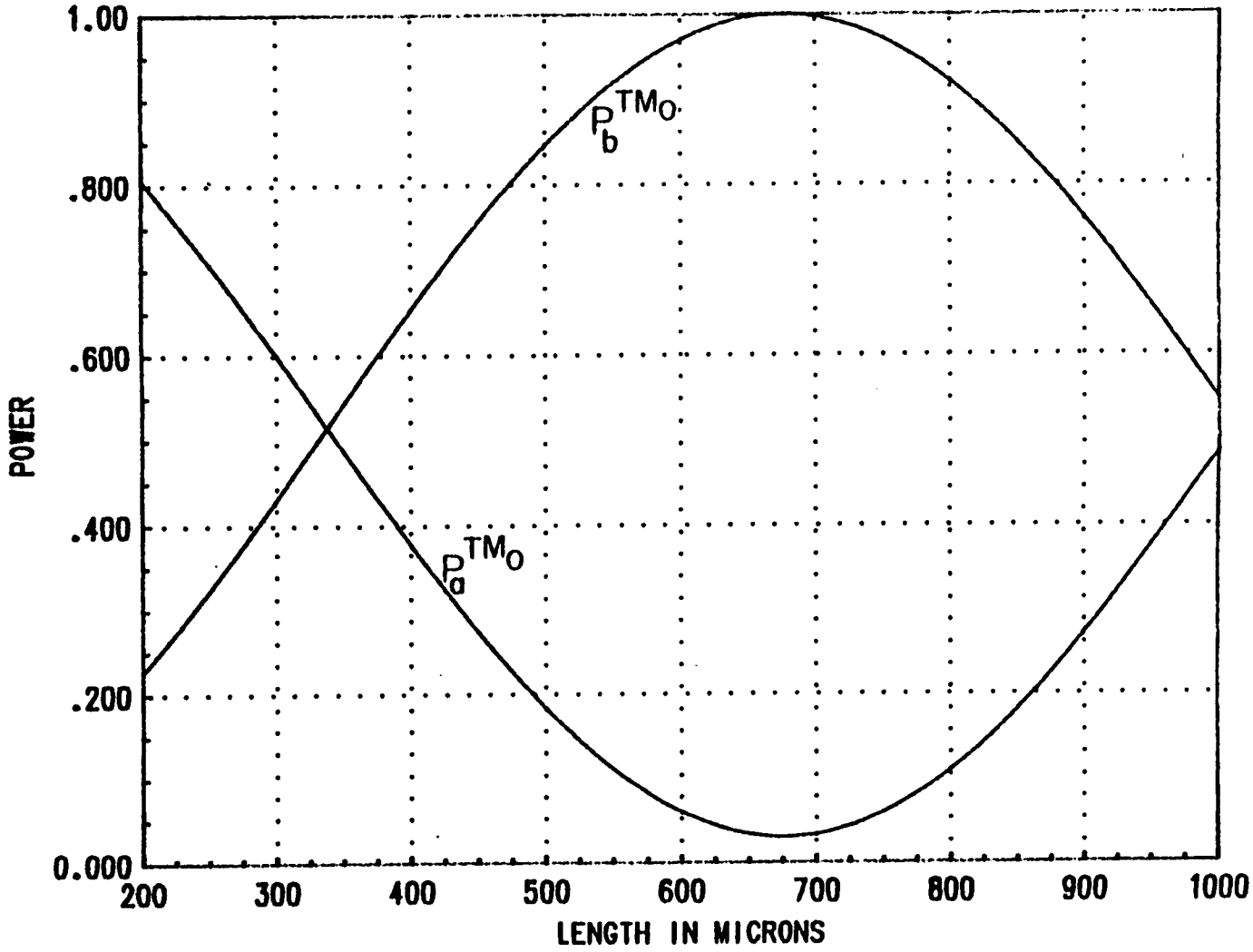

POWER IN WAVEGUIDES

a and b; TM MODES

Figure 4

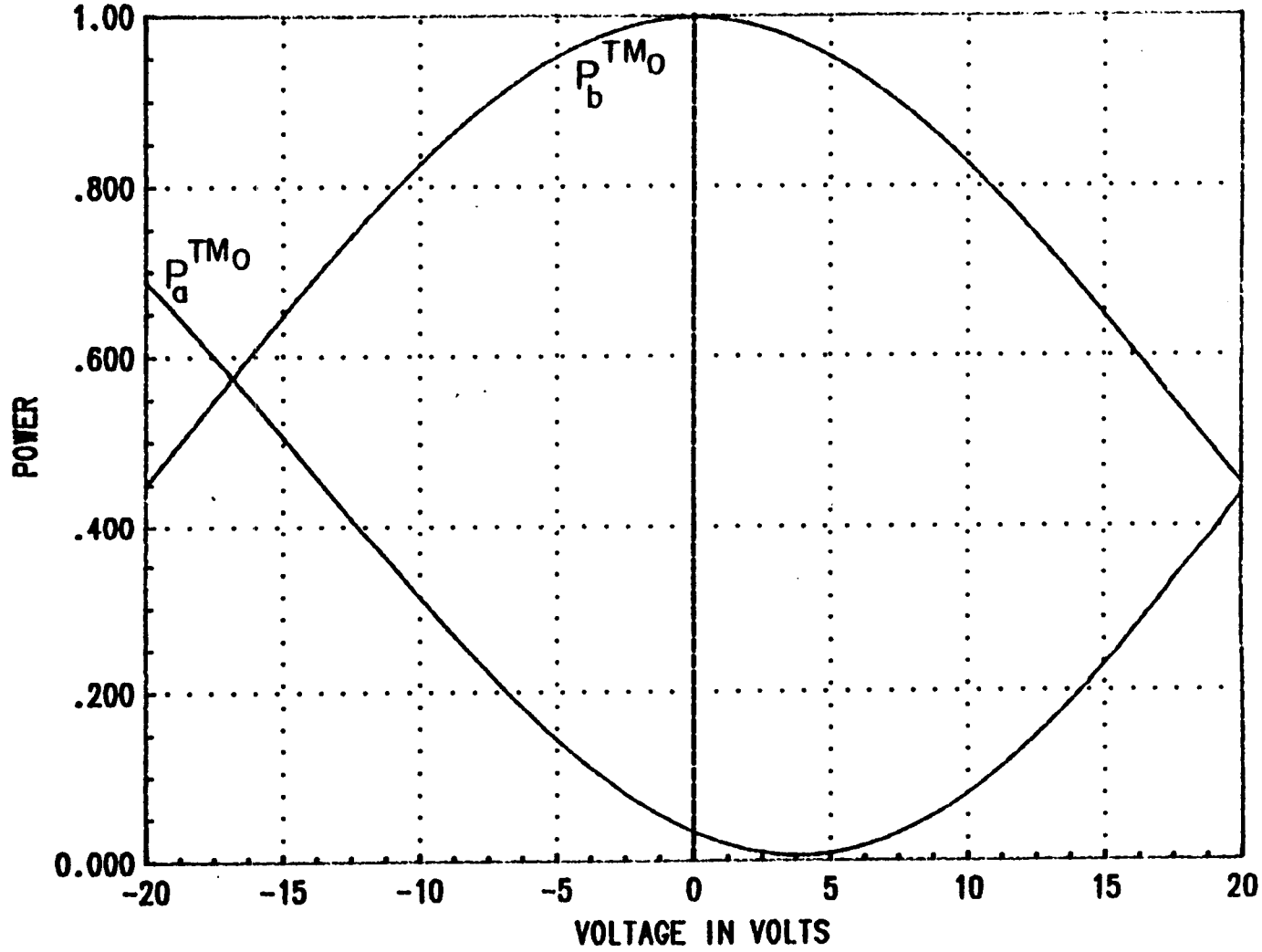

POWER IN WAVEGUIDES

a and b; TM MODES

Figure 5

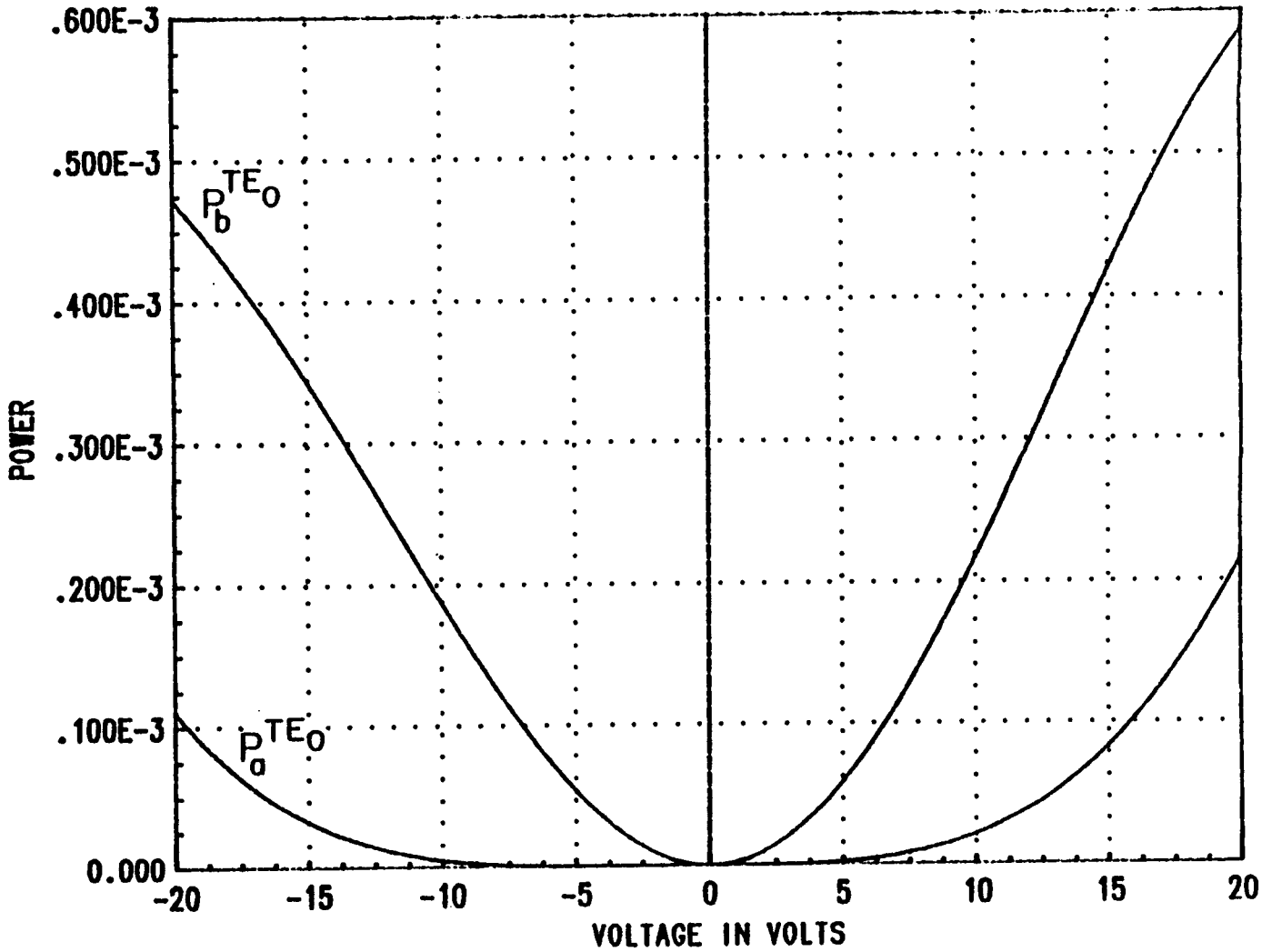

Figure 6

POWER IN WAVEGUIDES

a and b; TE MODES